

### **Abstract**

This is the user's manual for DEGAS 2 - A Monte Carlo code for the study of neutral atom and molecular transport in confined plasmas. It is intended to cover all aspects of DEGAS 2 from the user's point-of-view: obtaining the files, compiling them, setting up the input files, executing the code, and interpreting the output. References will be provided for the underlying physics, but the essential aspects will be highlighted. Information for programmers interested in modifying DEGAS 2 can be found within the source code itself. Links to some of the more useful ones are provided.





User's Guide for DEGAS 2  
*CVS Revision : 1.2<sup>1</sup>*

Daren Stotler and Charles Karney  
*Princeton Plasma Physics Laboratory*  
Randall Kanzleiter  
*Rensselaer Polytechnic Institute*  
Jaishankar S.  
*Institute for Plasma Research, India*

November 16, 2001

<sup>1</sup>This file is written in  $\text{T}_{\text{E}}\text{X}$ . A hyper-linked PDF file is generated from that source using `pdflatex`. The version number here is the CVS version number for the User's Manual itself. This document is now distributed as part of the DEGAS 2 code. The user can be best assured of concurrence between code and manual by referring to the version of the manual that came with the code. Copyright ©2001 PPPL. Permission is granted to make and distribute verbatim copies of this manual provided the copyright and permission notice is preserved on all copies. Permission is granted to copy and distribute modified versions of this manual under the conditions for verbatim copying, provided also that the entire resulting derived work is distributed under the terms of a permission notice identical to this one. Permission is granted to copy and distribute translations of this manual into another language, under the above conditions for modified versions.

# Chapter 1

## Introduction

### 1.1 Purpose of Monte Carlo Neutral Transport

The interaction of neutral atoms and molecules with the background plasma is an important component in the physics of fusion research plasmas. These neutrals affect both the particle and energy balance of the plasma, providing a source of new plasma and a channel for heat transport across the magnetic field that confines the charged particles. In addition, hot neutrals which leave the plasma volume can interact with the wall of the plasma chamber, sputtering impurities into the plasma and (in reactors) possibly damaging the wall. Finally, these hot neutrals can also be used for plasma diagnostics. Therefore, it is worth developing an accurate description of the neutral behaviour.

The theory of neutral particle kinetics[1] treats the transport of mass, momentum, and energy in a plasma due to neutral particles that are themselves unaffected by magnetic fields. This transport affects the global power and particle balances in fusion devices, as well as profile control and plasma confinement quality, particle and energy fluxes onto device components, performance of pumping systems, and the design of diagnostics and the interpretation of their measurements. Though analytic models (solving the Boltzmann equation for the neutrals or using the diffusion approximation), both single- and multi-species, have been used to study neutral transport, a variety of approximations must be made. Some numerical methods for solving the Boltzmann equation use simplified geometries and atomic physics. On the other hand, the Monte Carlo approach to integrating the Boltzmann equation can treat in great detail asymmetric geometries and complex atomic physics and wall interactions. Because of the similarity in the problems,

Monte Carlo neutral transport codes can build on the techniques developed for neutron transport in reactor design[2].

## 1.2 Need for DEGAS 2

The predecessor to DEGAS 2 was DEGAS[3], a widely used and well documented code. However, two events pointed out its limitations.

- The combined DEGAS-B2 code was too slow (about 100 Cray hours)[4]. The stronger the coupling between neutral and plasma species, the more difficult it is to arrive at a converged solution. In this case which looked at a high recycling divertor for a compact, high field reactor, hundreds or thousands of complete Monte Carlo profiles must be carried out in order to couple effectively to a fluid code.
- The problem physics was difficult to modify. In the radiative and detached divertor regimes being investigated for future reactors, it is believed that the list of important atomic processes will grow to include elastic collisions and molecular hydrogenic species other than ground state H<sub>2</sub>.

Hence, it was decided that a new code should be written which draws on the extensive experience at PPPL and that from Garching and Jülich. The philosophy behind DEGAS 2 was defined during 1992-1993:

- High speed,
- Flexibility,
- Ease-of-use,
- Well documented.

## 1.3 DEGAS 2 Features

An effort was made to realise the above mentioned objectives of DEGAS 2 by the following means:

- Improve speed relative to DEGAS by utilizing the “track length” estimator.

- Ensure flexibility by designing the code using quasi-object oriented programming techniques. The modifier “quasi” refers to the fact that DEGAS 2 is written in FORTRAN (compatible with FORTRAN 77 and FORTRAN 90). Even though the basic “classes” in the problem have been abstracted, the degree of encapsulation actually achieved (via pre-processor macros) in DEGAS 2 is limited. Furthermore, there is no provision for inheritance within this programming environment.
- Provide an easy-to-use and well documented code by writing it with the FWEB[7] package. FWEB provides the powerful preprocessing and macro facility which underlies the “quasi-object oriented” implementation and internal  $\TeX$  documentation.

Other significant features of DEGAS 2 include:

- Dynamic memory allocation for optimal performance in large problems,
- Operation on a number of UNIX platforms, compilable with both FORTRAN 77 and FORTRAN 90,
- Input and output data stored in self-describing, platform-independent binary files. Presently, the main code uses exclusively netCDF[8] (Network Common Data Format) files for input and output. However, a simple post-processing utility is included which generates graphics and data in HDF[9] (Hierarchical Data Format) files. Hopefully, a single format will be settled upon eventually.
- Parallel execution on distributed workstations and massively parallel computers. This is the most promising technique for improving the speed of DEGAS 2. The reason is that most of the future advancements in computer speed will result from increases in the number of processors. Parallel processing is practical to Monte Carlo since the amount of communication required per computation is small.
- High quality coding standards. Good programming practices such as use of the `implicit none` statement and an assertion facility help to ensure that the code works properly. This document will eventually describe a basic test suite which actually demonstrates that the code is correct. In the code design process, clarity has been given a high priority as well, facilitating readability and maintainability.

- Code versions numbered and documented with the “CVS” (concurrent version system) package.

# Chapter 2

## Background

### 2.1 Generic Monte Carlo Algorithms

Monte Carlo methods generally involve sampling from some “parent population”. The sampling process is usually facilitated by pseudo-random numbers generated via a numerical algorithm. The quantity or quantities sampled are then used as input to a subsequent (deterministic) calculation which results in the desired output. This process is repeated a number of times, so as to thoroughly sample the parent population, and a distribution of the output data is compiled. In some cases, only the mean of this distribution is of interest (as well as some estimate of its error), while in other cases, the distribution itself is the objective.

Note that the process being simulated need not be random. For example, Monte Carlo techniques may be the only way of computing the volume of some complex three-dimensional object. This is just one example of the versatility of Monte Carlo techniques. But, Monte Carlo is not always the most efficient solution for a problem because of the significant computational effort required. Two reasons for using Monte Carlo are:

1. No other solution is available.
2. The details of the problem are sufficiently important that no approximations can be tolerated.

In the case of particle transport, the latter reason is usually invoked. Examples of Monte Carlo particle transport include:

1. Neutron transport in fission devices,

2. Radiation transport,
3. Electron transport in semiconductors,
4. Neutral particle transport in plasmas.

### 2.1.1 Sampling a Distribution

The most fundamental process of a Monte Carlo simulation is the sampling of probability distributions. Typical examples for a particle simulations would be:

1. Choosing a velocity vector from a Maxwellian distribution,
2. Picking a particle from a spatially varying source,
3. Determining the distance to the next collision.

### 2.1.2 Sampling Distance to Next Collision

To illustrate the third case, consider particles with a total, macroscopic cross section  $\Sigma_t$ . We write the *probability density function* for having the next collision between  $x$  and  $x + dx$ ,  $p(x) dx$ , as:

$$p(x)dx = \Sigma_t \exp(-\Sigma_t x) dx. \quad (2.1)$$

Then, the *cumulative probability distribution*  $P(y)$ ,

$$P(y) = \int_0^y p(x) dx, \quad (2.2)$$

is the probability of having a collision for any  $x \leq y$ . Note that  $P(0) = 0$  and  $P(\infty) = 1$ .

As suggested by the above figure,  $P(y)$  can be sampled by choosing a uniformly distributed random number  $\xi$ , with  $0 \leq \xi < 1$ . For this example,  $P(y)$  is easily computed and inverted so that

$$y = -\frac{\ln \xi}{\Sigma_t}, \quad (2.3)$$

where we have surreptitiously replaced  $1 - \xi$  with  $\xi$  since both are uniform over the unit interval. Again the logic of this process, as depicted in the figure, is that if  $\xi$  is uniformly distributed, then numbers between  $\xi$  to  $\xi + \Delta\xi$  are chosen with the same frequency as particles having collisions between  $y$  and  $y + \Delta y$ . Thus,  $y$  is the sampled *distance to next collision*.

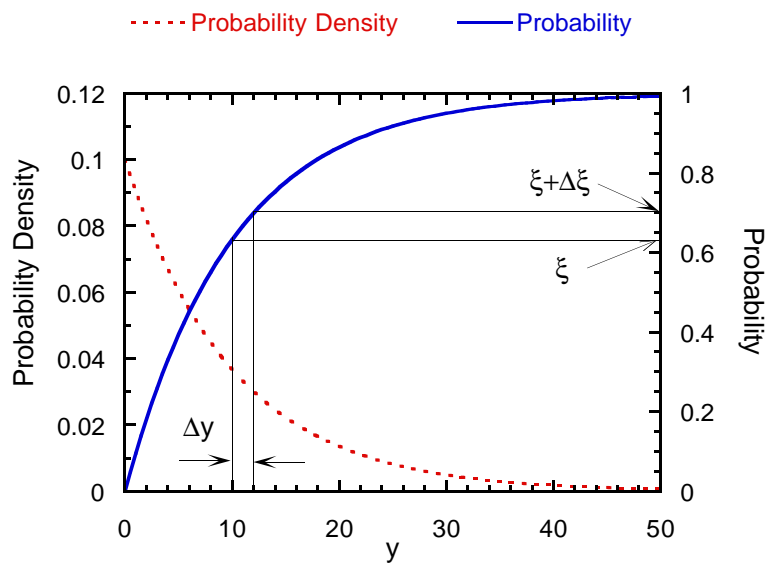


Figure 2.1: A uniformly sampled  $\xi$  value is translated into a sample of  $y$  distributed according to the “Probability Density” curve using the integrated “Probability” curve.

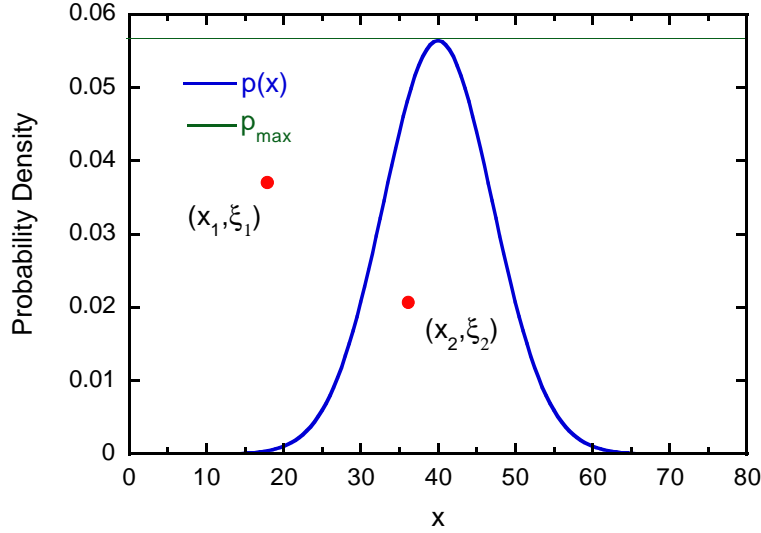


Figure 2.2: Values of  $x$  distributed according to  $p(x)$  can be sampled by uniformly selecting  $(x, \xi)$  pairs and tossing out ones with  $\xi > p(x)$ .

### 2.1.3 Sampling More Complicated Distributions

Because of the simplicity of the functional form of the collision probability density function, the distance to the next collision can be easily sampled using a single, uniform random number. If this were not the case, more general methods, such as this *rejection technique*, would have to be employed.

As an example, consider the sampling of a velocity  $v$  from a Maxwellian distribution,

$$p(v) = \frac{1}{\sqrt{\pi}v_{\text{th}}} \exp \left[ -\frac{(v - v_0)^2}{v_{\text{th}}^2} \right]. \quad (2.4)$$

For simplicity, limit the  $v$  values to  $|v - v_0| < Mv_{\text{th}}$  for some appropriate  $M$ .

Now, we choose a pair of random numbers  $(x, \xi)$  with  $x$  uniformly distributed over the interval  $v_0 - Mv_{\text{th}} \leq x < v_0 + Mv_{\text{th}}$  and  $\xi$  uniform over  $0 \leq \xi < p_{\text{max}}$ , where  $p_{\text{max}}$  is the maximum value of  $p(v)$ . If  $\xi < p(x)$ , accept this  $x$  as the sampled velocity. Otherwise, if  $\xi > p(x)$ , reject these  $(x, \xi)$  and sample another pair. That the resulting set of  $x$  values is distributed as required can be seen by studying the figure above. This figure also makes the case that the rejection approach may not be very efficient for sampling a Maxwellian (indeed, DEGAS 2 uses the well-known Box-Mueller method for this task).

In general, a rejection technique factors the probability density  $p(x)$  into two functions,  $p(x) = g(x)h(x)$ , where it is known how to sample  $x$  from the function  $g(x)$ . The acceptance condition is just  $\xi < h(x)$ . The Maxwellian example simply sets  $g(x) = 1$ .

## 2.2 Particle Transport

One of the main benefits of doing Monte Carlo particle transport is that most of the time the algorithm can be understood directly from a physical picture. Namely, we think of the code as tracking particles through a medium and having collisions with probabilities determined from the cross sections of the various collision processes. The outcome of those collisions is the same as for the actual physical particles, and so on. This is known as the *analog* description of Monte Carlo particle transport.

In this section, we want to give a rough idea of how this picture relates to the integral equations which provide the actual mathematical basis for Monte Carlo techniques. Only from these equations can we understand the *non-analog* techniques (the rejection technique described in the previous subsection is a non-analog technique) used to make the Monte Carlo process more efficient. We hope to familiarize the reader with the integral equations to the point where more detailed references[2, 10] can be readily digested.

From an analog point-of-view, we imagine a Monte Carlo particle simulation as consisting of four parts:

1. A way to sample an initial particle distribution,
2. A way to treat particles from one point in space to another,
3. Tools to treat “interesting things” that might happen along the way,
4. Some useful quantities to compute and record at each stage of the process.

The last of these, referring to “scores” and their “estimators” will be addressed in Sec. 2.3.

### 2.2.1 Motivating the Integral Equation

The initial particle distribution, or source, is given by a probability density function  $Q(x) > 0$ . We take  $x$  here to represent a point in phase space so that this function provides both the velocity and spatial distribution of the source.

The tracking of particles is described in the integral equation by a function  $L(y \rightarrow x)$  which gives the probability that a particle starting at a point  $y$  in phase space ends up at point  $x$ . This function includes the “interesting things” (collisions) that might happen along the way, as we will describe in the next subsection.

Using these two functions, we can write the *density of particles arriving at  $x$* ,  $\chi(x)$  as the sum of two pieces:

1. Arrivals directly from source:  $Q(x)$ .
2. Particles transported from elsewhere:

$$\int \chi(y)L(y \rightarrow x) dy \quad (2.5)$$

And we have

$$\chi(x) = Q(x) + \int \chi(y)L(y \rightarrow x) dy. \quad (2.6)$$

## 2.2.2 Transport and Collision Kernels

In order to describe the kernel  $L(y \rightarrow x)$  in more detail, substitute for  $y$  and  $x$  the phase space variables  $(\vec{r}, \vec{v})$  and a species index  $i$ . The kernel  $L$  can then be broken into two pieces:

$$L(\vec{r}', \vec{v}', i' \rightarrow \vec{r}, \vec{v}, i) = T(\vec{r}' \rightarrow \vec{r}; \vec{v}, i)C(\vec{v}', i' \rightarrow \vec{v}, i; \vec{r}), \quad (2.7)$$

where  $T(\vec{r}' \rightarrow \vec{r}; \vec{v}, i)$  is the (probability) density of particles leaving a collision at  $\vec{r}'$  and having a subsequent collision at  $\vec{r}$ . The “;” is used in the arguments of  $T$  and  $C$  to separate changing parameters (on the left) from those held fixed (on the right). Basically, sampling from  $T$  is as described in Section 2.1.2.

Collisions are described by  $C(\vec{v}', i' \rightarrow \vec{v}, i; \vec{r})$  which provides the probability that a particle of velocity  $\vec{v}'$ , species  $i'$  will have a collision resulting in a particle of velocity  $\vec{v}$ , species  $i$ . In practice,  $C$  is a sum over the physical reactions in which species  $i'$  participates.

## 2.2.3 Integral Equation Details

One of the problems with reading Monte Carlo particle references is that there are several slightly different “quantities of interest” equivalent to  $\chi(x)$ . Furthermore, there is no well-established notation for those quantities. In this subsection, we

attempt to list these various quantities and to provide a detailed form of an integral equation for later reference.

The quantity  $\chi(x)$  is called the *post-collision density*. The origin of this designation should be clear from the previous discussion. Equivalently, the integral equation can be written in terms of the *pre-collision density*  $\psi(x)$ . The two are related by

$$\psi(\vec{r}, \vec{v}, i) = \int d^3r' \chi(\vec{r}', \vec{v}, i) T(\vec{r}' \rightarrow \vec{r}; \vec{v}, i). \quad (2.8)$$

It is this pre-collision density which is most closely related to the more familiar particle flux  $\Phi$  and particle distribution function  $f$  by the definitions:

$$\psi(\vec{r}, \vec{v}, i) = \Sigma_t(\vec{r}, \vec{v}, i) \Phi(\vec{r}, \vec{v}, i) = \Sigma_t(\vec{r}, \vec{v}, i) |\vec{v}| f(\vec{r}, \vec{v}, i). \quad (2.9)$$

The integral equation for  $\psi$  bears a strong resemblance to that for  $\chi$ . We write it out here in detail to illustrate the details as well as to provide a reference point for the rest of the document and other reading:

$$\begin{aligned} \psi(\vec{r}, \vec{v}, i) &= S(\vec{r}, \vec{v}, i) \\ &+ \int_0^\infty dR \int d^3v C(\vec{v}', i' \rightarrow \vec{v}, i; \vec{r} - \vec{\Omega}R) \\ &\times T(\vec{r} - \vec{\Omega}R \rightarrow \vec{r}; \vec{v}, i) \psi(\vec{r} - \vec{\Omega}R, \vec{v}', i'), \end{aligned} \quad (2.10)$$

where

$$S(\vec{r}, \vec{v}, i) = \int_0^\infty dR Q(\vec{r} - \vec{\Omega}R, \vec{v}, i) T(\vec{r} - \vec{\Omega}R \rightarrow \vec{r}; \vec{v}, i), \quad (2.11)$$

and

$$T(\vec{r} - \vec{\Omega}R \rightarrow \vec{r}; \vec{v}, i) = \Sigma_t(\vec{r}, \vec{v}, i) \exp \left[ - \int_0^R dR' \Sigma_t(\vec{r} - \vec{\Omega}R', \vec{v}, i) \right]. \quad (2.12)$$

The actual form of the collision kernel  $C$  need not be written down here. Instead, in this document we'll only talk about it's implementation from an analog point of view. The only additional piece of information about it that we could add to the above equations is that  $C$  consists of a sum over the relevant collision processes involving species  $i'$ .

The approach of writing the path integrals as above instead of as general phase-space volume integrals with the path enforced via delta-functions[10] was copied from Case and Zweifel[11] We find that this leads to expressions which are easier to work with and think about.

## 2.3 Estimators

The objective of the Monte Carlo calculation is to evaluate integrals over the distribution function:

$$I(g) \equiv \int d^3r d^3v f(\vec{r}, \vec{v}) g(\vec{r}, \vec{v}). \quad (2.13)$$

For example, if we wish to estimate a reaction rate  $\rho \equiv \Sigma|\vec{v}|$ ,

$$I(\rho) = \int d^3r d^3v \Sigma \Phi(\vec{r}, \vec{v}). \quad (2.14)$$

Values of  $\rho$  are accumulated along the random walk of the neutral flight and used to estimate  $I(\rho)$ . The mathematical description of this accumulation process is called the *estimator* of  $I$ .

### 2.3.1 Simple Estimators

Consider a random walk  $\gamma$  which consists of  $k$  steps,  $(x_1, x_2, \dots, x_k)$ . I.e., the particle is absorbed or otherwise terminated at the  $k$ th step. The simplest estimator involves writing down the value of  $\rho$  at the point of absorption. Thus, the absorption estimator is

$$\xi_a(\gamma) = \frac{\rho}{\rho_a} w \chi_V, \quad (2.15)$$

where  $\rho_a$  is the absorption rate in the volume of interest  $V$  and  $w$  is the statistical weight of the particle (constant for this random walk process). The function  $\chi_V$

$$\chi_V(x_m) = \begin{cases} 1 & \text{if } x_m \in V \\ 0 & \text{if } x_m \notin V \end{cases}, \quad (2.16)$$

just permits the score to be localized to the volume of interest.

The expectation value of the estimator is just the sum over all possible random walks  $\gamma$  of the probability of each walk  $P(\gamma)$  times the corresponding estimator,

$$E(\xi_a) = \sum_{\gamma} P(\gamma) \xi_a(\gamma). \quad (2.17)$$

Obviously, only one data point is collected for each random walk.

We can instead accumulate a score at each step (scattering collision) of the random walk.

$$\xi_{c1}(\gamma) = \sum_{m=1}^k \left[ \frac{\rho_a(x_m)}{\rho_t(x_m)} \right] w \chi_V(x_m), \quad (2.18)$$

where  $\rho_t = \rho_a + \rho_s$  is the total reaction rate for the particle, with  $\rho_s$  being the scattering rate. The subscript  $c1$  denotes the first collision estimator described here. The expectation value of the estimator is again formally written as

$$E(\xi_{c1}) = \sum_{\gamma} P(\gamma) \xi_{c1}(\gamma). \quad (2.19)$$

Because of the greater amount of data accumulated along each particle track, the variance of this estimator will usually be smaller than that of the absorption estimator.

Consider now a random walk process in which absorption is forbidden. This is our first departure from the usual analog processes. Instead of an absorption, the weight of the particle is reduced at each scattering collision by its survival probability. So, at the  $m$ th step of the walk the weight of the particle is

$$w_m = w \prod_{j=1}^m \frac{\rho_s(x_j)}{\rho_t(x_j)}. \quad (2.20)$$

The flight must be terminated in some manner; the usual practice is to have it undergo Russian roulette[2] when  $w_m < w_{\min}$ , where  $w_{\min}$  is some specified minimum weight. The collision estimator for this nonanalog random walk process is then

$$\xi_{c2}(\gamma) = \sum_{m=1}^k w_m \left[ \frac{\rho_a(x_m)}{\rho_t(x_m)} \right] \chi_V(x_m). \quad (2.21)$$

For formal proofs that these expectation values do indeed yield  $I(\rho)$ , see Spanier and Gelbard[2].

### 2.3.2 Generalized Collision and Tracklength Estimators

Two principal estimators are used in DEGAS 2. One is a generalization of the collision estimator described in the previous subsection; the other is the tracklength estimator.

These estimators can be obtained by making a slight modification of the derivation given by Macmillan[45] (who had improved upon an earlier approach described by Spanier[46]). To make the connection to DEGAS 2 clearer, we replace the  $\Sigma$  and  $d$  variables of Macmillan with  $\rho$  and  $t$ .

Macmillan's paper, like the earlier one by Spanier, aims to derive the tracklength estimator. Collisions are described as either scatterings, rate  $\rho_s$ , or absorptions  $\rho_a$ . The starting point is the nonanalog random walk process described

in Sec. 2.3.1. The probability of an event occurring in a time interval  $dt$  is  $(\rho_s + \rho_a) dt$ . Again, the weight reduction factor applied at each scattering is  $\rho_s/(\rho_s + \rho_a)$ .

The trick used by Spanier is to introduce a fictitious “delta scattering” that has no impact on the particle’s trajectory or weight. These “pseudocollisions” are not unrelated to those of the original DEGAS code[3]. Additional flexibility in the final results is obtained by associating some fraction of the absorptions  $\alpha$  with the delta scatterings. To obtain the estimators used in DEGAS 2, we work with a total fictitious scattering reaction rate

$$\rho_{t,\delta} \equiv \rho_{s,\delta} + \alpha\rho_a, \quad (2.22)$$

where  $\rho_{s,\delta}$  is equivalent to Macmillan’s  $\Sigma_{s,\delta}$ . Then, the probability of a delta scattering in a time interval  $dt$  is  $\rho_{t,\delta} dt$ . At each delta scattering, the weight is reduced by a factor  $(\rho_{t,\delta} - \alpha\rho_a)/\rho_{t,\delta}$ . The probability of a real scattering in the same interval is  $(\rho_s + (1 - \alpha)\rho_a) dt$ ; at each such event, the weight is reduced by  $\rho_s/[\rho_s + (1 - \alpha)\rho_a]$ .

If a particle travels a time  $t$  in a region of constant parameters before having a real collision, the conditional probability of having  $n$  pseudocollisions is

$$P(n | d) = \frac{(\rho_{t,\delta}t)^n}{n!} \exp(-\rho_{t,\delta}d). \quad (2.23)$$

At each pseudo or real collision, we use the standard collision estimator for the nonanalog random walk, taken from Eq. (2.21):

$$\xi = \frac{\rho}{\rho_t^*} w, \quad (2.24)$$

where  $w$  is the current weight of the particle and

$$\rho_t^* = \rho_{t,\delta} + \rho_s + (1 - \alpha)\rho_a \quad (2.25)$$

is the overall total reaction rate.

The expected value of this estimator over the  $n$  collisions in the region is then

$$E(\xi | t) = \sum_{n=0}^{\infty} P(n | t) \frac{\rho}{\rho_t^*} \sum_{i=0}^n \left( \frac{\rho_{t,\delta} - \alpha\rho_a}{\rho_{t,\delta}} \right)^i, \quad (2.26)$$

where we have assumed that the initial weight of the particle is 1. The last factor represents the subsequent weight reductions with each pseudocollision.

Following Macmillan's evaluation of  $E(\xi | t)$ , we find that we can write

$$E(\xi | t) = c' \frac{\rho}{\rho_s + (1 - \alpha)\rho_a} + (1 - c')\rho \frac{1 - \exp(-\alpha\rho_a t)}{\alpha\rho_a}, \quad (2.27)$$

where

$$c' \equiv \frac{\rho_s + (1 - \alpha)\rho_a}{\rho_{t,\delta} + \rho_s + (1 - \alpha)\rho_a} \quad (2.28)$$

should be compared with Macmillan's  $c$ .

Macmillan's expression for the weight reduction after time  $t$  is exactly the same in our case:

$$E(w | t) = \exp(-\alpha\rho_a t) \frac{\rho_s}{\rho_s + (1 - \alpha)\rho_a}. \quad (2.29)$$

The factor at the end represents the weight reduction by the real collision at time  $t$ . If the particle travels a time  $t$  through the region without having a real collision, its weight should be reduced by just  $\exp(-\alpha\rho_a t)$ .

In this latter situation in which there is not a real collision at time  $t$ , only the pseudocollisions contribute to the score. An interesting difference from MacMillan's approach is that if we consider the limit  $\rho_{t,\delta} \rightarrow 0$ , we should get no score at all. In contrast, MacMillan's pure "collision estimator" still compiles a nonzero score as  $\Sigma_{s,\delta} \rightarrow 0$  through the  $\alpha\Sigma_a$  contribution to the pseudocollision cross section. Thus, MacMillan's "collision estimator" behaves somewhat like a track-length estimator if there are no collisions in a region. For simple scores, this behavior is desirable: lower variances will result in regions of small cross section. However, a few scores are sufficiently complex that averaging along the particle path cannot be done, and scoring can only be done at collisions. A pure collision estimator is required for handling such scores.

In the case of no real collision at time  $t$ , the expectation value for our estimator becomes:

$$E(\xi | t) = \frac{\rho}{\rho_t^*} \rho_{t,\delta} \frac{1 - \exp(-\alpha\rho_a t)}{\alpha\rho_a}. \quad (2.30)$$

Clearly,  $E(\xi | t) \rightarrow 0$  as  $\rho_{t,\delta} \rightarrow 0$ . The limiting expressions above for  $\rho_{t,\delta} \rightarrow 0$  can be obtained from MacMillan's with  $\Sigma_{s,\delta} \rightarrow -\alpha\Sigma_a$ .

We now consider the expressions used in DEGAS 2. We start by using  $\alpha = 1$  so that absorptions occur only at the delta scatterings. This is consistent with our use of the nonanalog random walk, i.e., suppressed absorption. The collision estimator is then given by  $\rho_{t,\delta} = 0$ ,

$$\xi_c \equiv \frac{\rho}{\rho_s} \exp(-\rho_a t) w \chi_V, \quad (2.31)$$

where  $w$  is the weight of the particle at the beginning of timestep  $t$  and we have inserted the characteristic function of  $V$   $\chi_V$  for completeness. At the end of the timestep (after the collision is scored) the weight is reduced by

$$w' = w \exp(-\rho_a t). \quad (2.32)$$

The particle track continues from there, and multiple scores may be made inside the volume  $V$ . If the flight travels through the volume  $V$  without a collision, no contribution to the score is made. However, the weight is still reduced by the factor in Eq. (2.32).

The track-length estimator is obtained with  $\rho_{t,\delta} \rightarrow \infty$ ,

$$\xi_t \equiv \rho \frac{1 - \exp(-\rho_a t)}{\rho_a} w \chi_V. \quad (2.33)$$

Note that Eq. (2.30) yields this same result in the case of no collisions. The same weight reduction, Eq. (2.32) is applied at the end of  $t$ . Conveniently, this allows us to use the same weight factor for both estimators (true in MacMillan's case as well).

Molecules and some other species are not treated with suppressed absorption. Instead, an ionizing collision terminates the flight (typically changing the species). The estimators for this case are obtained by setting  $\alpha = 0$  in the above expressions:

$$\xi_c \equiv \frac{\rho}{\rho_s + \rho_a} w \chi_V, \quad (2.34)$$

and

$$\xi_t \equiv \rho t w \chi_V. \quad (2.35)$$

There is no weight reduction in this case, and  $w$  retains its initial value for the duration of the flight.

### 2.3.3 Specification of Tallies

This section briefly covers the practical implementation of the estimators described in the previous subsection. DEGAS 2 currently features three primary types of estimators. These estimators are used in accumulating three types of tallies. The tally types are

1. test,
2. reaction,

3. sector.

These designations can also be viewed as characterizing the nature of the information contained in the function  $g$  of Eq. (2.13). The following discussion of the three estimators applies to the first two of these; there is only one estimator for the sector tallies.

The first estimator, associated with the accumulating test particle information, is just the track length estimator (see also Sec. 2.3.2),

$$\xi_g^{\text{TLE}} = w \frac{1 - \exp(-\sigma_i t_V)}{\sigma_i} g, \quad (2.36)$$

where  $t_V$  is the time the particle track spent in volume  $V$ ,  $w$  = weight at start of the time step. Compare this with Eq. (2.33). The function  $g$  can be a test particle attribute, such as mass, momentum, energy, or reaction-related, e.g., ion momentum source due to charge exchange. The latter  $g$  quantity enter the track-length estimator as averages over the background distribution[14].

The second type of estimator is the collision estimator,

$$\xi_g^{\text{CE}} = \sum_{m_s} w_{m_s} \frac{g}{\sigma_s}, \quad (2.37)$$

where the sum is over  $m_s$ , all scattering collisions within  $V$ . The quantity  $w_{m_s}$  is the weight at  $m_s$ th collision (by using the instantaneous weight rather than the initial weight, the exponential weight reduction factor that appears explicitly in Eq. (2.31) is incorporated automatically). Again,  $g$  is a test particle attribute.

There is an analogous expression for the collision estimator associated with a particular reaction,

$$\xi_g^{\text{CE}} = \sum_{m_j} w_{m_j} \frac{g}{\sigma_j}, \quad (2.38)$$

where the sum is now over  $m_j$  collisions of reaction  $j$  within  $V$ , The function  $g$  is some quantity related to the reaction and is likely something known only at collisions. One example of such a quantity would be the energy source due to  $\text{H}_2$  dissociation (i.e., the energy exchange is determined only once the product velocities have been determined).

The third type of estimator arises from the observation that many integrals of interest can be written as:

$$I(g) \equiv \int d^3r g(\vec{r}) \int d^3v f(\vec{r}, \vec{v}) = \int d^3r g(\vec{r}) n(\vec{r}). \quad (2.39)$$

This leads to the post-processing estimator. The requirement is that  $g$  not depend upon the test or background velocities. An example of this is the  $H_\alpha$  emission rate.

Information accumulated when a flight crosses a diagnostic sector (surface) is compiled in the sector tallies. The estimator is just  $wg$ , where  $w$  is the weight when the track hits the sector. Examples of the  $g$  functions include mass, incident angle, and energy. This is effectively a collision estimator.

There is also a “null” or “none” estimator that can be used, say, to eliminate the contribution of a particular reaction to a tally without having to remove that reaction from the problem.

For each tally, we need to specify

1. A descriptive label,
2. The type of tally (test, reaction, or sector),
3. Its geometry, [volume (per zone), surface (diagnostic sector), or detector (e.g., chord-integrated)],
4. The dependent variable (e.g., energy, background momentum,  $H_\alpha$  emission rate). The requested variables are matched directly against the labels in the atomic physics data files. If a new reaction and data file containing a new variable are added to the code, that variable can be used as the basis for a corresponding tally without having to modify the code.
5. The rank (or dimensionality) of the tally,
6. Its independent variables ( $1 \rightarrow$  rank) [e.g., zone, test particle species, energy bin (diagnostic sector), wavelength bin (detector)].
7. The estimator to be used (track-length, collision, post-processed, or null). For reaction tallies, the estimator chosen can vary with reaction. It may be advantageous to combine results from than one estimator, but no effort to implement such a capability has been made yet.
8. Any conversions that must be performed on the tally prior to output. Usually, these conversion will do some sort of scaling, e.g., by mass or volume. An important example is converting  $\vec{v}$  from Cartesian to cylindrical coordinates when scoring.

## 2.4 Tracking Procedure

The two previous subsections are tied together with an outline of the DEGAS 2 subroutine for following flights in Fig. 2.3.

The flight is initiated as it is sampled from the spatial and velocity distribution of a source. Conceptually, this step amounts to specifying  $\chi_0(\vec{r}', \vec{v}', i)$  using the source term  $Q(\vec{r}', \vec{v}')$ . The subscript 0 denotes the initial track for the flight.

The next stage of the algorithm involves computing the reaction rates  $\rho_s, \rho_a$ , etc. for the flight. Continuing flights which require a recomputation (due to crossing from one plasma region to another or to a change in species or velocity) repeat the main loop starting at this same point. The post-collision density  $\chi_n$  in Fig. 2.3 is intended to refer to them.

The time to the next collision is randomly sampled (Sec. 2.1.2) from the sum of the non-absorbing reaction rates using a random number  $\zeta$ .

The weight  $w$  is compared with some minimum weight to guarantee that the flight terminates at some point. The “End flight” process indicated in Fig. 2.3 actually represents a Russian Roulette procedure[2] which may allow the flight to live a little longer.

The transport kernel  $T$  translates the flight from position  $\vec{r}''$  to  $\vec{r}'$ . At the same time, this step represents the conceptual transition from post-collision density to pre-collision density  $\psi$ , Eq. (2.8). The tracking algorithm stops when  $t = t_{\max}$ , the flight crosses a zone boundary (denoting a change in plasma parameters), or a “sector” (a material or diagnostic surface; these will be discussed later in this document) is reached. If a zone boundary is crossed, the flight continues as is, although the rates must be recomputed. Processing a sector may result in the continuation or the termination of the flight, depending on the type of sector. Again, the details have been omitted for simplicity.

If the flight reaches  $t = t_{\max}$ , the implication is that it has had a collision. A particular collision is randomly chosen from amongst those possible for this particular flight. At this point, precollision scores are recorded and the collision itself is processed. Conceptually, this represents the transition via the operator  $C$  from  $\psi_{n+1}$  to  $\chi_{n+1}$ . If the reaction chosen results in no particles to track (e.g., in no neutral species; particles which DEGAS 2 has been instructed to track are called “test” particles), the flight is terminated. Test particles resulting from the collision are tracked in the same manner, starting with the computation of the reaction rates.

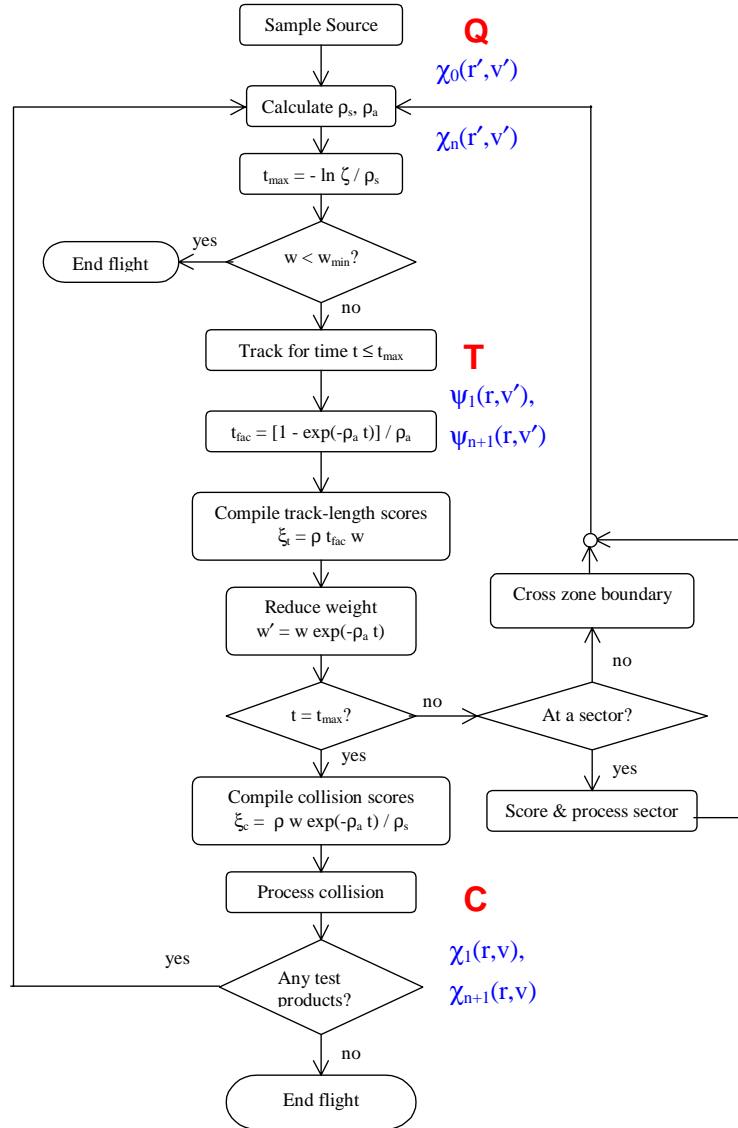


Figure 2.3: Flow chart of DEGAS 2 subroutine `follow`, showing the steps involved in tracking a flight from its birth to its termination. Note the weight reduction, and collision and tracklength estimators (Sec. 2.3). The operators from the integral equations are shown along with the pre- and post-collision densities. These labels tie the practical algorithmic operations to the equations in Sec. 2.2.3. Some details have been omitted for clarity.

## 2.5 Random Numbers

The concepts behind the random number generator used in DEGAS 2 are described in the file `random.web`. The documentation at the top of the file provides a nice introduction.

## 2.6 Geometry

The introduction to `geometry.web` provides a concise description of the fundamental elements of the DEGAS 2 geometry. Here's a link to the PDF version of this file. Note that most users will define geometries at a higher level, such as that provided by `readgeometry` and `boxgen`.

## 2.7 Atomic Physics

The interaction of electrons with hydrogen atoms and ions in a divertor plasma is complicated by having comparable collision and radiative decay times. The techniques for treating such systems were first described by Bates and McWhirter[5, 6]. The physical processes included in such a collisional-radiative model are:

1. Electron collisional excitation  $K_{e,mn}$  and de-excitation  $K_{d,mn}$ ,
2. Spontaneous radiative transitions  $A_{mn}$ ,
3. Electron collisional ionization  $K_{i,mn}$ ,
4. Three-body recombination  $K_{r,mn}$ ,
5. Radiative recombination  $\beta_m$ ,

where  $m$  and  $n$  are principal quantum numbers. For the two state terms, the initial state is the *second* number; the final is the *first*. This apparently backward notation allegedly has a mathematical origin.

A set of  $m$  equations describes the balance between these processes that determines the density of the  $m$ -th excited state of the atom,  $N_m$ ,

$$\frac{dN_m}{dt} = -N_m \left[ n_e \left( K_{i,m} + \sum_{n>m} K_{e,nm} + \sum_{n<m} K_{d,nm} \right) \right]$$

$$\begin{aligned}
& \left. + \sum_{n < m} A_{nm} \right] \\
& + n_e \left( \sum_{n > m} N_n K_{d,mn} + \sum_{n < m} N_n K_{e,mn} \right) \\
& + \sum_{n > m} N_n A_{mn} + n_e n_i (\beta_m + n_e K_{r,m}), \tag{2.40}
\end{aligned}$$

where  $n_e$  is the electron density and  $n_i$  is the density of ions corresponding to the atom under consideration ( $m \rightarrow \infty$ , effectively).

The basic assumption of the collisional-radiative model[5, 6] is that states above ground state will decay much more rapidly than the ground state will change. The evolution of the ground state is considered to be comparable to the transport time scales. This physical process is the one considered by the neutral transport code. In other words, the  $m = 1$  equation will essentially be solved by DEGAS 2 and  $N_1$  can be treated as an externally known quantity. The relatively rapid equilibration of the excited states permits the time derivatives of their densities to be set to zero. The set of equations for  $m > 1$  can then be solved,

$$N_m = \left( \frac{N_m^{(i)}}{N_1} \right) N_1 + \left( \frac{N_m^{(ii)}}{n_i} \right) n_i. \tag{2.41}$$

In practice, the solution of these equations involves:

1. Obtaining the various reaction rates,  $K_{e,mn}$ ,  $K_{d,mn}$ ,  $A_{mn}$ ,  $K_{i,mn}$ ,  $K_{r,mn}$ ,  $\beta_m$ , as a function of  $n_e$  and  $T_e$ ,
2. Solving the  $m > 1$  equations for each  $n_e$ ,  $T_e$  pair with  $N_1 = 1$  and  $n_i = 0$ , providing the ‘‘coupling to the ground state’’,
3. Solving the equations again with  $N_1 = 0$  and  $n_i = 1$ , yielding the ‘‘coupling to the continuum’’.

Tables of  $N_m^{(i)}/N_1$  and  $N_m^{(ii)}/n_i$  are thus obtained as a function of  $n_e$  and  $T_e$ .

With Eq. (2.41), the  $m = 1$  equation can become

$$\frac{dN_1}{dt} = -N_1 n_e S_{eff} + n_e n_i R_{eff} + \text{transport, etc.}, \tag{2.42}$$

with

$$S_{eff} = \sum_{m \geq 1} \left( \frac{N_m^{(i)}}{N_1} \right) K_{i,m}, \tag{2.43}$$

and

$$R_{eff} = - \sum_{m \geq 2} \left( \frac{N_m^{(ii)}}{n_i} \right) K_{i,m} + \sum_{m \geq 1} (\beta_m + n_e K_{r,m}). \quad (2.44)$$

$S_{eff}$  is thus the effective ionization rate of the ground state neutral, incorporating the multi-step processes associated with all of the excited states. Likewise,  $R_{eff}$  is the effective recombination rate. Both are functions of  $n_e$  and  $T_e$  and are tabulated along with selected values of the  $N_m^{(i)}/N_1$  and  $N_m^{(ii)}/n_i$  for use in DEGAS 2.

Excited state densities, e.g., for  $n = 3$ , are found with

$$N_3 = \left( \frac{N_3^{(i)}}{N_1} \right) N_1 + \left( \frac{N_3^{(ii)}}{n_i} \right) n_i. \quad (2.45)$$

Thus, the  $H_\alpha$  emission rate is given by  $N_3 A_{23} = 4.41 \times 10^7 N_3 \text{ cm}^{-3} \text{ s}^{-1}$ .

### 2.7.1 Electron Energy Exchange Rate

The expression used in `collrad` for the electron energy exchange is

$$\begin{aligned} \frac{dE_e}{dt} = & \text{Ry} (-N_1 n_e S_{eff} + n_e n_i R_{eff}) \\ & - \text{Ry} \sum_{\substack{m,n \\ n < m}} N_m A_{nm} \left( \frac{1}{n^2} - \frac{1}{m^2} \right) \\ & - n_e n_i \sum_{m \geq 1} \beta_m \left( \langle E_{rad,m} \rangle + \frac{\text{Ry}}{m^2} \right), \end{aligned} \quad (2.46)$$

where

- $\text{Ry} = 13.6 \text{ eV}$  (one Rydberg),
- the first term is the loss due to ionization,
- the second is the gain due to recombination.
- The sums represent lost photons from radiative transitions and radiative recombination,
- $\langle E_{rad,m} \rangle$  is the average energy of a recombining electron.

For the last item, we use the expression given by Reiter[14],

$$\langle E_{rad,m} \rangle = T_e \left[ \frac{3}{2} + \frac{T_e}{\beta_m} \frac{d\beta_m}{dT_e} \right]. \quad (2.47)$$

Using Eq. (2.41), Eq. (2.46) becomes

$$\frac{dE_e}{dt} = -Ry (N_1 n_e S_{eff} - n_e n_i R_{eff}) - N_1 E_{loss}^{(i)} - n_i E_{loss}^{(ii)}, \quad (2.48)$$

where the terms  $E_{loss}^{(i)}$ ,  $E_{loss}^{(ii)}$  represent the loss rates due to coupling to the ground state and continuum, respectively. Both are provided as tables as functions of  $n_e$  and  $T_e$  for use in DEGAS 2.

## 2.7.2 Solutions Used with DEGAS 2

The code we use to solve these equations, `collrad`, is based on the one described by Weisheit[17]. Rather than using Eq. (2.41), the original code used the assumption that ionization and recombination were in balance to determine the neutral density in terms of the ion density. The other change made to Weisheit's version of the code is that the cross section data have been updated as prescribed in the Janev-Smith database[15]. The resulting collisional-radiative data are believed to be in good agreement with ADAS. Although the `collrad` code is not itself distributed with DEGAS 2, it can be obtained from the DEGAS 2 authors (see Sec. 6.1).

The output data from `collrad` are contained in the file `ehr2.dat`. Earlier versions of this same file, `eh.dat` (as generated by Weisheit's original code) and `ehr1.dat` [generated with Weisheit's code modified to use Eq. (2.41)] are also included in the DEGAS 2 distribution since they were both used extensively with the original DEGAS code.

The `ehr2.dat` file contains

1. Ionization rate  $S_{eff}$  in  $\text{cm}^3 \text{s}^{-1}$ ,
2. Recombination rate  $R_{eff}$  in  $\text{cm}^3 \text{s}^{-1}$ ,
3. Neutral electron losses  $E_{loss}^{(i)}$  in  $\text{erg s}^{-1}$ ,
4. Continuum electron losses  $E_{loss}^{(ii)}$  in  $\text{erg s}^{-1}$ ,

5. Neutral “n=3 / n=1”,  $N_3^{(i)}/N_1$ ,
6. Continuum “n=3 / n=1”,  $N_3^{(ii)}/n_i$ ,
7. Neutral “n=2 / n=1”,  $N_2^{(i)}/N_1$ ,
8. Continuum “n=2 / n=1”,  $N_2^{(ii)}/n_i$ .

The portion of the file for each quantity consists of 15 separate sections (labeled by jn), corresponding to the various electron density values,

$$n_e(\text{jn}) = 10^{10+(\text{jn}-1)/2} \text{ cm}^{-3}. \quad (2.49)$$

Each section consists of 60 data values, one for each  $T_e(\text{j\tau})$ ,

$$T_e(\text{j\tau}) = 10^{-1.2+(\text{j\tau}-1)/10} \text{ eV}. \quad (2.50)$$

The index j\tau starts at 1 in the first column and row and proceeds row-by-row. There are 10 rows of 6 entries each.

## 2.8 Elastic Scattering

### 2.8.1 Neutral-Ion Elastic Scattering

*Note: this subsection was extracted from Ref. [18]. A few minor changes in notation have been made for consistency.* Only limited experimental data are available for ion-neutral elastic scattering at low energies. The monograph by Janev[13] is one of the most widely used data sources available, but only contains charge exchange at moderate to high collision energies and no data for elastic scattering. As divertor technology has progressed, low temperature operating environments have become a standard mode of operation. Under these conditions, both charge exchange and small-angle elastic scattering must be included in simulations. Below approximately 2 eV for  $D^+ + D$  collisions, separate treatment of small-angle elastic scattering and resonant charge exchange becomes impossible due to quantum mechanical effects. The need for a comprehensive treatment of ion-neutral elastic collisions at low energies motivated the Controlled Fusion Atomic Physics Data Center at ORNL to produce a collection of total differential elastic scattering cross sections for 31 various isotopic combinations of hydrogen atoms and molecules[19].

DEGAS 2 represents an improvement over the original DEGAS code in that the pseudo-collision algorithm originally employed in scoring results[3] is replaced with a track-length type estimator. This allows efficient determination of momentum and energy exchange with the background plasma over a wide range of background densities. The rate expressions used by the track-length estimator involve the momentum transfer (or diffusion) cross section,  $\sigma_d$ [20].

A general expression for the integral cross sections is[20]

$$\sigma_l = 2\pi \int_0^\pi (1 - \cos \theta)^l \sigma(\theta, E_r) \sin \theta d\theta, \quad (2.51)$$

where  $l = 0$  corresponds to the total elastic scattering cross section,  $l = 1$  to the diffusion cross section and  $l = 2$  to the viscosity cross section;  $\theta$  is the center-of-mass scattering angle,  $E_r$  is the relative energy of the collision, and  $\sigma(\theta, E_r)$  is the differential elastic scattering cross section. The total elastic collision cross section,  $\sigma_t$ , is used in Monte Carlo simulations to determine the time between elastic collisions. In this manner the size of the total elastic collision cross section influences the execution time of numerical simulations.

A simulation technique that reduces the total collision cross section while keeping the momentum transfer cross section invariant can be developed. Using the expression for  $\sigma_d$  and dividing Eq. (2.51) into small and large angle components,

$$\sigma_d(E_r) = 2\pi \int_0^{\theta_{\min}} C(E_r)(1 - \cos \theta)\delta(\theta - \theta_{\min})d\theta + 2\pi \int_{\theta_{\min}}^\pi (1 - \cos \theta)\sigma(\theta, E_r)d\theta. \quad (2.52)$$

Substituting  $\sigma(\theta, E_r)$  from the ORNL data set here and directly computing  $\sigma_d(E_r)$  [via Eq. (2.51)], allows Eq. (2.52) to be solved for  $C(E_r)$  given a particular value of  $\theta_{\min}$ . The resulting value of  $C(E_r)$  is then used in a similar expression for the viscosity cross section. This provides viscosity cross sections accurate to second order in  $\theta_{\min}$ . The value of  $\theta_{\min}$  is chosen so as to reduce the total elastic cross section as much as possible while retaining physical realism.

For low energy elastic collisions a significant portion of the collisions involve small-angle deflections. Due to this behavior, the majority of the reduction in total elastic cross section is obtained with a five-degree minimum scattering angle (Fig. 2.4). Minimum scattering angles greater than five degrees result in little computational savings. The resulting reduction in  $\sigma_t$  is approximately a factor of two at relative energies  $E_r > 10^{-1}$  eV. The values for  $\sigma_d$  are unchanged during application of a small-angle cut-off.

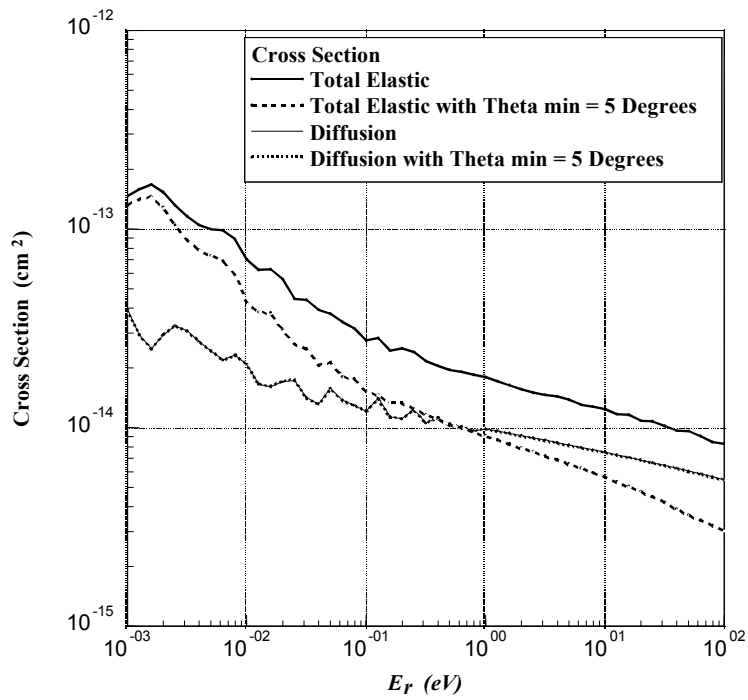


Figure 2.4: Comparison of total and diffusion cross sections for  $D^+ + D$  collisions with and without the small-angle cut-off approximation.

The use of this small-angle cut-off leads to an efficient algorithm for simulating the dynamics of elastic collisions in Monte Carlo simulations. Previous models based on classical collision kinetics for direct elastic scattering face difficulties in that the cross section is a rapidly varying function of the impact parameter[20]. This precludes the use of efficient table-look-up methods and forces a time consuming evaluation of the collision integral for each individual interaction.

Utilization of the differential elastic cross section,  $\sigma(\theta, E_r)$ , allows development of a table-look-up interpolation for both direct elastic scattering and resonant charge exchange. Following the work by Abou-Gabal and Emmert[21], we divide the total elastic cross section into  $n$  pieces and interpret the result as a cumulative probability distribution function,

$$P_i = 2\pi \int_{-1}^{\cos \Theta_i} \frac{\sigma(\theta, E_r)}{\sigma_t(E_r)} d(\cos \theta), \quad i = 0, 1, \dots, n. \quad (2.53)$$

Equation 2.53 is inverted to obtain the scattering angle as a function of relative energy and  $n$  equally spaced values of the cumulative probability spacing,  $\Theta_i(P_i, E_r)$ , where  $\Theta_i$  is the scattering angle in the center-of-mass frame. Examples of  $\Theta_i(P_i, E_r)$  for the  $D^+ + D$  and  $D^+ + D_2$  collisions at a center-of-mass energy of 1 eV are presented in Fig. 2.5. At this energy, inclusion of direct elastic scattering increases the probability that colliding particles undergo small angle deflections. Consideration of charge exchange alone would shift the probability distribution to favor collisions resulting in  $\Theta = \pi$ . As evident in Fig. 2.5,  $\Theta_i(P_i, E_r)$  for like-species collisions exhibits a higher probability of undergoing large-angle collisions compared to the ion-molecular collision case. This is due to the absence of a charge exchange contribution to the scattering function for ion-molecular elastic collisions. Monte Carlo collision processing begins with the sampling of a suitable ion from a Maxwellian distribution at the local ion temperature, yielding,  $E_r$ . The  $P_i$  are next sampled from a uniform distribution. The collision angle follows from a bi-linear interpolation into this data table without evaluation of complex integral functions.

Previous treatments of charge exchange in Monte Carlo algorithms employed a  $180^\circ$  collision scattering model in the center-of-mass frame. The approach is simple to implement, requiring just the exchange of the ion and neutral velocity vectors and yields a momentum transfer cross section of about  $2\sigma_{cx}$ , where  $\sigma_{cx}$  is the charge exchange cross section. This is, in fact, roughly equal to the total diffusion cross section in ion-neutral collisions,  $\sigma_d \sim 2\sigma_{cx}$  [22, 23, 24] The accuracy of this simple expression is demonstrated in Fig. 2.6, which compares the diffusion cross section with results for the “spin exchange” cross section from the ORNL

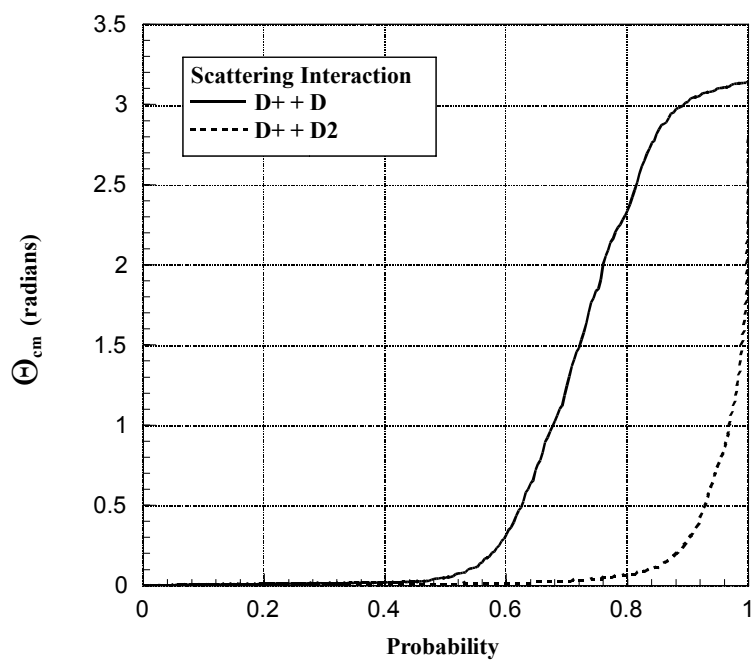


Figure 2.5: Scattering function  $\Theta_i(P_i, E_r)$  for  $D^+ + D$  and  $D^+ + D_2$  ion-neutral elastic interactions at an interaction energy of 1 eV.

data[19]. Spin exchange is defined as the exchange of the intrinsic quantum mechanical property of particle spin; for distinguishable particles this is equivalent to charge exchange. For like-species collisions, spin exchange and charge exchange are equivalent only within classical regimes. The relation  $\sigma_d \sim 2\sigma_{cx}$  holds within the classical regime above approximately 2 eV for  $D^+ + D$ . At lower energies, the particles must be treated as indistinguishable and separation of direct elastic scattering and charge exchange is no longer possible. At these low energies, spin exchange is no longer equivalent to charge exchange and the relation  $\sigma_d \sim 2\sigma_{cx}$  no longer holds. This illustrates the difficulties in treating ion-neutral elastic collisions by charge exchange alone under low-temperature detached conditions.

The addition of these data present the user with yet another option for handling hydrogen charge exchange in DEGAS 2. Figure 2.7 compares the new CFADC data (labeled “Krstic”) with previous versions and with experimental data. The cross sections have been plotted as a function of the relative velocity so that both the hydrogen and deuterium data can be included. The Krstic cross sections are the “spin exchange” cross sections described in Ref. [19]. They are thus *smaller* than the total elastic scattering cross sections that are to be used in DEGAS 2. This underscores the point that these new elastic scattering cross sections are intended to *replace* the existing charge exchange data, not used in addition to them.

The default data used heretofore in DEGAS 2 have been computed from the “Janev-Smith” fit[15]. This fit was derived from older data published by Barnett[25]. Barnett’s data were a compilation of various experimental results. Included was the work by Newman[26]. Why the Barnett compilation diverges slightly from the Newman data at the lowest energies is not clear. The Reviere[27] curve in Fig. 2.7 represents the charge exchange cross section employed in the original DEGAS code. Not surprisingly, they are used in DEGAS 2 in the `Degas_box_bench` example. Note that Reviere’s intended application was neutral beam penetration. Hence, the lack of agreement at divertor-relevant velocities is not surprising.

## 2.8.2 Neutral-Neutral Elastic Scattering

Low temperature (a few eV or less) plasma conditions may result in neutral densities that are comparable to the plasma density. In such cases, collisions amongst the neutral species can be important in determining the exchange of momentum and energy in the system. For example, hydrogen molecules generated at a surface typically have energies comparable to room temperature, say, 0.03 eV. Yet, these molecules may be surrounded by much more energetic atoms, say 3 to 5 eV, resulting from molecular dissociation or charge exchange. Elastic collisions be-

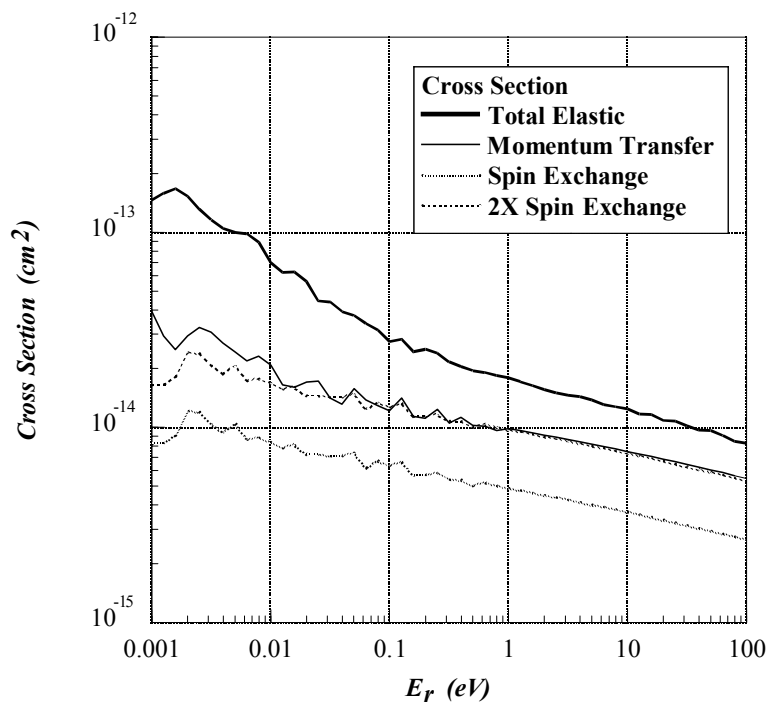


Figure 2.6: Comparison of diffusion and charge exchange cross sections for  $D^+ + D$  elastic collisions.

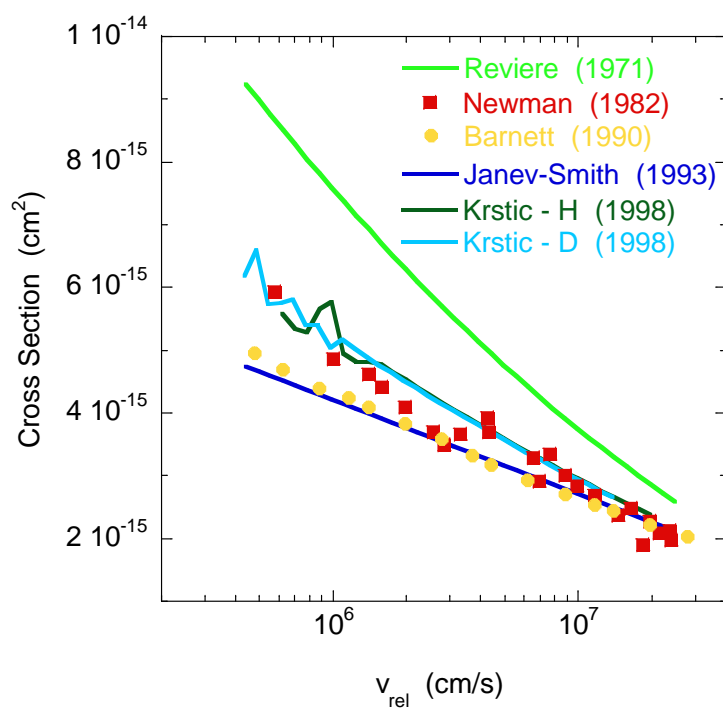


Figure 2.7: Comparison of various charge exchange cross sections. The curve labeled “Janev-Smith” represents the default data used in DEGAS 2 prior to the addition of the newer CFADC elastic scattering data, labeled here by “Krstic” (one curve for H, one for D).

tween the two species can significantly increase the molecules' energy, enabling them to penetrate much further into the plasma before becoming dissociated or ionized.

When the neutral-neutral mean free path is very short,  $K_n = \lambda_{\text{mfp}}/d \ll 1$  ( $d$  is a measure of the system size or of gradient scale lengths;  $K_n$  is the Knudsen number) cases, the most efficient approach would be to use a fluid model for the neutral species. This regime is also known as the “viscous flow” regime[28]. However,  $K_n$  is usually close to one in most fusion problems, even in vacuum regions. In that case, a kinetic treatment is required. Fortunately, such “transition regime” cases can be handled effectively with a Monte Carlo code. When  $K_n \gg 1$ , the “molecular flow” regime, neutral-neutral collisions can be neglected. For a practical discussion of these three regimes as they apply to the tokamak divertor, see Ref. [29].

The great difficulty with treating neutral-neutral collisions is that they make the problem nonlinear. Namely, the collision kernel is then a quadratic function of the neutral distribution function rather than a linear one. The exact problem is very difficult to solve, and one is forced to resort to approximations. Reiter et al. addressed this issue first with the EIRENE code and concluded that an iterative “BGK” approach (referring to the original algorithm developed by Bhatnagar, Gross, and Krook[30]; proposed independently by Welander[31]) was sufficient[32, 33]. The BGK approximation replaces the collision integral with a much simpler expression in which the distribution function relaxes to a Maxwellian distribution with a velocity independent collision time. A physically relevant result is ensured by determining the parameters of the Maxwellian distribution so as to enforce conservation of mass, momentum, and energy in the collisions. The collision time remains arbitrary and is chosen so as to reproduce measured viscosity and diffusion rates; this procedure is discussed in greater detail in Sec. 2.8.3.

Neutral-neutral collisions are included in DEGAS 2 in exactly the same way as in EIRENE. While more details on nature of the BGK algorithm are provided in Kanzleiter's thesis[34], the essential elements and references are covered in the more readily available Ref. [33]. The BGK algorithm approximates the binary collision integral for species  $i$  as

$$\frac{\partial f_i}{\partial t} \approx \frac{M_i - f_i}{\tau_i} + \sum_{j \neq i} \frac{M_{ij} - f_i}{\tau_{ij}}, \quad (2.54)$$

where the  $M$  represent Maxwellian distributions,

$$M_\alpha \equiv n_\alpha \left( \frac{m_\alpha}{2\pi kT_\alpha} \right)^{3/2} \exp \left[ -\frac{m_\alpha(\vec{v}_\alpha - \vec{U}_\alpha)^2}{2kT_\alpha} \right]. \quad (2.55)$$

Here, the individual particle velocity is  $\vec{v}_\alpha$ ; the mass  $m_\alpha$  is always that of the species represented on the left-hand side of Eq. (2.54). In Eq. (2.54), a single subscript refers to a physical species. Dual subscripts below refer to fictitious, “mixed” species introduced for the purpose of handling binary collisions between unlike neutral species.

Conservation of mass, momentum, and energy in the self-collision case yields

$$n_i = \int_{-\infty}^{+\infty} d^3v f_i(\vec{v}), \quad (2.56)$$

$$n_i m_i \vec{U}_i = \int_{-\infty}^{+\infty} d^3v m_i \vec{v} f_i(\vec{v}), \quad (2.57)$$

$$\frac{3}{2} n_i kT_i = \int_{-\infty}^{+\infty} d^3v \frac{1}{2} m_i v^2 f_i(\vec{v}). \quad (2.58)$$

Conservation of mass, momentum, and energy are also enforced in the mixed-species case to determine the  $M_{ij}$ . Additional constraints are obtained by requiring that the ratio of the momentum and energy relaxation rates is the same as for the full collision integral. The results are [32, 33, 34] are

$$\vec{U}_{ij} = \vec{U}_{ji} = \frac{m_i \vec{U}_i + m_j \vec{U}_j}{m_i + m_j}, \quad (2.59)$$

$$kT_{ij} = kT_i - \frac{2m_i m_j}{(m_i + m_j)^2} \left[ (kT_i - kT_j) - \frac{m_i}{6} (\vec{U}_i - \vec{u}_j)^2 \right]. \quad (2.60)$$

One additional important constraint on the collision times is obtained,

$$n_j \tau_{ij} = n_i \tau_{ji}. \quad (2.61)$$

With  $\tau_{ij} \equiv (n_j \langle \sigma v \rangle_{ij})^{-1}$  representing the typical time between physical species  $i$  and the fictitious species represented by  $M_{ij}$ , this becomes just

$$\langle \sigma v \rangle_{ij} = \langle \sigma v \rangle_{ji}. \quad (2.62)$$

May [32, 33] sets the values of the reaction rates for mixed collisions using empirical diffusion coefficients; the rates for self-collisions come from measured viscosity coefficients. The end result is that in both cases the reaction rate  $\langle \sigma v \rangle_i \propto T_i^{1/4}$

or  $\langle \sigma v \rangle_{ij} \propto T_{ij}^{1/4}$ . The validity of these expressions is examined in the next subsection.

The practical implementation of the algorithm is iterative. By default, the initial iteration of the code proceeds without neutral-neutral collisions. The reason for this is that the neutral “background” with which the test species collide initially has zero density. A nonzero density could be specified during the setup of the background, if desired. The fluid moments of Eqs. (2.57), (2.58), and (2.58) are computed at the end of the iteration and inserted into the background density, velocity, and temperature arrays for the neutral background species. The calculation is then restarted; this time the test neutral species scatter against the neutral background. At the end of the run, the fluid moments are again updated. The iterations continue either a specified number of times or until some convergence criterion is satisfied.

Accurately simulating neutral-neutral scattering requires greater care in setting up the geometry and deciding on the number of flights than is exercised in linear runs. First, the entire problem space must be divided up finely enough to resolve all anticipated spatial variations of the neutral density. In comparison, without neutral-neutral scattering, the vacuum regions can be treated as large monolithic zones. The variation of the neutral parameters between iterations is asymptotically limited by Monte Carlo noise. In other words, if too few flights are used, the background densities are not accurately determined, causing the elastic scattering of the test species to be doubly inaccurate. The variations in neutral density, etc. in a given simulation will be more effectively reduced by increasing the number of flights than by carrying out more iterations.

### 2.8.3 Validation of BGK Model and Rates

As described by May[32], the reaction rates for the BGK algorithm can be determined by matching physical quantities, the viscosity and diffusion coefficients, against measured values. However, since May’s thesis work and the publication of Reiter[33], the ORNL CFADC has computed differential scattering cross sections [19], analogous to those described in Sec. 2.8.1, for these neutral-neutral systems. In this subsection we will show that the two approaches are largely consistent, at least near room temperature.

We proceed in a manner analogous to May. Namely, we will obtain from the CFADC differential cross sections values for the viscosity and diffusion coefficients. These will be transformed into reaction rates that can be compared with those described in Sec. 2.8.2.

For self-collisions, consider the viscosity. The general expression derived in Chapman and Cowling[35] [their Eq. (10.1,4)] is

$$\mu_1 = \frac{5}{8} \frac{kT}{\Omega_1^{(2)}(2)}, \quad (2.63)$$

where  $\Omega_1^{(l)}(n)$  corresponds directly to the  $\Omega^{l,n}$  integrals described by Bachmann[20]. The subscript “1” here is to be associated with the cross section and refers to collisions of species “1” with itself (as opposed to collisions between species “1” and “2” which will be labeled with “12” below).

Likewise, we have for the diffusion coefficient [Eq. (9.81,1) in Ref. [35]],

$$D_{12} = \frac{3}{16} \frac{kT}{(n_1 + n_2)m_r\Omega_{12}^{(1)}(1)}, \quad (2.64)$$

where  $n_1$  and  $n_2$  are the species densities and  $m_r$  is the reduced mass for the system,  $m_r = m_1m_2/(m_1 + m_2)$ .

The  $\Omega^{(l)}(n)$  integrals represent averaging of the collision cross sections over Maxwellian distributions for both species. The `ratcalc` code is able to integrate these cross sections over a single Maxwellian distribution, namely, the  $I_{l,n}$  described in Reiter[14] and the documentation for `ratcalc`. Fortunately, the double integral we need here can be found as a limiting case of the single integral:

$$\langle I_{l,n} \rangle(u_p, u_n) = \lim_{u' \rightarrow 0} I_{l,n}(u'_p, u'), \quad (2.65)$$

where  $u_p'^2 \equiv u_p^2 + u_n^2$ , and  $u_p = \sqrt{2T_p/m_p}$  is the thermal velocity of the second species. Likewise,  $u_n = \sqrt{2T_n/m_n}$  is the thermal velocity associated with the Maxwellian distribution used in the averaging over  $u$ . The  $\langle I_{l,n} \rangle$  is then related to  $\Omega^{(l)}(n)$ ,

$$\langle I_{l,n} \rangle = 8 \left( \frac{u'_p}{u_p} \right)^n \Omega^{(l)}(n/2). \quad (2.66)$$

The same result is quoted in Ref. [20] and in [14], although in the latter case the variable equivalent to  $u'_p$  is incorrectly defined.

With these expressions, we can compute the single species viscosity and two species diffusion coefficients from the CFADC differential scattering cross sections. The corresponding expressions for the “Maxwell molecule” interaction [intermolecular force given by  $\kappa/r^5$ ; e.g., see Eq. (12.1,1) in Ref. [35]] are

$$\mu_1 = \frac{kT}{3\pi A_2(5)} \sqrt{\frac{2m}{\kappa}}, \quad (2.67)$$

where  $A_2(5) = 0.436$  is the result of a dimensionless integral. And from Eq. (14.2,2) of Ref. [35],

$$D_{12} = \frac{kT}{2\pi A_1(5)} \frac{1}{n\sqrt{\kappa_{12}m_r}}, \quad (2.68)$$

where  $A_1(5) = 0.422$  is the result of another dimensionless integration.

The reaction rates needed for the BGK algorithm are related to the constant in the Maxwell molecule force law by (see Ref. [36] or [32]),

$$\langle \sigma v \rangle_{11} = 2\sqrt{2}\pi A_1(5) \sqrt{\frac{\kappa}{m}}, \quad (2.69)$$

and

$$\langle \sigma v \rangle_{12} = 2\pi A_1(5) \sqrt{\frac{\kappa_{12}}{m_r}}. \quad (2.70)$$

Now, we can use Eq. (2.67) to eliminate  $\kappa$  in Eq. (2.69) in favor of  $\mu_1$ . Then, we can insert  $\mu_1$  as given by Eq. (2.63) to obtain an effective BGK reaction rate that has the same viscosity as that computed directly from the CFADC differential cross sections:

$$\langle \sigma v \rangle_{11} = 2.065\Omega_1^{(2)}(2). \quad (2.71)$$

The analogous procedure for the diffusion coefficient yields

$$\langle \sigma v \rangle_{12} = \frac{16}{3}\Omega_{12}^{(1)}(1). \quad (2.72)$$

Finally, we can use Eqs. (2.65) and (2.66) to replace the  $\Omega$  integrals with the equivalent integrals obtainable from `ratecalc`,

$$\langle \sigma v \rangle_{11} = \frac{2.065}{32} \lim_{u' \rightarrow 0} I_{2,4}(u'_p = \sqrt{2}u_p, u'), \quad (2.73)$$

and

$$\langle \sigma v \rangle_{12} = \frac{2}{3} \frac{u_p^2}{u_p^2 + u_n^2} \lim_{u' \rightarrow 0} I_{1,2}(u'_p = \sqrt{u_p^2 + u_n^2}, u'). \quad (2.74)$$

In evaluating the latter expression, we will assume that one of the species (e.g., molecules at the wall temperature) are much cooler than the other, i.e.,  $u_n \ll u_p$ . Equation (2.74) then becomes a function of only  $u_p$ .

The CFADC data exist only for the  $D + D_2$  and  $D + D$  systems (and isotopic equivalents; molecules are computationally intensive, hence, the absence of molecule-molecule data). These are compared with the May data in Fig. 2.8.

One concern with May's treatment of the  $D + D$  case is that the empirical viscosity formula quoted in Ref. [32] does not appear in the literature, nor is its origin clearly stated. The best guess for its origin is that it was obtained by rescaling the "Fuller" expression for the diffusion coefficient[37] into a viscosity using the theoretical expressions to relate the two. In Fig. 2.9, we compare May's expression with two that do appear directly in Ref. [37] ("Chung" and "Lewis") and with individual data points listed in the CRC Handbook[38]. The agreement of these values near room temperature ( $\sim 0.03$  eV) is expected. However, May's formula has a stronger temperature scaling than the others and exceeds them by about a factor of 15 at 10 eV. The relevant temperature range for this process is expected to be between 1 and 10 eV.

Figure 2.8 shows that at least near room temperature, May's expressions are also consistent with the CFADC data. However, in the 1 to 10 eV range, they are considerably larger than the CFADC values, suggesting that the values used in DEGAS 2 (and EIRENE) may be too large. We will demonstrate in Sec. 3.7.2 that the temperature dependence ascribed to these rates by May is inconsistent with Eq. (2.62).

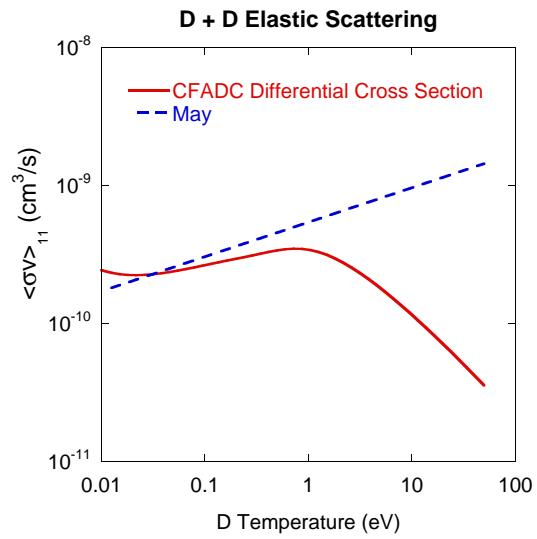
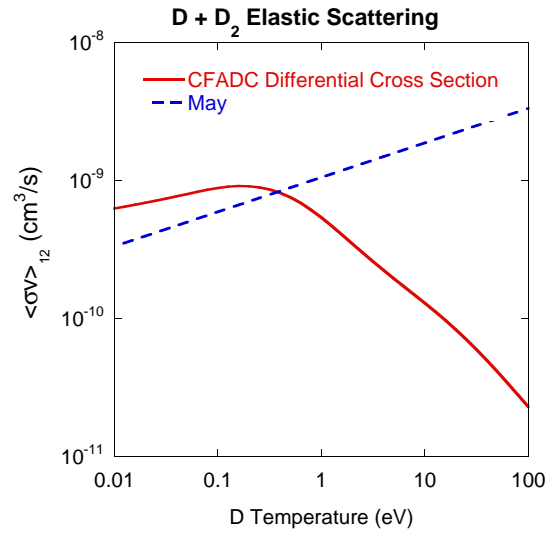


Figure 2.8: Comparison of reaction rates for the  $D + D_2$  and  $D + D$  systems. The original rates suggested by May[32] and effective rates computed from the CFADC data are shown.

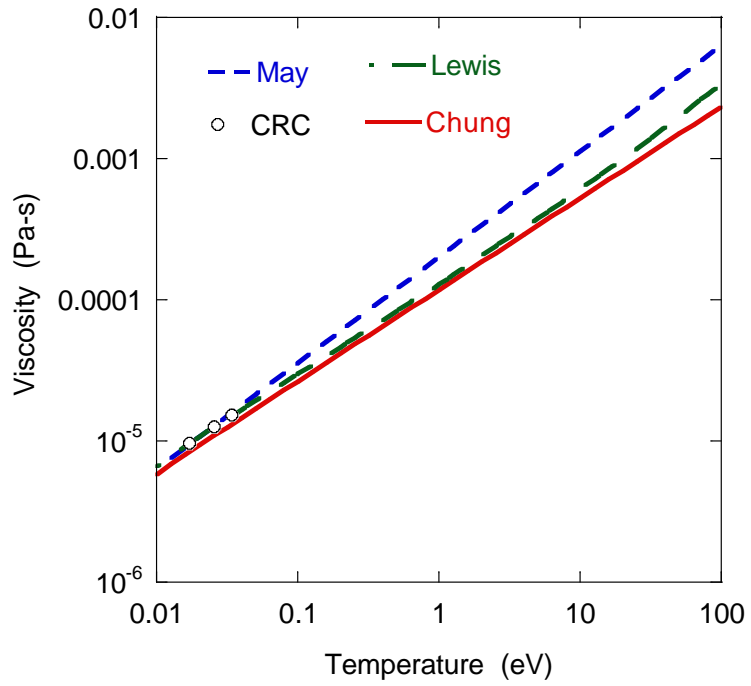


Figure 2.9: Comparison of viscosity formulas from May[32], Reid[37] (the “Chung” and “Lewis” expressions), and the CRC Handbook[38].

# Chapter 3

## Running DEGAS 2

### 3.1 Getting DEGAS 2

DEGAS 2 can be obtained from the anonymous FTP site at Princeton Plasma Physics Labs (PPPL). It can be found in the directory `/pub/degas2`. The procedure for getting it is:

```
ftp ftp.pppl.gov
user: anonymous
Password: < your email address >
ftp> cd pub/degas2
ftp> binary
ftp> get degas2.tar
ftp> bye
```

If you want to download DEGAS 2 through your browser now, here's a link to it. Currently, there are three forms:

1. `degas2.tar` An uncompressed tar file (extract with:

```
tar xf degas2.tar
```

2. `degas2.tar.Z` The tar file compressed with the `compress` utility. To extract the code,

```
uncompress degas2.tar.Z
tar xf degas2.tar
```

3. `degas2.tar.gz` The tar file compressed with the `gzip` utility. To extract the code,

```
gunzip degas2.tar.gz
tar xf degas2.tar
```

There are a number of older versions of the code in this directory. The most recent is always linked to the names listed above. Please consult with the authors if you think you need an earlier version.

## 3.2 Getting Supporting Tools

DEGAS 2 relies on several pieces of utility software. In some cases (netCDF), these utilities are absolutely required. These utilities can be obtained from the indicated sites. You will probably want to have your system administrator download, compile, and install these packages system-wide for your convenience.

### 3.2.1 GNU Software

The DEGAS 2 Makefile automates several chores, including generating and compiling FORTRAN code, as well as weaving T<sub>E</sub>X files from from the FWEB source. The Makefile also controls the application of platform-specific lines of code and compilation options. Although not completely necessary, using DEGAS 2 without using GNU Make to run this Makefile would be extraordinarily inconvenient. The `gmake` (the GNU Make utility) can be found at <ftp://prep.ai.mit.edu/gnu/make/>

Likewise, the Emacs editor is not essential, but its use simplifies a number of tasks. For instance, Emacs provides a facility which allows the user to search for variable and routine names across many files. For example, say you're editing `randomtest.web` and you'd like to see the source code for subroutine `next_seed` called there. All you have to do is execute the Emacs command `M-. next_seed` (it will ask for the name of the tags file; the default value of `TAGS` is correct and you just need to hit `Enter` here). All of DEGAS 2 source and header files are included in this list of tags. Additional facilities such as a tag-query-replace (e.g., to change *all* occurrences of a variable name) are available. See the Emacs Info file under the node "Tags" for more information.

### 3.2.2 netCDF

netCDF provides a device-independent binary file format. Furthermore, these files are self-describing. Most of the effort required to read and write these files is handled by macros. These are documented in the file `netcdf.hweb`. By adding the commands in `src/.emacs` to your `.emacs` file, Emacs will be able to convert automatically these files to text and back to binary for perusal and editing. netCDF is fully documented in the Info facility of Emacs. The netCDF libraries are required to run DEGAS 2 since virtually all of the input data is stored in netCDF files. The associated netCDF utilities `ncdump` (for translating a netCDF file into human-readable text) and `ncgen` (for generating a netCDF binary file from a text file) are useful for reading and making minor changes to DEGAS 2 input files. Two short scripts, `ncdump-filter` and `ncgen-filter`, allow Emacs to invoke these utilities via the commands in the `.emacs` file. These are not part of the netCDF distribution and are included amongst the DEGAS 2 source files for your convenience. These should be copied to a directory which is covered by your shell's `PATH` variable.

An additional note: if you use `ncgen`, be sure to either specify the `-b` or `-o netcdf_filename` option to let the utility know that you want it to generate a netCDF file (see: `man ncgen`).

netCDF (see Sec. 3.2.2) can be obtained from `ftp://unidata.ucar.edu/pub/netcdf/netcdf-3.4.tar.Z`. Other compression formats and files are also present in this same directory. See the link to "FAQ" for the answers to frequently asked questions.

### 3.2.3 FWEB

The FWEB package provides a facility for code documentation as well as a powerful preprocessor. The typesetting abilities of FWEB allow authors to insert  $\TeX$  (or  $\LaTeX$ ) comments into their code. In DEGAS 2, the preprocessor is utilized extensively for writing macros which allow the code seen by the user to be significantly more powerful than pure FORTRAN. In fact, the code can be processed into FORTRAN 77 or FORTRAN 90 as needed. However, FWEB is *not optional*. The user must have access to at least its `ftangle` executable on some system in order to generate compilable FORTRAN files (once generated, these can be copied to other systems for compilation). For examples of the overall structure of FWEB programs, see the `*.web` files; most of the macros are located in the header `*.hweb` files. FWEB is fully documented in the Info facility of Emacs.

FWEB (version 1.62) (see Sec. 3.2.3) is available at `ftp://ftp.pppl.gov/pub/fweb/fweb-`

1.62.tar.gz

To typeset DEGAS 2 source code in “human-readable” formats such as DVI, PostScript, or PDF, the user will need FWEB’s `fweave` utility and a version of  $\text{T}_{\text{E}}\text{X}$  or  $\text{L}_{\text{A}}\text{T}_{\text{E}}\text{X}$ .

$\text{L}_{\text{A}}\text{T}_{\text{E}}\text{X}$  is available in lots of places. To begin with, see the official CTAN  $\text{T}_{\text{E}}\text{X}$  network page at <http://www.tex.ac.uk/ctan>. The distribution in use at PPPL is called `teTeX`, <ftp://ctan.tug.org/tex-archive/systems/unix/teTeX/1.0/distrib/sources>.

### 3.2.4 Concurrent Version System

The UNIX CVS (Concurrent Version System) utility is used to coordinate work on a code by a number of authors. The central DEGAS 2 source code is maintained in a CVS repository. Users planning to coordinate with the code authors should become familiar with CVS. Users who will do extensive code development on their own will find CVS a valuable tool in tracking their work. The average end-user should be able to work effectively without ever dealing with CVS.

The CVS repository is a central, safe version of the code; authors check out copies in their own disk space in order to work on the code. By doing a `cvs update`, a given author can update his local sources to incorporate changes others have saved to the central repository. The `cvs commit` command allows him to save his own changes to the repository.

The Info page for CVS is the best reference for commands. The manual page is complete, but lengthy. The man page for `rcsintro` may also be helpful as an introduction. Many `cvs` commands may be executed from within Emacs. See the Emacs Info page on `Pcl-cvs` for more details.

### 3.2.5 HDF

HDF is another device-independent binary file format. At present, HDF files are used only by the `geomtesta` utility as a convenient format for transferring the code results in graphical form for processing by commercial products.

The HDF libraries can be obtained from <ftp://ftp.ncsa.uiuc.edu> Note that as of HDF version 4, some of the netCDF functionality is implemented in HDF. To avoid conflicts with the official netCDF libraries, do not install the netCDF portion of the HDF distribution.

### 3.2.6 Triangle

Jonathan Shewchuck's `Triangle` program is used by the `definegeometry2d` code to break polygons up into triangles. The home for `Triangle` is <http://www.cs.cmu.edu/quake/triang>. The `Triangle V. 1.3` was used in writing `definegeometry2d`. Anyone downloading a more recent version should notify the `DEGAS 2` authors. The `DEGAS 2 Makefile` will expect to find the `Triangle` files, `triangle.c`, `triangle.h`, etc., in `$HOME/Triangle`. If your copy is installed elsewhere, you can either create an appropriate link or modify `Makefile`.

## 3.3 Structure of the DEGAS 2 File System

Here is an example structure of the directories under the top-level `degas2` directory. Those labeled with “(D)” represent source and data directories maintained with CVS. The others are created by the user as described in the compiling section. Note that the `Makefile` assumes that this `degas2` directory sits in the directory pointed to be the `$HOME$` environment variable on your workstation. If you have installed the code elsewhere, see Sec. 3.6.3.

**data** Input atomic and surface physics data and information (D)

**src** All source code (D)

**Doc** Location of the various formats of this document and ancillary files (D)

**examples** Input and output files from example and benchmark runs (D)

**Aladdin** Source code and data for use with IAEA Aladdin package (D)

**ALPHA** Object and executable files for Dec Alpha machines

**SUN** Object and executable files for Sun Solaris and SunOS machines

**CRAY** Pre-processed source code for export to Cray computers

**tex** Intermediate files and final DVI documentation files generated from source code

If you need to have multiple run directories for a given system (e.g., focussed on different problems or using different compilers), you can create additional directories with names like `SUN-foo` where “foo” is any string you like.

## 3.4 Components of the Code

DEGAS 2 is not a single code (not now anyway), but a complex package of setup, test, simulation, and post-processing tools. Which ones are needed depend on the user's objectives and familiarity with DEGAS 2. A few additional "targets" are listed in the Makefile. These are either sufficiently out of date or infrequently used to warrant mention here.

### 3.4.1 Main Code

Virtually every user will be running these executables, usually in this order.

**problemsetup** Reads a text file describing the species, materials, atomic, and surface physics required for the current problem. The code accesses the required "reference" data, and compiles them into a netCDF file (the `problem.nc` file).

**definegeometry2d** Generates a DEGAS 2 netCDF geometry file from from a text input file. Input files for simple geometries may be generated manually; more complex geometries can be specified via other computer generated text files files referenced by the input file. For example, `definegeometry2d` is able to read data produced by the DG package (part of the B2-Eirene or SOLPS distribution) or by UEDGE. Of the three tools for setting up DEGAS 2 geometries `definegeometry2d` is the most flexible.

**readgeometry** Generates a DEGAS 2 netCDF geometry file from an existing DEGAS, UEDGE, or SONNET geometry description. This package has largely been superseded by `definegeometry2d`. However, users with legacy input files for the old DEGAS code will still want to use `readgeometry`. A short text input file helps `readgeometry` through the transformation process.

**defineback** Uses a short text input file to control the mapping of plasma data in external text files onto the DEGAS 2 geometry. Designed to be used in conjunction with `definegeometry2d`, `defineback` can utilize data produced by other codes. However, `defineback` is not yet mature and is, consequently, a little "rough around the edges".

**readbackground** Plasma data in an external file is mapped onto the zones of the DEGAS 2 geometry. Presently, only DEGAS and UEDGE files can be used; readgeometry and readbackground read the same data file.

**updatebackground** Is similar to readbackground, but is intended for use in iterations with the UEDGE code *only*. The source information generated by the initial run of readbackground is stored in a separate file (`oldsourcefile`, Sec. 3.5.1). On subsequent iterations, small changes in the source terms are accounted for by allowing non-unit weighting factors at each source segment. Once the accumulated changes exceed a certain size (specified by parameters in the sources class), the DEGAS 2 source sampling arrays are re-initialized (i.e., to once again use unit weights) and the `oldsourcefile` is rewritten. The effectiveness of this procedure is currently being evaluated and should be considered as experimental.

**tallysetup** This code specifies the types of “scores” (the essential output of the code), along with their dependencies, which will be computed in the DEGAS 2 run. Although the input files(s) should not be modified by the novice user, this code needs to be run to factor the values of physics and geometry parameters for the problem at hand into the specification of these scores.

**flighttest** The core of DEGAS 2. This program launches, follows, and scores the Monte Carlo trajectories which make up a DEGAS 2 simulation. (The name is a holdover from early versions in which this did tracking with a minimum of hardwired physics).

**outputbrowser** Reads the output netCDF file generated by `flighttest` (in addition to all other netCDF files for the problem) and allows the user to interactively browse its contents. A script facility is provided for batch-like operation.

**geomtesta** Another inappropriately named routine which serves as the principal post-processing code for DEGAS 2. Although originally designed as a diagnostic for the geometry, it has proven too easy to continue extending this code to warrant development of an honest post-processing tool. The DEGAS 2 input and output files are read in by the code. Using the geometry information, the zone-based plasma and neutral data are transcribed onto a high density uniform rectangular mesh and dumped into the HDF files suitable for further manipulation by commercial products such as IDL and Noesys.

### 3.4.2 Other Setup Routines

These are occasionally used to add new atomic or surface physics reactions, or to generate new atomic and surface physics data files.

**datasetup** This routine possibly belongs in the first list. It reads text files describing the complete lists of elements, species, reactions, materials, and plasma-material interactions available to DEGAS 2 and generates the corresponding DEGAS 2 netCDF files. These lists are occasionally referred to in the code as the "reference" lists; the input file for `problemsetup` specifies subsets of these lists. A new reaction is added to DEGAS 2 by inserting the requisite information into the "reactionfile" and rerunning `datasetup`. The new reaction can then be added to the problem input file.

**ratecalc** A routine for computing averages of atomic physics cross sections. Since it is designed to read data from the Aladdin database, `ratecalc` is presently limited in its flexibility. The principal application thus far has been the generation of reaction rates and higher moments for charge exchange and other interactions between atoms, molecules, and ions.

**reactionwrite** A simple routine designed to translate collisional radiative data for the electron impact ionization of hydrogen from the format used by the old DEGAS code into netCDF files (ionization and recombination) for DEGAS 2. This code has been run a handful of times as needed to keep up with changes in the content and format of the atomic physics data files.

**pmiwrite** Is analogous to `reactionwrite`, but handles almost all of the plasma-material interaction data. Presently, two data files from the old DEGAS code and one from EIRENE are used as input. A few processes describable without external data are also included. This code can be used, in a somewhat clumsy manner, to add new plasma-material interaction data to DEGAS 2 using either one of these three existing data bases or via a new datafile (with the rest of the code serving as an example).

**boxgen** Is the third of geometry / background generation tool provided with DEGAS 2. It is intended to serve as an example of how to generate geometry and background files from scratch. As the name implies, `boxgen` sets up a simple box geometry with a linearly varying plasma. However, no input file for `boxgen` has been developed; all modifications have to be effected through direct source code modification. The typical user in search of a

simple linear geometry to study can be overwhelmed by the complexity of the code encountered there. For this reason, the `definegeometry2d / defineback` pair may be more suitable for setting up simple problems.

### 3.4.3 Test Routines

**reactiontest** Can be run after `problemsetup` to check the computation of the reaction rate, and collision products (including velocities and scoring data) for a given reaction.

**pmitest** The analog of `reactiontest` for plasma-material interactions. Again, this code can be executed for a given problem once `problemsetup` has been run. Since the velocity distributions of some plasma-material interactions are described statistically, `pmitest` is also set up to average the outcome of a given interaction over a specified number of trials and print out a list of the product velocities for external manipulation.

**sourcetest** Tests the distribution in phase space of the source terms for a particular problem. Since the source is described in the “background” `netCDF` file, `readbackground`, `boxgen`, or something equivalent must be run prior to using this routine. Like `pmitest`, the code is able to run many trials, compute averages, and printout data from each individual trial.

**dataexam** Provides the user with a convenient interface to the atomic physics data files. Although `netCDF` files can be converted to a human-readable text form, interpreting those data is since DEGAS 2 collapses the multi-dimensional structure components of the atomic physics data into a single one-dimensional array. This routine reads the “raw” (at the “reference” level) data files prior to their insertion into the problem `netCDF` file and, thus, can be run at any time. An analogous routine for the plasma material interactions is needed.

**sysdeptest** Tests several system-dependent features of DEGAS 2. This would be run only if the code was being ported to a new operating system or if the operating system on a currently supported architecture underwent a significant upgrade.

**randomtest** Is used to verify that DEGAS 2 will give the same results on different architectures (provided the random number seeds are set the same!).

### 3.4.4 Miscellaneous Routines

**matchout** Is used to compare the current DEGAS 2 output netCDF file with another from an equivalent run (i.e., all of the arrays must be exactly the same size) on the command line. The most frequent use of `matchout` is to verify that two separate runs have yielded results which are the same to within roundoff error. Because of the size of the output netCDF file, verifying this by visually comparing the files is impractical.

**matcheir** Is specifically designed for comparing with output from the EIRENE code. The name of the EIRENE file is specified on the command line. See Sec. (the same physics benchmark).

**datamatch** Provides a means for comparing the contents of the two netCDF data files specified on the command line.

## 3.5 Input Files

The essential inputs to a Monte Carlo neutral transport code are:

- The identity of the “test” species (usually neutral in plasma problems) that are of interest,
- The identity and phase space distributions of the “background” (typically electrically charged in plasma problems) species with which the test species will interact,
- The interaction processes between the test and background species. The relative probability of these processes as a function of the test and local background properties are required as well as a prescription for specifying the outcome of each interaction.
- The simulation geometry, including a framework for holding the background species data, as are a means for tracking the test species through the background.
- The boundaries of the geometry, including a prescription for specifying the outcome of interactions between the test species and these boundaries.

DEGAS 2 utilizes several text based input files for controlling the actions of its component executables (see Sec. 3.4). In this section we will discuss a few of these input files. The more complex input files are described in their respective codes; links to the documentation for those files will be given instead. More detailed information on running DEGAS 2 will follow in later sections.

These text input files are, for the most part, read with the same set of text processing utilities that adhere to the following guidelines. In some cases, particularly those involving files generated by other codes, the files are read directly with formatted FORTRAN read statements.

1. Spacing and blank lines are ignored. The user is free to utilize white space in whatever way facilitates reading and maintaining the input file.
2. Comments, either a complete line or at the end of a line, are begun with a # sign.
3. File names can be a relative or full path name.

### 3.5.1 degas2.in

`degas2.in` is the input file which controls (most of) the other input files. Each line consists of DEGAS 2's symbolic name for the file (this can be changed only by modifying `readfilenames.hweb` and `readfilenames.web`) followed by the path name for the file to be used in the current problem. The order of the lines in this file is unimportant.

```
elementsfile ../data/elements.nc
backgroundfile bk_users.nc
geometryfile ge_users.nc
problemfile pr_users.nc
reactionfile reactions.nc
speciesfile ../data/species.nc
aladinfile ../data/aladinput.nc
aladoutfile ../data/aladoutput.nc
elements_infile ../data/elements.input
problem_infile pr_users.input
reaction_infile reactions.input
species_infile ../data/species.input
materials_infile ../data/materials.input
```

```
materialsfile ../data/materials.nc
pmi_infile ../data/pmi.input
pmifile ../data/pmi.nc
cramdproblemfile cramdprob.nc
tallyfile tally_uers.nc
outputfile degas2_uers_out.nc
oldsourcefile os_uers.nc
```

Note that some of these are outdated or rarely used (unused entries may be deleted from the file, if desired). Most of the files come in pairs with the name `XXX_infile` corresponding to a text input file and `XXXfile` being a netCDF file generated by a program like `datasetup`, `problemsetup`, etc.

### **3.5.2 elements\_infile**

`elements_infile` lists all of the elements available to DEGAS 2 for use in constructing the species (see Sec. 3.5.3). Additional detail is given at the beginning of the file `elementsetup.web`.

### **3.5.3 species\_infile**

Inputs for species are contained in the file with the symbolic name `species_infile`. Additional detail is given at the beginning of the file `speciessetup.web`.

### **3.5.4 reaction\_infile**

The file `reaction_infile` describes all of the reactions available in DEGAS 2. Additional detail is given at the beginning of the file `reactionsetup.web`.

Note that adding a new reaction to this file involves two tasks beyond inserting the appropriate lines in `reaction_infile`. First, the netCDF file for the atomic physics data must be generated (see Sec. 3.9). The second task would be to write subroutines for setting up the products and handling collisions (see Sec. 3.9.3). This would be necessary only if a new reaction type were being added.

### 3.5.5 `ratecalc` Input

The `ratecalc` code is used to compute atomic physics reaction rates from cross section data, as well as a few other tasks. The code is documented internally. Follow this link to the introductory section to learn more.

### 3.5.6 `materials_infile`

The materials described in `materials_infile` are essentially just labels which will be used in conjunction with the plasma material interactions (see Sec. 3.5.7) to specify how test species interact with non-transparent surfaces. Additional detail is given at the beginning of the file `materialsetup.web`.

### 3.5.7 `pmi_infile`

The file `pmi_infile` describes all of the plasma-material interactions (PMI) available in DEGAS 2. Additional detail is given at the beginning of the file `pmisetup.web`.

### 3.5.8 `problem_infile`

As noted already in the section describing the DEGAS 2 components (see Sec. 3.4), there are two levels of physics input to DEGAS 2. The input files noted thus far comprise the reference level: in practice, the sum total of the data available to the code (although in principle it could be smaller). The second level is the problem level of data. This prescribes the species, reactions, materials, and PMI which will serve as the physical model to be used in carrying the simulation at hand. In some parts of the (internal) code, these are also referred to as the subset data since they represent a subset of the reference data (see also Sec. 3.9 and Fig. 3.2).

Additional concepts alluded to above in connection with the reaction input file (see Sec. 3.5.4) are those of test species and background species. Most simply, test species are the ones DEGAS 2 will track as they collide off of background species. The use of the word species here is important: both of the test and background lists are subsets of the “species” list (see Sec. 3.5.3). One more precise distinction between the two species types is that we assume that we know the distribution function (in space and velocity) of the background species; in fact, such information is required input to DEGAS 2. On the other hand, we are attempting

to *compute* the test species distribution function, moments of which serve as the primary output of DEGAS 2.

More information about the input file can be found at the beginning of the file `problemsetup.web`.

### **3.5.9 readgeometry Input**

The documentation for `readgeometry` input is maintained in the source code, `readgeometry.web`. For readers of the PDF version of this manual, here's a link to the corresponding PDF file.

### **3.5.10 definegeometry2d Input**

The documentation for `definegeometry2d` input is maintained in the source code, `definegeometry2d.web`. For readers of the PDF version of this manual, here's a link to the corresponding PDF file.

### **3.5.11 defineback Input**

The documentation for `defineback` input is maintained in the source code, `defineback.web`. For readers of the PDF version of this manual, here's a link to the corresponding PDF file.

### **3.5.12 readbackground Input**

Currently, the only possible inputs to `readbackground`— are the `UEDGE` (a specifically formatted text file generated during `UEDGE` post-processing) and `DEGAS` formats (an input file for the old `DEGAS` code). This routine makes some specific assumptions about the contents of these files. Since this situation is unsatisfactory from a number of viewpoints, a better long-term approach is being contemplated. For that reason, no additional documentation is provided at this point.

### **3.5.13 tally\_infile**

The documentation on the input file for `tallysetup` is maintained in the source code, `tallysetup.web`. This link will take the reader to the corresponding PDF file. The `tally` class contains more extensive and detailed information.

### 3.5.14 outputbrowser Input

This post-processing utility can be run interactively or with an input file. When run interactively, the session is logged into a script file called `outputscript` (in the run directory) which can be subsequently used as input to `outputbrowser`. Details on the use of `outputbrowser` and on the format of the script file can be found in the introduction to the file `outputbrowser.web`.

### 3.5.15 geomtesta Input

The post-processing utility `geomtesta` produces HDF files which can be viewed using the freeware utility `ximage`. However, commercial products such as IDL or Noesys from Research Systems, Inc. provide convenient tools for generating images and manipulating the data contained in these files.

The input to `geomtesta` is called `geometry.inp` and consists of 4 lines:

1.  $(x, y, z)$  coordinates of an origin
2.  $(x, y, z)$  unit vector giving one axis,
3.  $(x, y, z)$  unit vector giving a second axis,
4. length of each of the two sides.

For example,

```
-0.013 0.0 -0.008
1 0 0
0 0 1
0.056 1.088
```

The code just plots the data on a 2-D slice through the 3-D problem space. Specifying the slice requires: an origin (first line), a vector for each edge of the slice (second and third lines), and the length of each edge (fourth line). Since most DEGAS 2 applications will involve either cylindrical or toroidal symmetry, i.e., with the  $y$ -coordinate ignorable, the specification of the vectors is usually going to be as in the example. In general, though, one could take a slice which goes in the third direction as well. The vectors do not need to be orthogonal.

## 3.6 Compiling DEGAS 2

The Makefile has been written to compile on a variety of architectures and operating systems. Those currently supported and their corresponding symbols (in brackets) are:

1. Sun Solaris [SUN],
2. IBM AIX [IBM],
3. Digital OSF1 [ALPHA],
4. Silicon Graphics IRIX [SGI],
5. Linux, NAG F95, Portland Group F90, and Lahey-Fujitsu F95 compilers [LINUX], (The code will work with the Lahey-Fujitsu compiler, but may run very slowly. This will likely be remedied in a subsequent version of the compiler.)
6. Others (e.g., [CRAY]) are available for cross-compilation.

By default, the Makefile assumes that the DEGAS 2 main directory exists at `$HOME/degas2`. If you unpacked the `tar` file in some other location, you'll need to tell the Makefile where to look (see Sec. 3.6.3). Blindly change directory names is not recommended. Some flexibility is again provided; see below for details.

### 3.6.1 Basics

Let's start by compiling the `randomtest` utility (see Sec. 3.4.3) on a Sun system. To use other systems, replace `SUN` with the appropriate symbol from the above list.

First, change to the main DEGAS 2 directory and create the `SUN` subdirectory:

```
cd ~/degas2
mkdir SUN
cd SUN
cp ../src/Makefile .
```

Once the Makefile is present here, it will “update itself” with respect to the copy in the `src` directory when needed. To get an idea of how `ftangle` works, just “make” the main FORTRAN file for `randomtest`:

```
gmake randomtest.f
```

At some point, you may want to visually compare this file with the original source code `randomtest.web` (in the `src` directory, with the other source files) to gain an appreciation for the amount of work the FWEB macros do in DEGAS 2. For more information on these macros, see the documentation in `array.hweb` and the other header files.

Now, finish making `randomtest`:

```
gmake randomtest
```

To run `randomtest`, just type

```
./randomtest
```

The output to the right of the “=” sign should match the numbers in parentheses.

### 3.6.2 Making Documents

Generating “woven” (i.e., using FWEB’s `fweave` utility) documentation is similar:

```
cd ~/degas2
mkdir tex
cd tex
cp ../src/Makefile .
gmake randomtest.dvi
```

The DVI file can then be printed or viewed (using `xdvi`), as desired. In fact, the Makefile also provides additional “targets”, e.g., `randomtest.print` (uses `lpr` to print to your default printer), `randomtest.view` (launches `xdvi`) for you, and `randomtest.ps` (a PostScript file generated via `dvips`). You can generate woven documents for all of the “.web” source files. For some of the more useful ones, see Sec. 3.13.

You could also just generate the  $\text{\TeX}$  file (again, from the `degas2\tex` directory),

```
gmake randomtest.tex
```

You could then use `latex`, `pdflatex`, or whatever other  $\text{\TeX}$  application you wished.

### 3.6.3 Adjustments to Makefile

A number of the default settings in the Makefile can be overridden by placing the desired values in a file called `Makefile.local` in the working (e.g., `SUN`) directory. Some of the more frequently changed variables are:

- `DEBUG=no` turns on optimization. The default `DEBUG=yes` is required for debugging.
- `DEGASROOT=somedir` will tell Makefile to find the main DEGAS 2 directory at `somedir/degas2`. `somedir` should be an absolute path name. E.g.,

```
DEGASROOT = /u/somedir
```

- `FORTTRAN90=yes` switches from using the default FORTRAN 77 compiler to FORTRAN 90. Be aware that only some of the FORTRAN 90 compilers available work satisfactorily. Some will compile the code, but run slowly. Others will not work at all.
- `FCF77`, `FCF90` tell Makefile which “normal” (non-MPI) compiler to use.
- `MPI=yes` will enable the MPI commands in the source code and direct the Makefile to use the MPI compiler flags.
- `FCMPI77`, `FCMPI90` tell Makefile which MPI compliant compiler to use.
- `NETCDFV2=yes` tells DEGAS 2 that your system has only the older version 2 of the netCDF library (by default, DEGAS 2 expects version 3).
- The Makefile will accommodate more than one working directory on a given machine provided the additional directory has a name like `SUN-junk`, where “junk” is some string meaningful to you.
- If you would like to have more than one source directory, we recommend creating a new `degas2` directory hierarchy somewhere else in your file system and use the `DEGASROOT` variable to get the Makefile working there (you can set up symbolic links to common directories such as `data`).

### 3.6.4 Cross-Compiling

As an example of how to cross-compile, here are the procedures for making `randomtest` on the NERSC Crays. This assumes that you have access to AFS from your local workstation (and at NERSC, of course):

```
mkdir <some-afs-directory>/degas2/CRAY
ln -s <some-afs-directory>/degas2/CRAY ~/degas2/CRAY
cd ~/degas2/CRAY
cp ~/degas2/src/Makefile .
gmake randomtest
```

This will use `ftangle` on the local workstation to generate the FORTRAN source code files from the FWEB files in the `src` directory. It is advisable to set up a `Makefile.local` (see Sec. 3.6.3) in this directory that contains the same flags that will be used on the remote machine, particularly `DEBUG`, `FORTTRAN90` and `MPI`.

Then, log on to the remote machine and do:

```
ln -s <some-afs-directory>/degas2 ~/degas2
cd <some-work-directory>/CRAY
cp ~/degas2/CRAY/Makefile .
make randomtest
```

In addition to the usual variables in `Makefile.local`, one needs to add `STANDALONE=no`. This will tell `make` that the FORTRAN (e.g., `.f`) files have already been generated on your local workstation, and that it can find them in `~/degas2/CRAY` on the remote machine, which should be linked back to your local workstation via AFS.

The `degas2/data` directory will likely also be needed on the remote machine. You can manually copy the directory and its contents to the remote machine (e.g., via `ftp`) or keep a copy in the AFS directory and use a link to allow the code on the remote machine to find the files. E.g., for the second option, starting on the local workstation:

```
cd ~/degas2
cp -R data <some-afs-directory>/degas2
```

And on the remote machine

```
cd <same-work-directory>
ln -s <same-afs-directory>/degas2/data data
```

Be aware that in either case, the `data` directory could eventually get out of sync with the one on your local workstation. If this is a likely possibility, one could consider also linking the `data` directory on the local workstation to the one in the AFS directory, making the latter the only real copy.

### 3.6.5 Miscellaneous Targets

The Makefile provides some other occasionally useful targets. Please see the Makefile for more details.

- `clean` removes source, object, and other unessential files. This is pretty thorough and indiscriminate; use with caution.
- `TAGS` updates the Emacs tags table (see Sec. 3.2.1). You may need to do this if you substantially altered any of the source files or have other reason to believe that the tags table is out-of-date. You would run `gmake TAGS` from the `src` directory only.
- `depend` updates the Makefile dependencies (in `Makefile.depends`). Do this if the header file dependencies of one or more executables have been changed or if you believe that the dependencies are out of date. Note that source code (i.e., object files) dependencies are explicitly stated in the Makefile and must be updated by hand.
- `foof` dumps out values of some of the internal Makefile variables. This is useful for debugging Makefile problems.

### 3.6.6 CVS Access to DEGAS 2

Properly privileged (in the UNIX sense) authors of DEGAS 2 will be given access to the CVS (see Sec. 3.2.4) repository for the code. With this access, one can obtain the latest version of the source with:

```
setenv CVSROOT /afs/pppl.gov/common/cvs
cd
cvs co degas2
```

(this will place the code in `~/degas2`; see also Sec. 3.6.3). Of course, the command setting the `CVSROOT` variable can be more conveniently executed from a login (e.g., `~/login`) or shell startup script (e.g., `~/cshrc`). The user will also have access to all older versions of the source and data files through the appropriate CVS commands. More importantly, the user will be able to *update* the CVS repository. For this reason, such access is controlled by the primary authors of DEGAS 2. Contact them if you feel that you can contribute to the DEGAS 2 source code (see Sec. 6.1).

## 3.7 Examples

The `examples` directory contains several documented DEGAS 2 examples, with input output, and auxiliary files. They are included not only for instructive purposes, but also for verifying that successive versions of the code give the same results. Namely, the user should be able to download the code and generate exactly (to within roundoff error) the results contained within each of the example subdirectories. Any discrepancies should be reported to the primary code authors (see Sec. 6.1).

### 3.7.1 Analytic fluid bench

This simple run demonstrates that DEGAS 2 matches the results of an analytic model in the fluid limit. More information on this comparison can be found in the IAEA proceedings[12] or on the Web as a PostScript or PDF file.

To run this example, follow these steps:

1. **Set source code switch.** The source code file `boxgen.web` has within it a few different settings available which can be selected by changing the value of the flag `BOXRUN`. With this file open in an editor, change the line

```
@m BOXRUN 0
```

so that it now reads

```
@m BOXRUN 32
```

Save the file and exit the editor.

2. **Switch to the example directory.** If the main DEGAS 2 directory sits within your home directory:

```
cd ~/degas2/examples/Analytic_fluid_bench
```

3. **Copy the degas2.in file into your working directory.** E.g., if you are working on a Sun,

```
cp degas2_boxgen.in ../../SUN/degas2.in
cd ../../SUN
```

(overwriting any degas2.in file you may have had there already!).

4. **Prepare reference data.** This example uses the standard reference data files in the data directory. Hence, this step can be skipped if those files have not been altered since you downloaded the code.

```
gmake datasetup
./datasetup
```

5. **Prepare problem data.** This and subsequent steps are *not* optional! Note that the degas2.in file points back to the examples directory for the problem input file (see Sec. 3.5.8).

```
gmake problemsetup
./problemsetup
```

6. **Generate geometry and background files.** The boxgen program takes care of both of these:

```
gmake boxgen
./boxgen
```

7. **Set the number of flights.** The background file bk\_boxgen.nc contains the specification of the number of flights to be run. Open this file in an editor (Emacs will be the most convenient) and find the line

```
source_num_flights = 100 ;
```

Change the “100” to either “1600” or “6400”. The example contains the output for both cases. Save the file and exit the editor.

**8. Set up the tallies.**

```
gmake tallysetup
./tallysetup
```

**9. Run the code.**

```
gmake flighttest
./flighttest
```

10. **Check the text output.** The file `density.out` can be directly compared with either `density_1600.out` or `density_6400.out`, depending on the number of flights. The numbers in here have only five digits of precision. If an exact match is not obtained, something is amiss. Please contact the code authors (see Sec. 6.1) if you feel that a problem exists with the code as you downloaded it.
11. **Check the binary output.** You can use the `matchout` utility (see Sec. 3.4.4) to do this.
12. **Compare with the analytic solution.** The file `soln_32` contains the columns:
- x** Distance along the problem space in meters.
  - N1(x)/N(0)** Relative density (to density at  $x = 0$ ) predicted by one analytic model (see the above references) solution.
  - N2(x)/N(0)** Relative density predicted by a second analytic model solution.
  - Ti(x)** Ion temperature profile.
  - Ni(x)** Ion density profile.
- The columns of the `density.out` file contain
- (a) First zone number. These zones correspond directly to the  $x$  values in the `soln_32` file.
  - (b) Second zone number. This is always 0 since this is a 1-D problem.

- (c) Neutral hydrogen density in  $\text{m}^{-3}$ . To normalize this column, divide the whole column by the value in the first row. Since this corresponds to the first value of  $x$  in `soln_32` and *not* to  $x = 0$ , multiply the whole column by the relative density from the analytic solution at the first value of  $x$ , normalizing the DEGAS 2 result to the analytic solution at one point.
- (d) Relative standard deviation of the neutral density (see Sec. 4.4).
- (e) Neutral hydrogen pressure in pascals.
- (f) Relative standard deviation of the neutral pressure.
- (g) The last two columns are no longer used and should be filled with zeroes.

### 3.7.2 Neutral-Neutral Scattering Examples

The initial implementation of the BGK algorithm for handling neutral-neutral collisions (see Sec. 2.8.2) in EIRENE has been tested by comparison with analytic expressions for the time dependence of the relaxation of a distribution function (both in self-collision and mixed-species collision systems) and against models describing the Couette flow problem.[32] The relaxation benchmarks have been repeated with DEGAS 2, but have not been formally made into an example run and will not be discussed here. Further details can be provided upon request. However, the Couette flow problem can be set up with only a few minor modifications to the code and does make a suitable example.

#### Couette Flow

The Couette flow problem of fluid mechanics involves the flow of fluid between two parallel, sliding plates. The fluid is assumed to have “no slip” boundary condition at the plates. The viscosity of the fluid drags along adjacent fluid elements, resulting in a velocity gradient between the boundary velocities represented by the two plates.

In this example, two semi-infinite plates are a distance  $d$  apart in the  $x$  direction. At present, the plates have a finite extent in the  $z$  direction with mirror boundary conditions at  $z_{\min}$  and  $z_{\max}$ . Periodic boundary conditions are enforced in the  $y$  direction so that the problem is effectively infinite in that direction. Eventually, the  $z$  direction will also have periodic boundary conditions. Particles are

initialized at the  $x = 0$  plate with a thermally distributed velocity to which a constant velocity in the  $y$  direction,  $v_{y0}$ , is added; this represents the velocity of the plate. The second plate at  $x = d$  is treated as stationary. Particles striking it are assumed to be re-emitted with a thermal distribution pointed in the  $-x$  direction. Particles striking the  $x = 0$  plate are absorbed. Hence, in the no collision limit, particles make only one round trip across the box.

The choice of the distributions used at the plates is crucial to reproducing the analytic models. In particular, the ‘‘Maxwell flux’’ distribution [10] must be used. This distribution describes a recycling thermal flux of particles moving in a particular direction (in this case, perpendicularly away from the wall). This is the distribution used in some of the PMI data files, such as in `h2_des_maxw_mo`. In this example, however, the distributions of the particles coming off of the two plates are enforced through hardwired code, not through the data files.

The initial velocity is chosen from the distribution

$$Q(\vec{v}) \propto v_x \exp \left\{ -\frac{m}{2kT} [v_x^2 + (v_y - v_{y0})^2 + v_z^2] \right\}. \quad (3.1)$$

Note the plate velocity  $v_{y0}$  in the exponent. For particles ‘‘reflected’’ at the  $x = d$  surface,  $v_{y0} \equiv 0$ . This is just a thermal (Maxwellian) distribution multiplied by  $v_x$ , the velocity in the direction normal to the surface and is required for describing sources that simulate a recycling process.

A brief digression will clarify the relationship between this *source* distribution and the thermal distribution that characterizes the particles in the volume of the fluid. Consider the number of particles of arbitrary volume distribution  $f$  that recycle at, say, the  $x = 0$  surface in a time interval  $\Delta t$  (a source distribution specifies a density in phase space per unit time). For particles in the velocity interval  $v_x \rightarrow v_x + dv_x$ , this is  $f dv_x A \Delta x$ , where  $A$  is the area of the recycling surface and  $\Delta x = v_x \Delta t$  is the distance over which particles with velocity  $v_x$  can reach  $x = 0$  in  $\Delta t$ . So, the phase space density of the recycling particles per unit time (dividing this number by  $\Delta t$  and  $dv_x$ ) is  $\propto v_x f$ . Another way of saying this same thing is that the source needs to emphasize the faster particles in the distribution since more of them will reach the recycling surface in a given time interval. One upshot is that the average energy of the source particles is  $\langle E \rangle_{\text{source}} = 2T$  while the average energy in the volume (for  $v_{y0} = 0$ ) is the familiar  $3/2T$ .

For clarity, we note that the volume distribution function in the free-molecular limit is

$$f(\vec{v}) = f_+(\vec{v}) + f_-(\vec{v}), \quad (3.2)$$

$$f_+(\vec{v}) = \frac{n}{2} \left( \frac{m}{2\pi T} \right)^{3/2} \exp \left\{ -\frac{m}{2T} [v_x^2 + (v_y - v_{y0})^2 + v_z^2] \right\}, \quad v_x > 0 \quad (3.3)$$

$$f_-(\vec{v}) = \frac{n}{2} \left( \frac{m}{2\pi T} \right)^{3/2} \exp \left[ -\frac{m}{2T} (v_x^2 + v_y^2 + v_z^2) \right], \quad v_x < 0 \quad (3.4)$$

With this distribution, one can show that the fluid pressure is

$$P = \frac{2}{3} \langle nE \rangle = nT + \frac{1}{6} m v_{y0}^2. \quad (3.5)$$

The fluid velocity is

$$\begin{aligned} \langle \vec{v} \rangle &= \langle \vec{v} \rangle_+ + \langle \vec{v} \rangle_- \\ &= \frac{1}{2} v_{y0} \hat{y} + 0, \end{aligned} \quad (3.6)$$

so that  $|\langle \vec{v} \rangle| = v_{y0}/2$ . To compute the fluid temperature used in the BGK distributions, we need to subtract the drift energy,

$$T = \frac{P}{n} - \frac{1}{3} m \langle \vec{v} \rangle^2 \quad (3.7)$$

$$= T + \frac{1}{12} v_{y0}^2. \quad (3.8)$$

The primary physical quantity appearing in the analytic models[39, 40, 41] of Couette flow is the x-y component of the stress tensor,

$$\Pi_{xy} \equiv \int d^3v \, m v_x v_y f(\vec{v}) - nm U_x U_y, \quad (3.9)$$

where  $\vec{U}$  is the first (velocity) moment of  $f$  (the flow velocity). Note that while we should have  $U_y \neq 0$ ,  $U_x$  should be identically 0 since there is no net flow in the  $x$  direction. In the molecular-flow regime, the distribution function is not changed by collisions as the particles move across the box. Furthermore, particles coming from the  $x = d$  side of the box make no net contribution to  $\Pi_{xy}$  (since the integrand is an odd function of  $v_y$ ). Inserting Eq. (3.3), we find

$$\Pi_{xy}^{\text{fm}} = \frac{nm}{4} \left( \frac{8T}{\pi m} \right)^{1/2} v_{y0}. \quad (3.10)$$

As collisions become more important, the plate velocity information is dissipated into random motions of the fluid to a greater and greater extent, and  $\Pi_{xy}$  falls below  $\Pi_{xy}^{\text{fm}}$ .

The variational theory of Cercignani[40, 41] yields a relatively compact formula for  $\Pi_{xy}$  that matches the numerical results of Willis[39] to within 0.5%. With  $\delta = 1/K_n$ ,

$$\frac{\Pi_{xy}}{\Pi_{xy}^{\text{fm}}} = \frac{a + \sqrt{\pi}\delta}{a + b\delta + c\delta^2}, \quad (3.11)$$

where for the case of a BGK collision operator,

$$\begin{aligned} a &= \frac{4 - \pi}{\pi - 2} \\ b &= \frac{\pi^{3/2}}{2(\pi - 2)} \\ c &= 1. \end{aligned} \quad (3.12)$$

The  $x$ - $y$  component of the stress tensor is computed along with other test particle data during tracking. However, final processing of that information into a usable form is only done when the COUETTE macro is enabled in `flighttest.web`.

The Couette flow problem can be simulated in DEGAS 2 with only a few code modifications to set up the required boundary conditions (at the moment, the required particle distributions cannot be specified completely by input or data files). Because the problem is relatively simple, it represents a good starting point for learning how to use neutral-neutral collisions in DEGAS 2.

Most of these changes are invoked with a COUETTE FWEB macro inserted into the files

To run this example, follow these steps:

1. **Set source code switches.** The source code file `boxgen.web` has within it a few different settings available which can be selected by changing the value of the flag `BOXRUN`. With this file open in an editor, change the line

```
@m BOXRUN 0
```

so that it now reads

```
@m BOXRUN 41
```

Save the file and exit the editor. The files `plate.web`, `sources.web`, and `flighttest.web` each have the line

```
@m COUETTE 0
```

near the top. Edit these files, changing the “0” to a “1” in each case (be sure to revert to the default setting of “0” before running other problems).

2. **Switch to the example directory.** If the main DEGAS 2 directory sits within your home directory:

```
cd ~/degas2/examples/Couette_flow
```

3. **Copy the degas2.in file into your working directory.** E.g., if you are working on a Sun,

```
cp degas2.in ../../SUN/degas2.in
cd ../../SUN
```

(overwriting any degas2.in file you may have had there already!).

4. **Prepare reference data.** This example uses some nonstandard data files so, unlike the previous example, datasetup must be run. Note that the degas2.in file points back to the examples directory for the input files needed here and in subsequent steps.

```
gmake datasetup
./datasetup
```

5. **Prepare problem data.**

```
gmake problemsetup
./problemsetup
```

If you look at the problem input file, you will see that there is only one reaction, that for the neutral-neutral collisions. Note also that the test species D2 also appears in the list of background species (the usual background species e and D+ appear here just because boxgen expects them to be there; they are not used in this simulation).

6. **Generate geometry and background files.** The boxgen program takes care of both of these (be sure that the BOXRUN macro has been set to 41):

```
gmake boxgen
./boxgen
```

7. **Set the number of flights.** The background file `bk_boxgen.nc` contains the specification of the number of flights to be run. Open this file in an editor (Emacs will be the most convenient) and find the line

```
source_num_flights = 100 ;
```

The results in this directory were obtained with 10 BGK iterations of 4000000 flights each. Such a run could easily require more than a day if run on a single processor (this run was executed in about an hour using 14 400 MHz Pentium PCs). You can probably run a smaller number of flights (say, 100000) and still get reasonable results. Save the file and exit the editor.

8. **Set up the tallies.**

```
gmake tallysetup
./tallysetup
```

9. **Run the code.**

```
gmake flighttest
./flighttest
```

The number of BGK iterations is controlled by the value of the `bgk_max` macro in `flighttest.web`. The value used here is 10. If you just want to get an idea of how the calculation proceeds, you can choose a smaller number. Note that the macro parameters controlling the convergence tests, `bgk_cvg_dens` and `bgk_cvg_pres`, are set to ridiculously small values ( $10^{-8}$ ) to ensure that all 10 iterations are completed.

10. **Check the text output.** At each iteration, the code writes out the test species density and other data in a file with a name of the form `densityxx.out` where `xx` is replaced by the iteration number. The contents of these files are analogous to those of the other examples (the density and pressure for each zone are in the third and fifth columns, respectively; see the description in Sec. 3.7.1), except for the last two columns. These are normally not used; here, they contain the values and standard deviations of the  $x$ - $y$  stress tensor,  $\Pi_{xy}$ . The comparison of those values with theory will be discussed below.

At the end of each iteration, the background netCDF file (`bk_bgktest.nc`) is also updated (overwritten) with the density, velocity, and temperature of the neutral background species. A third file, `cvg_global.txt`, will provide information on the global progress of the BGK iterations towards convergence. The four columns are:

- (a) Iteration number,
- (b) Test species number,
- (c) Global fractional change in density (dimensionless); this is compared with `bgk_cvg_dens` to decide whether or not to stop the iterations.
- (d) Global fractional change in pressure. (dimensionless); this is compared with `bgk_cvg_pres` to decide whether or not to stop the iterations.

Note that on most machines this file does not appear until the unit is closed at the end of the run.

These files can be directly compared with the corresponding files in the `examples` directory. If you have repeated the run at the above-described length, you should be able to match the text files exactly. The level of agreement in the netCDF file should be several digits (perhaps as many as 10). If a satisfactory match is not obtained, something is amiss. Please contact the code authors (see Sec. 6.1) if you feel that a problem exists with the code as you downloaded it.

11. **Check the binary output.** You can use the `matchout` utility (see Sec. 3.4.4) to do this. Again, you should expect the largest differences to be  $\sim 10^{-8}$  or better.
12. **Compare with the analytic solution.** The rightmost set of data in the `densityxx.out` file are the stress tensor values,  $\Pi_{xy}$ . Ideally, these are constant across the problem space. Some deviation exists here due to Monte Carlo noise. You can compute the free molecular value from Eq. (3.10). With both of these numbers in hand, you can compare with Eq. (3.12). To do that, you need to know  $\delta$ . The explicit formula used is

$$\delta = \frac{n\langle\sigma v\rangle d}{\sqrt{2T/m}}, \quad (3.13)$$

where  $n = 10^{20} \text{ m}^{-3}$  (enforced in `flighttest.web` by code enabled with the `COUETTE` macro),  $\langle \sigma v \rangle = 1.1 \times 10^{-16} \text{ m}^3/\text{s}$  (from the `d2d2_bgktest.nc` file),  $d = 0.1 \text{ m}$  (set in `boxgen.web`), and  $m = m_{\text{D}_2} = 6.689 \times 10^{-27} \text{ kg}$  (also from `boxgen.web`). One would expect the temperature  $T$  of the fluid to be equal to that of the wall by virtue of the initial conditions. However, in cases where the energy associated with the plate velocity  $v_{y0}$  is significant compared with  $T_{\text{wall}}$ , the actual temperature of the fluid is slightly higher than that of the wall as is indicated by Eq. (3.8). In fact, this example with  $v_{y0} = 1000 \text{ m/s}$  shows better agreement with the theoretical result Eq. (3.12) if  $T$  is set to the simulated fluid temperature (e.g., from the `bk_bgktest.nc` file).

With  $T = T_{\text{wall}} = 0.0258 \text{ eV} = 4.1336 \times 10^{-21} \text{ J}$ , we find  $\delta_{\text{wall}} = 0.9894$ . Plugging this into Eq. (3.12),

$$\left( \frac{\Pi_{xy}}{\Pi_{xy}^{\text{fm}}} \right)_c (\delta_{\text{wall}}) = 0.6047. \quad (3.14)$$

The free-molecular stress, Eq. (3.10), is  $\Pi_{xy}^{\text{fm}}(T_{\text{wall}}) = 0.20978 \text{ Pa}$ . If we average the 10 values for  $\Pi_{xy}$  in the `density10.out` file, we get  $\Pi_{xy,\text{sim}} = 0.13051 \text{ Pa}$  and

$$\left( \frac{\Pi_{xy}}{\Pi_{xy}^{\text{fm}}} \right)_{\text{sim}} = 0.6215. \quad (3.15)$$

This would qualify as pretty good agreement. However, if we average the fluid temperature values in the `bk_bgktest.nc` file, we get  $T_{\text{sim}} = 4.5866 \times 10^{-21} \text{ J}$ . Then,  $\delta_{\sim} = 0.9393$ , and

$$\left( \frac{\Pi_{xy}}{\Pi_{xy}^{\text{fm}}} \right)_c (\delta_{\text{sim}}) = 0.6157, \quad (3.16)$$

about a factor of two better agreement. Now, one might argue that we should also use  $T_{\text{sim}}$  in computing  $\Pi_{xy}^{\text{fm}}$ . However, the free-molecular stress, Eq. (3.10) was computed directly from the general distribution function for arbitrary  $v_{y0}$  so that  $T = T_{\text{wall}}$  in that formula, without any ambiguity. Qualitatively speaking, for small  $\delta$  the character of the source distribution dominates. As  $\delta$  approaches or exceeds 1, the temperature of the fluid in the volume,  $T_{\text{sim}}$  computed from Eq. (3.8), better describes the distribution. The better agreement is shown over a range of inverse Knudsen numbers and two values of  $v_{y0}$  in Fig. 3.1.

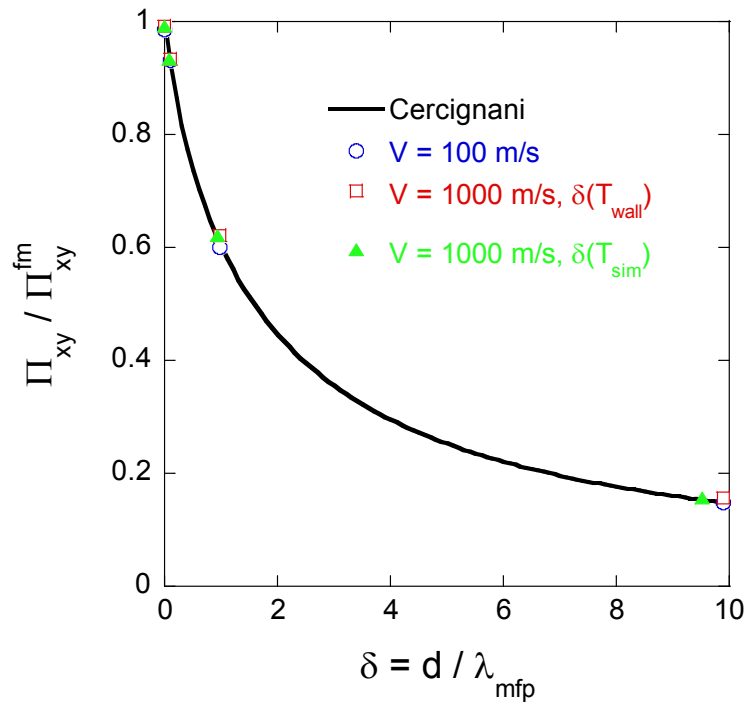


Figure 3.1: Comparison of 8 DEGAS 2 simulations (symbols) of the Couette flow problem with the analytic expression for the normalized shear stress Eq. (3.12) obtained by Cercignani[40, 41]. Two different plate velocities  $V = v_{y0}$  were used in the simulations. For the higher velocity, better agreement with the analytic expression is obtained if the inverse Knudsen parameter is computed from the actual fluid temperature from the simulation,  $T_{\text{sim}}$ , rather than the wall temperature,  $T_{\text{wall}}$ .

## C-Mod 1-D: Conservation Checks

This example demonstrates a run with complete hydrogen physics in a simple geometry. In particular, this run includes both neutral-ion and neutral-neutral elastic scattering processes. The complexity of the physics also makes for a good demonstration of DEGAS 2's conservation checks.

Experiments by Pitcher et al. [48, 49] on the Alcator C-Mod tokamak indicated that the flow of neutral gas through material structures around the plasma was being limited by its diffusion rate through the divertor plasma. Pitcher [49] developed a semi-analytic model that reproduced this behavior. An attempt was made to precisely reproduce the results of that model with DEGAS 2. The overall effort consisted of several simulations in which the model assumptions were gradually relaxed towards those consistent with normal DEGAS 2 operation. This example is from a simulation in having atomic and surface physics assumptions more like a normal DEGAS 2 run. The remaining difference from a “full physics” DEGAS 2 run (apart from the greatly simplified geometry) is that the neutral source is a gas puff rather than a recycling source. The full physics and geometry simulations are described in Ref. [50].

To run this example, follow these steps:

1. **Set source code switch.** The source code file `boxgen.web` has within it a few different settings available which can be selected by changing the value of the flag `BOXRUN`. With this file open in an editor, change the lines

```
@m BOXRUN 0
@m SOLN 1
```

so that they now read

```
@m BOXRUN 40
@m SOLN 0
```

Save the file and exit the editor. The second parameter disables the analytic solutions that are used in the original `boxgen` example (Sec. 3.7.1).

2. **Switch to the example directory.** If the main DEGAS 2 directory sits within your home directory:

```
cd ~/degas2/examples/CMod-1D
```

3. **Copy the degas2.in file into your working directory.** E.g., if you are working on a Sun,

```
cp degas2.in ../../SUN/degas2.in
cd ../../SUN
```

(overwriting any degas2.in file you may have had there already!).

4. **Prepare reference data.** This example uses some nonstandard data files so, unlike the previous example, datasetup must be run. Note that the degas2.in file points back to the examples directory for the input files needed here and in subsequent steps.

```
gmake datasetup
./datasetup
```

5. **Prepare problem data.**

```
gmake problemsetup
./problemsetup
```

6. **Generate geometry and background files.** The boxgen program takes care of both of these. Be sure the BOXRUN macro was set to 40:

```
gmake boxgen
./boxgen
```

7. **Set the number of flights.** The background file bk\_boxgen.nc contains the specification of the number of flights to be run. Open this file in an editor (Emacs will be the most convenient) and find the line

```
source_num_flights = 40000 ;
```

Save the file and exit the editor.

8. **Set up the tallies.**

```
gmake tallysetup
./tallysetup
```

## 9. Run the code.

```
gmake flighttest
./flighttest
```

The code will execute 5 iterations automatically, each with 40,000 flights. The number of BGK iterations is controlled by the parameter `bgk_max` in `flighttest.web`; the default setting is 5. The BGK iterations can alternatively be controlled by the convergence parameters `bgk_cvg_dens` and `bgk_cvg_pres`. The corresponding tests monitor global measures of the changes in the density and pressure of the BGK species. Note that these can be satisfied only if there are sufficiently many flights to achieve a correspondingly high precision in the local density and pressure values, no matter how many BGK iterations are run. In this example, the parameters chosen are such that `bgk_max` will be governing the number of iterations.

10. **Check the text output.** At each iteration, the code writes out the test species density and other data in a file with a name of the form `densityxx.out` where `xx` is replaced by the iteration number. The contents of these files are analogous to those of the other examples (the density and pressure for each zone are in the third and fifth columns, respectively; see the description in Sec. 3.7.1).

At the end of each iteration, the background netCDF file (`bkoned.nc`) is also updated with the density, velocity, and temperature of the neutral background species. This file can be used to restart the BGK iterations, e.g., with an increased number of flights. A third file, `cvg_global.txt`, provides information on the global progress of the BGK iterations towards convergence. The four columns are:

- (a) Iteration number,
- (b) Test species number,
- (c) Global fractional change in density (dimensionless); this is compared with `bgk_cvg_dens` to decide whether or not to stop the iterations.
- (d) Global fractional change in pressure. (dimensionless); this is compared with `bgk_cvg_pres` to decide whether or not to stop the iterations.

Note that on most machines this file does not appear until the unit is closed at the end of the run. The output netCDF file from this run is included as well.

These files can be directly compared with the corresponding files in the `examples` directory. The numbers in the text files have only five digits of precision and should be matched exactly. The level of agreement in the netCDF file should be several digits (perhaps as many as 10). If a satisfactory match is not obtained, something is amiss. Please contact the code authors (see Sec. 6.1) if you feel that a problem exists with the code as you downloaded it.

11. **Check the binary output.** You can use the `matchout` utility (see Sec. 3.4.4) to do this. Again, you should expect the largest differences to be  $\sim 10^{-8}$  or better.
12. **Examine test particle balances** To simplify examination of the conservation checks, an input script for the `outputbrowser` code is included, `bgkbalances`. The results are in `bgkbalances.out`. The checks can be performed for the density, momentum, and energy of each of the test species. Since D2+ does not move, the checks on it are satisfied trivially and are not considered further.<sup>1</sup> For each quantity, the procedure consists of totaling the negative of the quantity lost to the walls (the "current out" tally), the quantity coming in from the walls (the "current in" tally), and the "source rate" tally. The last item is further broken down by reaction (or source) to provide an indication of the relative importance of each process. For this example, we consider only the *X*-component of the momentum (dimension #1) since the problem does not vary in the other two directions. For this case, the following totals are obtained:

### particles

$$D \quad 5 \times 10^{16}$$

---

<sup>1</sup>In fact, the values of the "total" tallies for D2+ are all determined by roundoff errors. For this reason, you will not likely match these values exactly. You should convince yourself that they are numerically much smaller than the other totals. If you use `matchout` to compare with the reference output netCDF file, these D2+ totals will also stand out as apparently significant discrepancies.

$$D_2 \ 3 \times 10^{15}$$

**momentum 1**

$$D \ -4 \times 10^{-7}$$

$$D_2 \ -2 \times 10^{-8}$$

**energy**

$$D \ 4 \times 10^{-2}$$

$$D_2 \ -4 \times 10^{-3}$$

In addition, a global check involving the background particle number can be performed:

$$\begin{aligned}
 &+ \text{ Total source of deuterium atoms (the puff source),} \\
 &\quad +4.0 \times 10^{21} \\
 &- \text{ Total number of deuterium atoms lost to the walls,} \\
 &\quad -(3.36841 \times 10^{22} + 2. \times 3.95601 \times 10^{21}) \\
 &\quad +(3.12591 \times 10^{22} + 2. \times 4.58939 \times 10^{21}) \\
 &- \text{ Total number of deuterium atoms lost to the plasma (D+ source rate),} \\
 &\quad -2.84170 \times 10^{21} \\
 &= 6. \times 10^{16}
 \end{aligned}$$

There should always be a small remainder in the energy and momentum balances; its magnitude appears to roughly coincide with the accuracy provided by `outputbrowser`. This remainder results from the enforcement of a

minimum weight via Russian roulette in subroutine `follow`. By default, that minimum weight is  $10^{-3}$  of the initial weight. The Russian roulette procedure is set up so as to not lose mass. However, it will conserve momentum and energy only on the average (i.e., after many flights). You can demonstrate this effect by reducing the minimum weight (`WMIN` in `flight.web`) to, say,  $10^{-7}$ . Doing so will make the run substantially longer. To see the difference in the conservation checks, you may need to examine the output `netCDF` file directly (hint: run `outputbrowser` first to get “rough” values for these quantities and then use the search facility in Emacs to locate the corresponding data in the output `netCDF` file).

13. **Transfers between BGK species.** In looking at the energy and momentum transfers between BGK species, you should notice that no sources appear for the background partners. The reason for this is that the transfers to and from these species do not have a clear physical meaning; all relevant information can be obtained from the corresponding test species.

However, the transfers between BGK test species, say between D and D2 here, are significant. The process `d2d_neut` (see the “momentum source vector by reaction” and “energy source by reaction” sections of `bgkbalances.out` under reaction 11) transfers energy and momentum between the background D2 and the test D (problem species, “`problem_sp`”, number 6); likewise, `dd2_neut` (reaction number 12) connects the background D and test D2 (`problem_sp` 7). One would expect that in a converged state these two transfer rates would be equal (this actually goes into the derivation of the algorithm). In this example, they are (to within the error bars),

mom. 1 to D: $-9.39835 \times 10^{-3}$	mom. 1 to D2: $+9.19450 \times 10^{-3}$
energy to D: $-4.21074 \times 10^2$	energy to D2: $+4.13512 \times 10^2$

(The molecules come off the wall at low energy and are being heated by the warmer atoms that arise from elastic scattering with the plasma ions and from dissociation.)

For this to occur, the reaction rate for these two processes must be numerically identical. The original implementation of the BGK algorithm in EIRENE had the same temperature dependent expression for the two rates. However, because the temperatures of D2 and D species are different in

general, the resulting rates had different numerical values. The initial implementation of the BGK algorithm in DEGAS 2 repeats this same mistake.

To see the difference, you can modify the `degas2.in` file to point to the `reactions.input` and `reactions.nc` files in the data directory.

When you run the code again (you at least need to rerun `problemsetup` first), you will find something like the results contained in `bgkbalances_default.out`:

mom. 1 to D: $-4.71320 \times 10^{-3}$	mom. 1 to D2: $+7.04233 \times 10^{-3}$
energy to D: $-2.04504 \times 10^2$	energy to D2: $+3.36294 \times 10^2$

This error in the default rates will be corrected in a subsequent version of the code.

- Other results.** For reference purposes, this directory contains output files from a single iteration (on a Sun with `DEBUG=yes`) with 1000 flights. These output files contain the string `1K`. The primary purpose of these files is to serve as a known, reproducible point of contact for testing subsequent code modifications. It also demonstrates that these conservation checks hold even if the code is run with relatively few flights. To duplicate these files, you will need to stop the BGK iteration process after the first (zeroth, actually) iteration. The easiest way to do this is to insert the line:

```
bgk_iteration=FALSE
```

as the last executable statement in subroutine `bgk_test` near the end of `flighttest.web`.

You may notice that the tallies used for the conservation checks predominantly utilize collision estimators while the standard (zone-resolved) tallies are based on track length estimators. The reason is that the former will explicitly demonstrate conservation of mass, momentum, and energy since they are computed using the instantaneous test particle attributes. The track length estimators will generally provide more accurate values for the code output, but will exhibit conservation only in a statistical sense. You can demonstrate this by replacing the estimator lists in each of the “total” tallies with the lists from the corresponding zone-resolved tallies.

## 3.8 Run Control Parameters

Several run control parameters are contained in the `sources` class. Ideally, these would be set by the user in a dialog box just prior to the run. For now, they must be changed manually by editing the background netCDF file. The following subsections describe the features, roughly in order of usefulness to the average user:

### 3.8.1 Checkpoints

By default, the DEGAS 2 output netCDF file is written only at the end of the run. Each source group can be broken up into an integral number of pieces with an intermediate output file being written after each such checkpoint. The array `so_chkpt (grp)` contains the number of checkpoints for source group `grp`. If `so_chkpt (grp)` is 0, no file is written. If 1, an intermediate output file will be written at the end of the source group, and so on.

The intermediate output file does not contain post-processed results and cannot be used with post-processing utilities. The raw data there are suitable only for a restart of the code.

### 3.8.2 Restarting

The two main uses of the restarting capability are

1. To complete an interrupted (and checkpointed) run without having to restart from the beginning,
2. To increase the number of flights in a run to improve statistics.

In both cases, the user needs to change the value of the flag `so_restart` from its default value of `FALSE` (represented by 0 in the background netCDF file) to `TRUE` (1). The code will expect to find an existing output file, with the name specified in the `degas2.in` file. This can be either an intermediate output file from a checkpoint or a completed one generated at the end of a run.

The restarted run will extend the number of flights to the value specified in the background netCDF file (by `so_nflights`). A few different situations may arise:

1. If the number of flights is the same as those in the output file, no additional flights are run. This feature permits the data in an intermediate output file to be post-processed into a “completed” output file.
2. If the previous checkpointed run was interrupted, the restarted run resumes from the point of the last checkpoint and completes the specified number of flights. The results should match those that would have been obtained if the run were to have run to completion on the first try.
3. If the user wishes to increase the number of flights for the *last* source group of a completed run, the code will compute the required number of flights. The results will be the same as if the flights were all done at once.
4. If the user wishes to increase the number of flights in *more than one* source group, the code will extend the run accordingly. However, the results *will not* exactly match those obtained in a single run of the same length. The reason is that by default a run uses a continuous random number chain for all source groups. In a restart, that chain is resumed at its end. Hence, the first source groups will be using random numbers for these new flights different from those they would have had in a single run. Note that the resulting run should still be *statistically equivalent* to the single run. The “spaced seeds” option has been added to provide a workaround to this minor shortcoming of the restart procedure.

### 3.8.3 Seed String

Prior to version 2.6 of DEGAS 2, the initial random number seed was hardwired in `flighttest.web`. The user can now change the initial seed (and, hence, the entire random number chain) via `so_seed_string` in the background `netCDF` file.

The preferred mechanism for specifying the initial seed is as a character string. This is transformed into the appropriate integer representation using routines in `random.web` (see Sec. 2.5). The default value is “12”. Reasons to use different values include

1. An unexpected, but perhaps not statistically significant, result has been obtained. A repeat of the run with a different random number seed will aid in establishing the validity of the result,

2. The DEGAS 2 code package contains several tools for statistically analyzing results (e.g., `matchout` and `matcheir`). By changing the random number seed, the effectiveness of these statistical comparisons can be evaluated.

### 3.8.4 Spaced Seeds

If the user anticipates needing to extend a multiple source group run to a larger number of flights (e.g., to achieve a desired variance) and insists that the results match those of a single run, the flag `so_spaced_seeds` should be set to `TRUE` (1) in the initial run. With this option enabled, the code will set the initial seed for each source group to be 100000000 (set by `so_seed_spacing`) flights apart. Each source group in a restarted run will then be able to “pick up where it left off”, up to a total of 100000000 flights.

To minimize the chances of compromising the integrity of the random number chain, `so_spaced_seeds` should be left at its default `FALSE` (0) value, unless the user truly needs to be able to extend the run and match the single run results.

### 3.8.5 Direct Sampling

The default (random) method of sampling the initial particle source in DEGAS 2 leads to a source distribution that differs from the ideal, input distribution by a fraction of order  $1/\sqrt{N}$  ( $N$  being the number of flights). Yet, if we were to take those same  $N$  flights and divide them up by hand amongst the source segments, we would obtain an error of order  $1/N$ . Such an approach is impractical in general as it requires specifying the number of flights once and for all at the beginning of the run (a restart would not be possible) and the possibility of overlap in the initial source positions would arise if the number of flights were large enough.

An equally effective alternative can be developed based on hashing algorithms described by Knuth[47]. The idea is to replace the pseudo-random number  $\xi$  usually used in the source sampling process with

$$\xi = (x + i/\phi) \bmod 1, \tag{3.17}$$

where  $x$  is a single, fixed random number,  $i$  is the flight number, and

$$\phi^{-1} = \frac{\sqrt{5} - 1}{2} \tag{3.18}$$

is the golden ratio. This value yields the desired distribution properties (as can be verified using `sourcetest`), but minimizes the possibility of overlap by ensuring that  $\xi$  is far from low order rational numbers.

The sampling method used is governed by the flag `so_sampling`. The default value of `so_random` yields the usual random sampling procedure. This is the recommended value for most applications. The new, direct sampling method is selected by setting `so_sampling` to `so_direct`. This method was installed to see if it would lead to more efficient iterations in coupling DEGAS 2 to plasma transport codes.

## 3.9 Adding Reactions and PMI

### 3.9.1 Overview of Data Format

The same, basic approach is used to store all reaction- and PMI-related data in DEGAS 2. First, the data for each reaction or PMI is stored in its own netCDF file. That file contains:

1. Name of reaction,
2. Number of dependent variables,
3. Organization of data for each dependent variable (“table” or “fit”),
4. Rank of each dependent variable (number of independent variables),
5. Character name for each dependent and independent variable,
6. Number of values of each independent variable (for tabular data),
7. Data table, a single one-dimensional array. Indices into this array are computed on the fly based on the number of values used for each independent variable.

For more details, see the description of the cross section class. The corresponding information for PMI is in the description of the PMI format class.

The only general tool available for creating new data files is `ratecalc` (see Sec. 3.4.2 and the `ratecalc` file itself). Example input files for `ratecalc` can be found in the `data` directory. Two other routines `reactionwrite` and

`pmiwrite` (again see Sec. 3.4.2) read existing text files and write the data out into `netCDF` files. These two routines can be used as examples for generating specific data files.

At run time, all of the reaction data files specified in the problem input file (see Sec. 3.5.8) (and only those) are read in. The reaction rates (for PMI, the corresponding quantity is termed the “yield”) and the descriptions of their independent variables and other characteristics are compiled into one set of arrays. The information is organized in a similar manner to that of the original data files, but with an additional index corresponding to the problem reaction number. Additional processing is done to replace character strings with integer indices, to make for more efficient searches. Again, all of the actual reaction rate data values are stored as a single 1-D array with macros used to provide simple access to individual entries for a particular reaction. The reaction rate is used in computing the current mean free path of the flight and in choosing amongst the flight’s possible reactions when a collision is indicated.

All other data present in the reaction data files is compiled into a set of “handling” arrays, indicating that their primary purpose is to control the specification of collision product velocities for that reaction. In addition to an index for problem reaction number, there is one for dependent variable number. The collision routines will search these data arrays for required information and will stop code execution (in `DEBUG` mode, anyway) if they are not found. The flow of data through the various `DEGAS 2` classes is shown in Fig. 3.2.

The data format, evaluation routines, and scoring mechanisms are designed so that specific quantities can be scored just by adding the appropriate data to the data file and creating a corresponding tally with that quantity as the dependent variable.

One aspect unique to the PMI is that specification of the outgoing velocity distribution necessarily involves a “fit” since standard `FORTRAN` will not permit a function (in this case, the function which interpolates the data tables) to return a vector.

### 3.9.2 An Example: Bateman Format Data

A particularly involved example of a PMI is the specification of “Bateman format” data[3, 44]. A few uses of this for reflection processes are currently in the code. A large set of data for PMI in an improved version of this format will soon be added.

For each incident energy and polar angle pair,  $(E_{in}, \theta_{in})$ , we have a conditional

## DEGAS 2 PHYSICS CLASSES

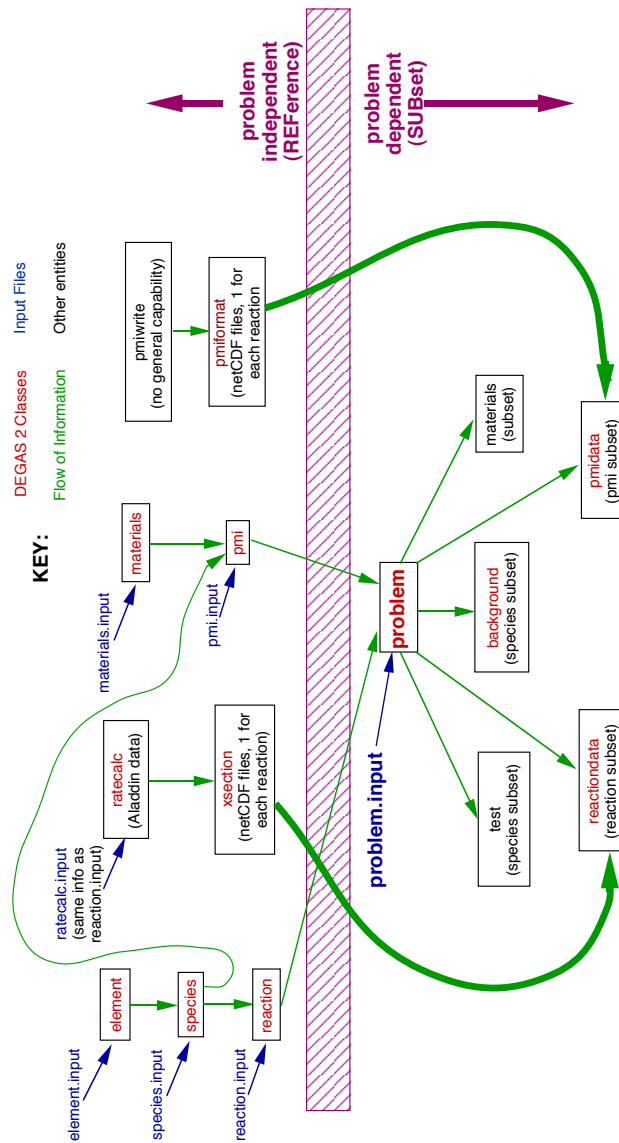


Figure 3.2: Flow of atomic and surface physics data through various DEGAS 2 classes during preprocessing.

distribution for the product atom

$$P_{E_{\text{in}},\theta_{\text{in}}}(v, \alpha, \phi)v^2 dv \sin \alpha d\alpha d\phi, \quad (3.19)$$

where  $\alpha$  and  $\phi$  are the outgoing polar and azimuthal angles, respectively.

This distribution is sampled from three separate 1-D distributions. First, the outgoing velocity  $v_0$  is specified by

$$f_{E_{\text{in}},\theta_{\text{in}}}^1(v) = \int \int P_{E_{\text{in}},\theta_{\text{in}}}(v, \alpha, \phi) \sin \alpha d\alpha d\phi. \quad (3.20)$$

The outgoing polar angle  $\alpha_0$  obeys the distribution

$$f_{E_{\text{in}},\theta_{\text{in}}}^2(\alpha) = \int P_{E_{\text{in}},\theta_{\text{in}}}(v_0, \alpha, \phi) d\phi. \quad (3.21)$$

And, finally, the outgoing azimuthal angle  $\phi_0$  is taken from

$$f_{E_{\text{in}},\theta_{\text{in}}}^3(\phi) = P_{E_{\text{in}},\theta_{\text{in}}}(v_0, \alpha_0, \phi). \quad (3.22)$$

The inverse cumulative distribution,  $F(\omega) = G^{-1}(\omega)$ , with

$$G(x) = \omega = \int_0^x f(y) dy, \quad (3.23)$$

is specified, say, 5 values of  $0 < \omega < 1$ . For example, for a normally incident  $\theta_{\text{in}} = 0$ , ( $E_{\text{in}} = 1$  eV H atom being reflected off of Fe, the data are

$$R_N(E_{\text{in}}, \theta_{\text{in}}) =$$

$$8.27750\text{E}-01$$

$$F^1(\xi) =$$

$$1.99146\text{E}+00 \quad 2.25513\text{E}+00 \quad 2.32691\text{E}+00 \quad 2.36544\text{E}+00 \quad 2.40806\text{E}+00$$

Interpolation into this array with a random number  $\xi$  yields  $\sqrt{E_{\text{out}}}$ , and thus  $v_0$ .

$$F^2(\eta, \xi) =$$

$$\begin{array}{ccccc} 5.16532\text{E}-01 & 6.99576\text{E}-01 & 8.11503\text{E}-01 & 8.99906\text{E}-01 & 9.67300\text{E}-01 \\ 3.70481\text{E}-01 & 6.11799\text{E}-01 & 7.63020\text{E}-01 & 8.72539\text{E}-01 & 9.61285\text{E}-01 \\ 3.80010\text{E}-01 & 6.18834\text{E}-01 & 7.63825\text{E}-01 & 8.75375\text{E}-01 & 9.61256\text{E}-01 \\ 3.57688\text{E}-01 & 5.95520\text{E}-01 & 7.51752\text{E}-01 & 8.59766\text{E}-01 & 9.57489\text{E}-01 \\ 3.48497\text{E}-01 & 5.17881\text{E}-01 & 6.53833\text{E}-01 & 7.79846\text{E}-01 & 9.23956\text{E}-01 \end{array}$$

A 2-D interpolation into this table with the same first random number  $\xi$  and a second one  $\eta$  gives  $\cos \theta_0$ .

$$F^3(\zeta, \eta, \xi) =$$

-9.54674E-01	-5.93616E-01	-4.55439E-03	6.11607E-01	9.54292E-01
-9.39719E-01	-5.34726E-01	7.70975E-02	5.91124E-01	9.38723E-01
-9.47749E-01	-5.99118E-01	-5.34413E-03	5.58645E-01	9.59176E-01
-9.52932E-01	-5.09963E-01	1.11845E-01	6.68895E-01	9.59592E-01
-9.63812E-01	-6.32861E-01	2.84474E-02	6.49311E-01	9.65024E-01
-9.49486E-01	-5.27460E-01	4.71202E-02	5.40823E-01	9.43092E-01
-9.18789E-01	-5.34890E-01	3.87104E-03	5.97719E-01	9.43635E-01
-9.35546E-01	-5.66353E-01	-6.17420E-02	5.65376E-01	9.28863E-01
-9.39133E-01	-5.88361E-01	4.03247E-02	5.36441E-01	9.41553E-01
-9.42917E-01	-5.66390E-01	4.88304E-03	5.72368E-01	9.58254E-01
-9.59566E-01	-6.35221E-01	-7.50576E-02	5.72627E-01	9.59374E-01
-9.43053E-01	-6.23133E-01	-8.35145E-02	5.13894E-01	9.33565E-01
-9.42753E-01	-6.40605E-01	-1.50300E-02	5.51493E-01	9.32335E-01
-9.28625E-01	-5.03451E-01	3.69856E-02	6.04412E-01	9.51354E-01
-9.47567E-01	-5.75171E-01	6.78900E-02	6.17675E-01	9.61149E-01
-9.42125E-01	-6.25972E-01	-6.74072E-02	5.10579E-01	9.26111E-01
-9.24288E-01	-5.62514E-01	-6.67559E-02	5.49679E-01	9.57450E-01
-9.45958E-01	-5.88903E-01	6.07203E-02	5.98492E-01	9.45981E-01
-9.64714E-01	-6.17340E-01	-2.49212E-02	5.61052E-01	9.49261E-01
-9.59291E-01	-6.47473E-01	-8.40439E-02	4.58677E-01	9.33637E-01
-9.43142E-01	-5.25077E-01	4.79891E-02	6.22436E-01	9.53027E-01
-9.43214E-01	-5.90395E-01	2.32011E-02	5.42675E-01	9.35411E-01
-9.40994E-01	-4.99927E-01	7.81558E-02	6.19613E-01	9.44418E-01
-9.35018E-01	-5.38589E-01	8.60652E-02	6.47157E-01	9.51505E-01
-9.49873E-01	-5.38587E-01	8.93784E-02	6.39298E-01	9.66431E-01

A third random number  $\zeta$  is used with the other two in a 3-D interpolation of this table to obtain  $\cos \phi_0$ . The re-use of these random numbers in interpolating these three separate dependent variables means that DEGAS 2 has to treat the random numbers as fixed independent variables, just like electron density or ion temperature, rather than generating the random numbers on the fly in the interpolation process. Hence, the appearance of `1st_random_number`, `2nd_random_number`, and `3rd_random_number` in the independent variables list (see the PMI format class).

So, each file for such PMI contains

1.  $R_N(E_{\text{in}}, \theta_{\text{in}})$ ,

2.  $F^1(\xi, E_{\text{in}}, \theta_{\text{in}})$ ,
3.  $F^2(\eta, \xi, E_{\text{in}}, \theta_{\text{in}})$ ,
4.  $F^3(\zeta, \eta, \xi, E_{\text{in}}, \theta_{\text{in}})$ .

Again, all of the data values are stored in a single 1-D array with the array behavior specified by macros (see the PMI format class).

### 3.9.3 Reaction Processing Routines

Need to create “set products” and “products” routines, as well as collision and track-length routines if new type.

## 3.10 Defining Radiation Detectors

The user defines “groups” of detector “views”. Each view needs to be defined only once and can be used in more than one group. A view is defined by:

1. Two points,
  - The first is taken as the starting point,
  - The second fixes direction.
2. Angular halfwidth (i.e., each view consists of a cone with apex at the starting point),
3. An averaging algorithm, used to simulate 3-D behavior with a cone defined in 2-D (see below). The two techniques available now are
  - Uniform weighting,
  - Circular weighting.
4. A binning variable,
  - Only examples are “none” and “wavelength,”
  - To use “wavelength”, would also need to specify a minimum, maximum, and the number of wavelength bins.

The actual variables are defined and described in the detector class.

Views are machine specific and not frequently changed. For these reasons, the user will need to specify them via specific lines of code in `readgeometry` or `boxgen` (both have working examples).

### 3.10.1 Signal Computation

The contribution from each zone to a view is precomputed so that the signal can be quickly determined during or after the run from volumetric emission.

The 2-D viewing cone is divided into 30 subchords / degree. The code expects, but does not insist (a warning will be printed), that the apex of the cone does not fall inside a plasma or vacuum zone. Each subchord is tracked from the apex to the start of a plasma or vacuum zone. From there, the distance the subchord traverses through each zone is computed. The subchord is terminated when it reaches a solid zone; this is the actual end point. The resulting contribution made to the view by zone  $j$ , call it  $f(z_j)$ , is for  $i = 2N + 1$  uniformly weighted subchords

$$f(z_j) = \sum_{i=-N}^N d_{i,j} w_i / V_j, \quad (3.24)$$

where  $d_{i,j}$  is the distance along subchord  $i$  through zone  $j$ , and  $V_j$  is the volume of zone  $j$ . The relative weight of each subchord is  $w_i$  with

$$w_i^{\text{uniform}} = \frac{1}{4\pi(2N + 1)}, \quad (3.25)$$

and

$$w_i^{\text{circular}} = \frac{1}{2\pi^2 N \sqrt{1 - (i/N)^2}}. \quad (3.26)$$

The units of  $f$  are  $\text{m}^{-2}/\text{st}$ .

These zone contributions can then be used during execution of the main code or during post-processing to compute, say, the  $\text{H}_\alpha$  signal  $S_\alpha$  in the absence of recombination (see Sec. 2.7) as

$$S_\alpha = \sum_j N_1(z_j) \left[ \frac{N_3}{N_1} A_{23} E_{23} \right] f(z_j), \quad (3.27)$$

where  $N_1$  is the number of neutral H atoms in zone  $j$ . The bracketed quantity is interpolated from the input data file, with  $E_{23}$  being the energy of the Balmer- $\alpha$

transition, and other quantities defined in Sec. 2.7. Note, however, that the code is completely general regarding wavelength and origin of radiation. Other line emission rates can be scored in an analogous if the appropriate data are present in the input data files. Again note that the views cannot be toroidally directed. If needed, this option could be incorporated with relative ease.

### 3.11 Sectors and Diagnostic Surfaces

The default behavior for a surface in DEGAS 2's tracking algorithm is to stop the flight momentarily (to check for a zone boundary) and then to continue. In some instances, these surfaces need to do more, e.g.,

1. If that surface represents the interface between a plasma or vacuum zone and a material (solid) or exit zone, the quantities describing the flight must be altered to represent the effect of that next zone,
2. If the user wishes to monitor the passing of a flight through a particular surface, the flight's parameters must be noted and used to update the appropriate tallies.

To address these needs, DEGAS 2 utilizes the *sector* concept. The most general description of a sector is a coupled surface and a zone. More specifically, the surface should be a bounding surface of a cell comprising the zone (the orientation is important; see below). The function used to define sectors takes as an optional argument a second zone. If provided, the function will verify that the input surface is indeed an interface between the two zones. The programmer should use this option whenever possible as a consistency check.

Solid zones in DEGAS 2 are typically physically larger entities than plasma zones. E.g., many plasma zones may be in contact with the same solid zone. Although this approach simplifies specification of the geometry, it prevents local variations in the properties of the solid zone, such as material temperature or recycling coefficient. Instead, we will use the sectors to store data such as these. In contrast, each plasma zone has associated with it local data, such as plasma temperature and density. By including the plasma zone number in the sector definition, the sectors have access to the properties of both the material and plasma at the interface between the two. The particular properties required may vary with the model used process the flights as they strike the interface. The existing geometry setup routines (`definegeometry2d`, `readgeometry` and `boxgen`)

define take care of the definition of these sectors. In the first two cases, little or no input is required from the user.

Sectors can also be defined for purely diagnostic use. The zones adjacent to the sector surface can be of any type. A given sector may be used to specify more than one diagnostic (e.g., one may track particle current, another might tally particle energy).

Because of the inherent differences between interfaces of different types, the sectors must be categorized into subclasses:

**target** The interface between a plasma zone and a solid zone,

**wall** The interface between a vacuum zone and a solid zone,

**exit** The interface between a vacuum or plasma zone and an exit zone,

**diagnostic** A diagnostic sector.

**plasma** A sector type used in an earlier version of the code, retained only for backward compatibility.

**vacuum** A sector type used in an earlier version of the code, retained only for backward compatibility.

To facilitate output organization, sectors have labels associated with them, `strata` (for groups of sectors) and `sector_strata_segment` (for an individual segment). The user can specify these in an arbitrary manner. `readgeometry` provides some keywords for this purpose.

Additional details on the sector subclass properties can be found in the documentation on the sector class.

### 3.11.1 Diagnostic Sectors

Diagnostic sectors are defined in a manner closely paralleling that of detectors. Diagnostic sector groups are used to identify sectors of similar functionality. Both `readgeometry` and `boxgen` define default diagnostic groups using the non-diagnostic sectors set up by those routines:

**Wall and Target Counts** Includes all wall and target sectors. No independent variable is associated with this diagnostic group; it is only capable of summing a particular test particle property (which will be specified by a corresponding tally, particle mass, for example).

**Exit Counts** Includes all exit sectors. No independent variable is associated with this diagnostic group either.

**Wall and Target Energy Spectrum** Specifies the particle energy as the independent variable. As in the “Counts” groups, some as-yet-unspecified particle property will be tracked. The difference is that the tally will be divided up into the energy bins defined for this group.

**Wall and Target Angle Spectrum** Similar to the “Energy Spectrum” group, but the independent variable is the angle of incidence of the particle.

In addition, the definition of diagnostic only sectors and a corresponding group (“Throat sectors”) is illustrated in `readgeometry.web`.

The particle properties to be associated with these diagnostic groups for the purpose of defining tallies may be directionally dependent. For instance, the particle current leaving and entering a zone may be specified separately. Details will be given in Sec. 2.3.3.

## 3.12 Output File

The output netCDF file (`outputfile` in `degas2.in`) contains the tally data in four arrays:

1. Sorted by the neutral source group, prior to post-processing,
2. Summed over neutral sources, prior to post-processing,
3. Sorted by neutral sources, after post-processing,
4. Summed over neutral sources, after post-processing.

All have standard deviation data, but their interpretation is not guaranteed for the latter two since the impact of post-processing (especially the addition of post-processed scores to a tally) is not accounted for. If the output file is the result of a checkpoint dump (Sec. 3.8.1), keep in mind that post-processing has not been done. Navigating these large arrays is extremely tedious and not recommended except as a last resort. Instead, the user should utilize `outputbrowser`. There is a separate output array for data to be passed to 2-D fluid plasma code.

A couple of text output files, largely of historical origin, are generated. The `density.out` file has been described already in Sec. 3.7.1. The `sources.out`

and `testdata.out` files are unformatted files used to transfer data to the UEDGE code. All of the information in them is accessible through `outputbrowser`, so no further description of them will be given.

### **3.13 Other Documentation**

The file `classes.web` contains an extensive description of what the code looks like internally. Most of the common variables (i.e., the contents of the `hweb` header files) are documented here as well. Try following [this link](#) if you want to have a look at it now.

# Chapter 4

## EIRENE Benchmark

### 4.1 Introduction

Since UEDGE was first coupled to EIRENE and since EIRENE is currently the most widely used neutral transport code in the field, the first step in coupling DEGAS 2 is to perform a benchmark against EIRENE. A simple slab, “single-null” geometry and plasma generated by UEDGE is used as input to both codes. An initial effort was performed without recombination. Essential information from that documentation has been included here for completeness.

This chapter describes a second round of benchmark exercises in which recombination is accounted for. The plasma  $T_{e,i} \sim 1$  eV near plate in this case. For reasons to be explained below, several numerical differences between the codes are accentuated under these conditions. We will describe here the isolation and elimination of most of these differences, enabling us to get agreement of densities and plasma sources to within 5%. In the process we have developed a means for quantitatively comparing the code results.

The following sections will:

1. Describe the geometry, boundary conditions, and UEDGE plasma,
2. Qualitatively compare “out of the box” code results,
3. Describe how code results are quantitatively compared,
4. Explain several differences between the codes, eliminating or minimizing them when possible,
5. Characterize the level of agreement between the codes,

6. Go through a performance benchmark and optimization of DEGAS 2.

## 4.2 Problem Description

The geometry is intended to be a 2-D slab representation of a toroidally symmetric single-null scrape-off layer. The resulting “box” is 1 m long, extending from a mirror boundary at  $Z = 0$  to a molybdenum target plate at  $Z = 1$  m. Only half of the scrape-off layer is being simulated; hence, the appearance of the mirror. The radial width is 0.05 m. An exit is used to represent the core boundary at  $R = -0.01$  m between  $Z = 0$  and  $Z = 0.75$  m. The outer wall at  $R = 0.04$  m is assumed to be made of molybdenum. The section representing the wall adjacent to the private flux region, at  $R = -0.01$  m between  $Z = 0.75$  m and  $Z = 1$  m, is also taken to be made of molybdenum. Finally, a mirror surface at  $Z = 0.75$  m extending from  $R = -0.01$  m to  $R = 0$  creates a private flux region above it. The length of the box in the third dimension is 1 m, although periodic boundary conditions are established at both ends.

The UEDGE mesh has a nonuniform spacing with 64 zones in the  $Z$  direction and 32 in  $R$ . The geometry and plasma data are provided to DEGAS 2 in a file generated during UEDGE post-processing by the BASIS utility. The electron temperature and density computed by UEDGE with its fluid neutral transport model are shown in Figs. 4.1 and 4.2.

## 4.3 “Out of the Box” Results

Figures 4.3 and 4.4 show how the atomic deuterium densities computed by EIRENE and DEGAS 2 using the UEDGE plasma compare with roughly standard physics. The word “roughly” is meant to imply that some of the changes to be described later in this chapter have been incorporated into these simulations. For EIRENE, the random number problem (see Sec. 4.5.2) has been remedied. For DEGAS 2, the treatment of reflection used on the molybdenum surfaces uses the EIRENE data, including the attempts to mimic EIRENE’s extrapolation behavior (see Secs. 4.5.3 and 4.5.4).

The peak EIRENE density is about  $3 \times 10^{20} \text{ m}^{-3}$ . For DEGAS 2, the peak is only about  $2 \times 10^{20} \text{ m}^{-3}$ . In Sec. 4.5, we will list the causes of this discrepancy and describe the techniques we use to eliminate or minimize them.

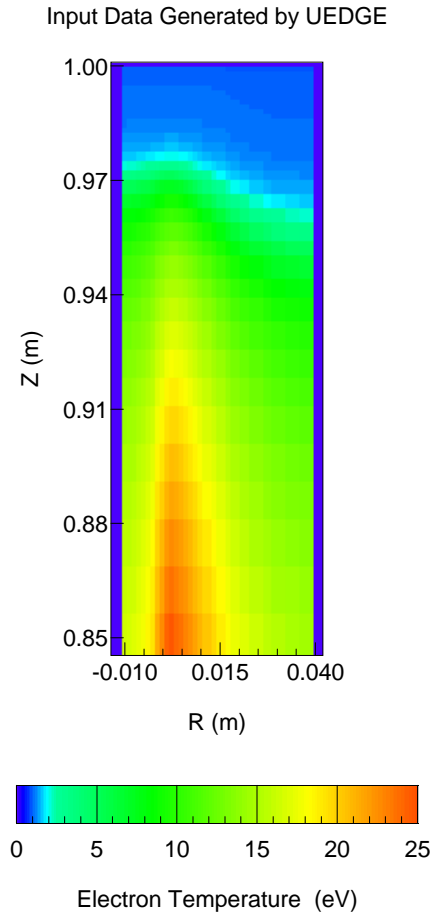
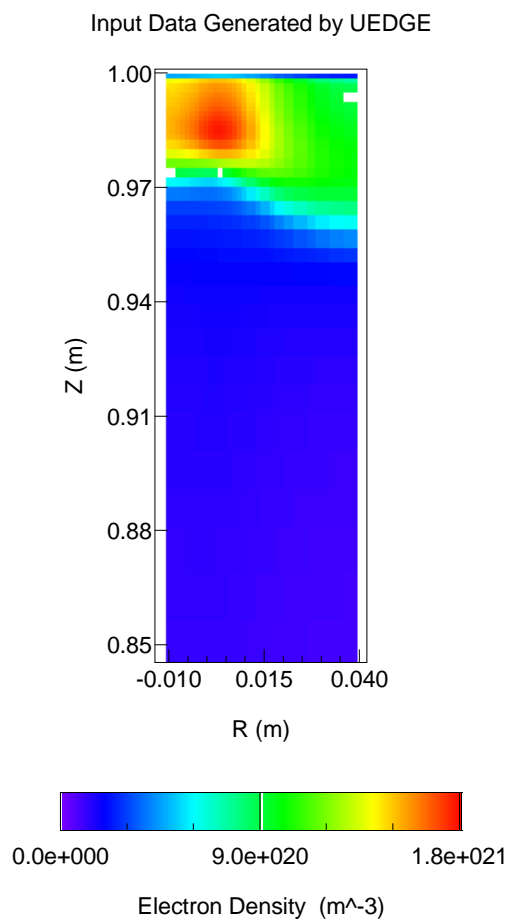


Figure 4.1: Electron temperature near the target ( $Z = 1$  m) as computed by UEDGE with its fluid neutral model.

electron\_density\_x2

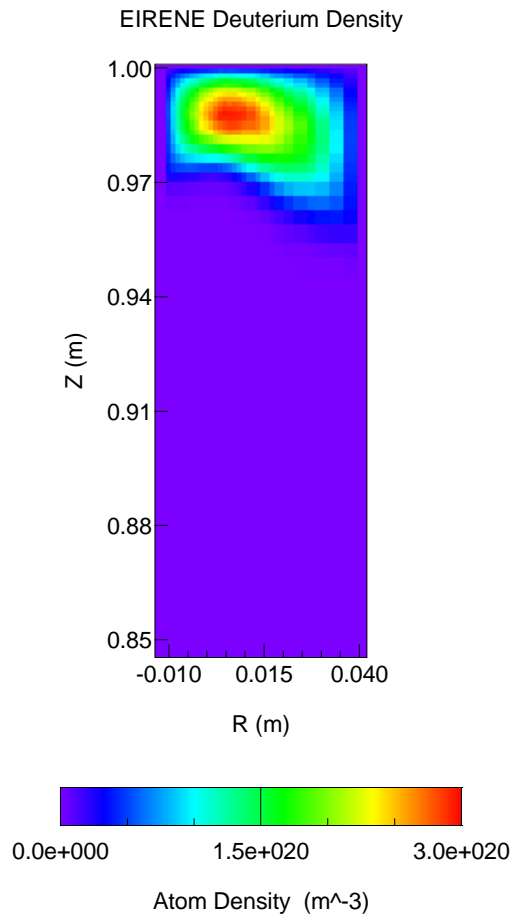


Dec 22 1998

Page 1 of 1

Figure 4.2: Electron density near the target ( $Z = 1$  m) as computed by UEDGE with its fluid neutral model.

D\_density\_10\_x

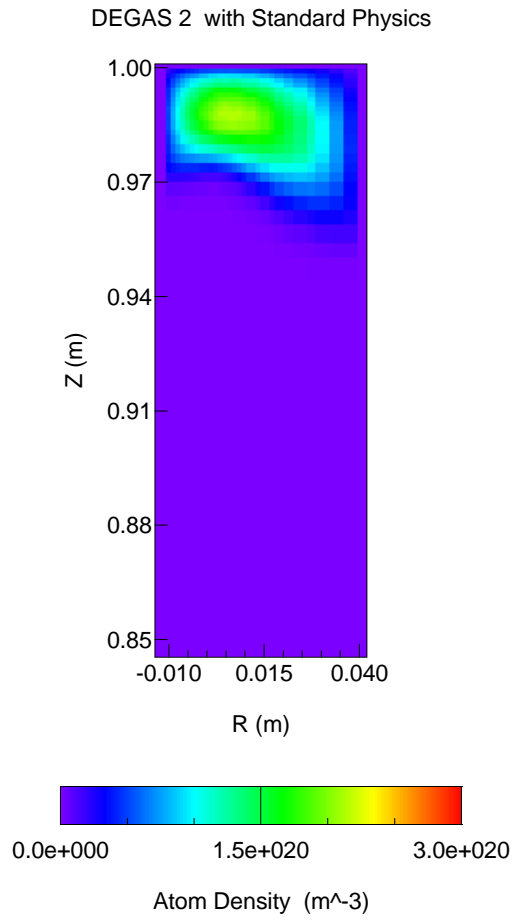


Jan 04 1999

Page 1 of 1

Figure 4.3: Neutral deuterium atom density computed by EIRENE.

spD\_density\_x



Jan 04 1999

Page 1 of 1

Figure 4.4: Neutral deuterium atom density computed by DEGAS 2 using “standard physics”.

## 4.4 Statistical Basis for Comparisons

Because Monte Carlo codes provide only a statistical description of a result, e.g., the neutral density at a particular point in space and an estimate of its error, comparisons between codes require some care. Differences between codes smaller than the standard error in their results cannot be discerned, as this section will demonstrate. We will describe a quantitative procedure for comparing code results which can be used to tell if the differences cannot be statistical in nature.

The standard error decreases with  $1/\sqrt{N}$ , where  $N$  is the number of flights, and can in principle be made as small as desired. For the problem at hand, we've used 80,000 flights for each of the source groups, resulting in standard errors of a few percent near the plate for simple tallies such as the neutral atom density. The differences between EIRENE and DEGAS 2 remaining after the steps described in Sec. 4.5 have been taken are slightly larger than this, so raising the number of flights further would not be useful.

Both DEGAS 2 and EIRENE compute the recombination contributions to the source terms (e.g., subtracting recombination rate from the ion particle source) directly and add them to the final Monte Carlo results at the end of the run. DEGAS 2 does provide the option for computing these contributions in the standard Monte Carlo way (as a check), but the statistical error is increased substantially. Comparison of the code results is, thus, further complicated because the computed variance estimates cannot be used directly with the final output results. Rather, our statistical comparisons must be made *without* these “post-processing” contributions.

DEGAS 2 has two sets of output arrays:

1. One written before post-processing and containing relative standard deviations,
2. One with the post-processing results and no variance data.

The screen output generated by EIRENE likewise contains results without these post-processing contributions and their relative standard deviations, provided they were requested in the input file. These data along with the first of the two DEGAS 2 output array sets will be analyzed with the procedure outlined here.

The principal basis our statistical comparison is the Central Limit Theorem[2]. Say we have the density score in a particular zone from a run of  $K$  flights; call it  $\mu_K$ . This result is effectively a sample drawn from a parent population; call its

mean  $m$  and the standard deviation  $\sigma$ . The objective of the Monte Carlo method is to estimate this mean  $m$ .

The Central Limit Theorem then says that the relative error

$$\epsilon_{\text{rel}} \equiv \frac{|\mu_K - m|}{\sigma_K}, \quad (4.1)$$

where  $\sigma_K = \sigma/\sqrt{K}$  is the standard error, has a Maxwellian distribution. That is, the probability that  $\epsilon_{\text{rel}} < 1$  is 68.3%,  $< 2$  is 95.4% and  $< 3$  is 99.7%.

To apply this directly to our situation, we would need to:

- Do many runs of both codes,
- Find values of  $m$  for each code which are consistent with those results,
- Compare the  $m$  values between codes,
- Repeat the process for each zone.

Such a process is too lengthy to permit extensive comparisons of different variables and input conditions. We propose using instead a simpler, compromise procedure. Say we have a density score from DEGAS 2  $\mu_K^D$  and one from EIRENE  $\mu_{K'}^E$ . We begin by *postulating* that they have the same  $m$ . If this is true, the random variable  $z \equiv \mu_K^D - \mu_{K'}^E$  has mean  $m_z = 0$ . Then, if each of the codes' standard deviation estimates  $s_K^D$  and  $s_{K'}^E$  are also consistent with  $\sigma$ , one can show that the distribution of  $z$  about its mean 0 will have a standard deviation

$$s_{z,K,\text{eff}} = \sqrt{(s_K^D)^2 + (s_{K'}^E)^2}, \quad (4.2)$$

This is just what one expects from propagation of errors.

We are not done yet in that applying this would still require many runs of both codes. However, we do have many zones in each run. *If* the scores in each zone are uncorrelated with other zones, we could treat the value of

$$\epsilon_{z,\text{rel}} = z/s_{z,K,\text{eff}} \quad (4.3)$$

in each zone as a separate sample and compile a distribution of  $\epsilon_{z,\text{rel}}$  by comparing the results in each zone. If we find this distribution to be Maxwellian, we may infer that our postulates are correct, i.e., the codes are giving the same results. If the distribution strongly deviates from a Maxwellian, we can suspect that the codes do not agree.

The extent to which scores in two zones are correlated depends on many factors. Since we do not require precise statistical agreement between the codes (a few percent of systematic error is acceptable), we will assume that the effect of these correlations is too small to prevent this test from detecting significant (more than a few percent) differences.

One other consideration is that the Central Limit Theorem only applies for “large enough  $K$ ”. For a given zone, this effectively means a “small enough relative standard deviation”. For these comparisons, both codes produce relative standard deviations near the target of a few percent. If we restrict the comparison to zones with relative standard deviations below some value, say  $\sigma_{\max} = 20\%$ , we should still have a large number of zones to work with.

Note that the codes output the relative standard deviation,  $\sigma/(m\sqrt{K})$ . To get  $\sigma_K^D$  we multiply the output relative standard deviation by  $\mu_K^D$ .

## 4.5 Code Differences

### 4.5.1 Atomic Physics

The common ancestry of EIRENE, DEGAS, and DEGAS 2 is apparent in their atomic physics data. All three codes rely upon the molecular data in the Janev book[13] (see Sec. 4.5.5, however). The reaction rates are explicitly the same in all three codes, as are the dissociation energies, and the electron energy loss rates. Note also that since the scoring of momentum transfer to the plasma in EIRENE is relatively new, its implementation is incomplete: there is no momentum transfer for the molecular dissociation processes. However, given the dominance of the other momentum sources, this should not be a problem. DEGAS 2 tracks all three components of the momentum transfer in all reactions.

This version of EIRENE (with the present input file) uses the reaction rate for charge exchange in the Janev book[13]. No attempt is made to ensure that the sampled background ion velocities are consistent with the charge exchange cross section[3]. Furthermore, the momentum and energy transfer expressions are correct only in the limit of  $\langle\sigma v\rangle = \sigma v$  (see Sec. 4.5.6). More recent versions of the code certainly do better than this[14].

The DEGAS 2 standard charge exchange data comes from the Janev-Smith database[15], with consistently computed reaction rates, and energy and momentum transfer rates[14]. The simulation described in Sec. 4.3 used these data. For subsequent runs, data equivalent to those in EIRENE will be substituted.

DEGAS 2 and EIRENE each rely on their own collisional radiative[14] codes for the multi-step electron-impact ionization and recombination of hydrogen data. These two codes have been compared several times in the past. The basic difference is that the EIRENE code, AMJUEL, is based upon the Johnson-Hinnov ionization cross sections[16]. The data used in DEGAS 2 are described in Sec. 2.7.

Figures 4.5 and 4.6 compare the rate data. The AMJUEL ionization rates are noticeably lower for  $T_e < 10$  eV. This is likely responsible for most of the differences between the densities in Figs. 4.3 and 4.4. The energy loss rates agree. However, when normalized to the ionization rate, to give the energy lost per ionization, the differences of Fig. 4.5 are factored in.

Figure 4.7 shows that the recombination rates agree well. The reason is that the Johnson-Hinnov[16] recombination cross section data are used in both collisional radiative codes. The energy exchange rates agree for  $T_e < 10$  eV, but disagree at higher temperatures. This quantity includes the average energy of a radiatively recombining electron; the expression used to compute it involves[14]  $d\langle\sigma v\rangle_{\text{recombination}}/dT_e$ . Apparently, the AMJUEL values were obtained by differentiating a fit to  $\langle\sigma v\rangle_{\text{recombination}}$ . The values used in DEGAS 2, however, were obtained by differentiating closed form expressions for  $\langle\sigma v\rangle_{\text{recombination}}$  and should be correct.

As with charge exchange, in Sec. 4.3 DEGAS 2 used the `ehr2.dat` data. For subsequent runs, the AMJUEL data will be used in both codes.

## 4.5.2 Source Sampling

The ion current distribution to the target is sampled according to the relative fractions of current striking each segment (i.e., each radial zone). Likewise, the probability distribution used in sampling the “birth” zone of a recombining ion is given by the fraction of the total recombination occurring in that zone. Whether or not a code is correctly sampling these distributions can be easily determined. For DEGAS 2, the `sourcetest` utility was written to do just this (see Sec. 3.4.3). Cruder means were used to extract the requisite data from EIRENE.

Figure 4.8 shows that the two codes are able to match the input distribution (to within the error bars). To make the comparison quantitative, we use a  $\chi^2$  test[42]. The result is  $p$ , the probability that sampled distribution matches the parent distribution. For the 5000 samples used in generating Fig. 4.8, the DEGAS 2 results yield  $p = 0.97$ . For EIRENE, we get  $p = 0.69$ . Since  $p$  in both cases is not too much smaller than 1, we conclude that the input distribution is being adequately sampled.

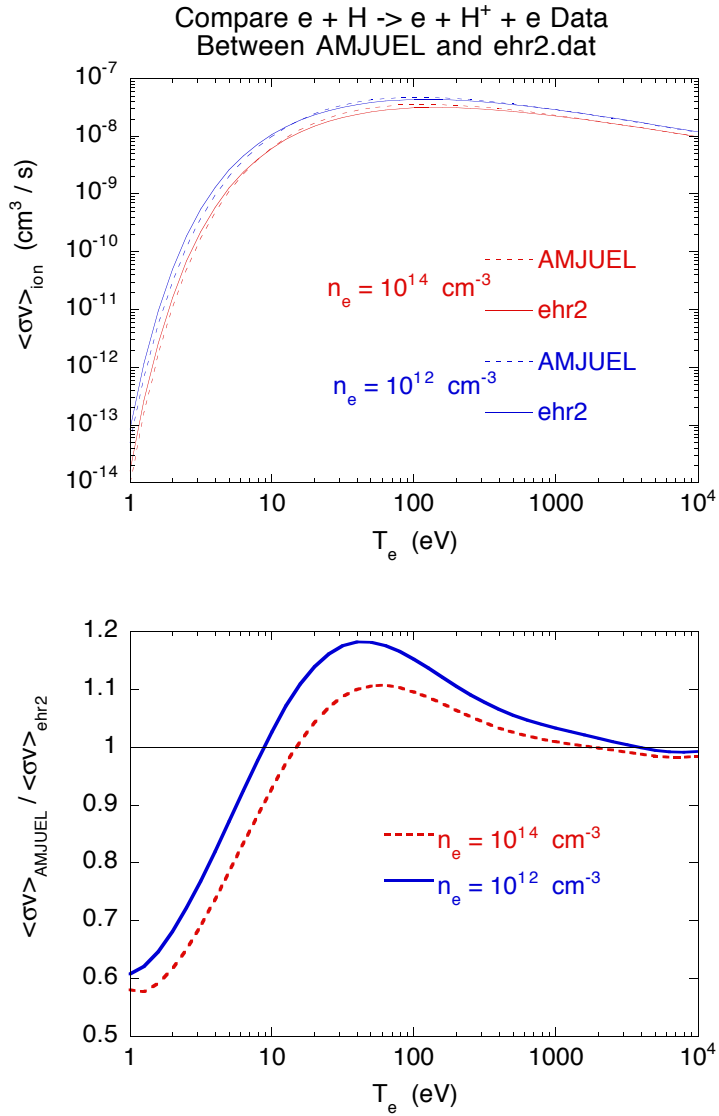


Figure 4.5: Comparison of effective collisional radiative electron impact hydrogen ionization rate from EIRENE's AMJUEL data file and from DEGAS 2's IRLS code (contained in the publicly distributed file `ehr2.dat`) at densities of  $10^{18} \text{ m}^{-3}$  and  $10^{20} \text{ m}^{-3}$ . The lower figure shows the ratios of the rates computed by the two codes.

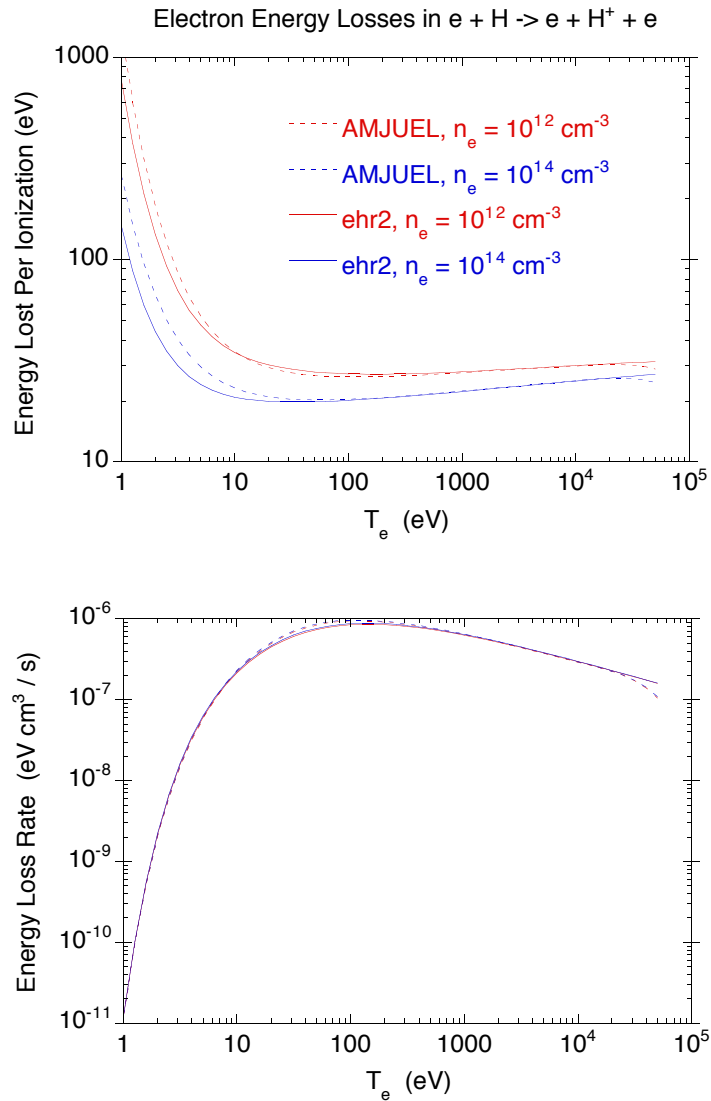


Figure 4.6: Comparison of effective collisional radiative electron energy loss rate from EIRENE's AMJUEL data file and from DEGAS 2's IRLS code (contained in the publicly distributed file `ehr2.dat`) at densities of  $10^{18} \text{ m}^{-3}$  and  $10^{20} \text{ m}^{-3}$ . The upper figure shows the energy lost per ionization; the lower gives the power lost.

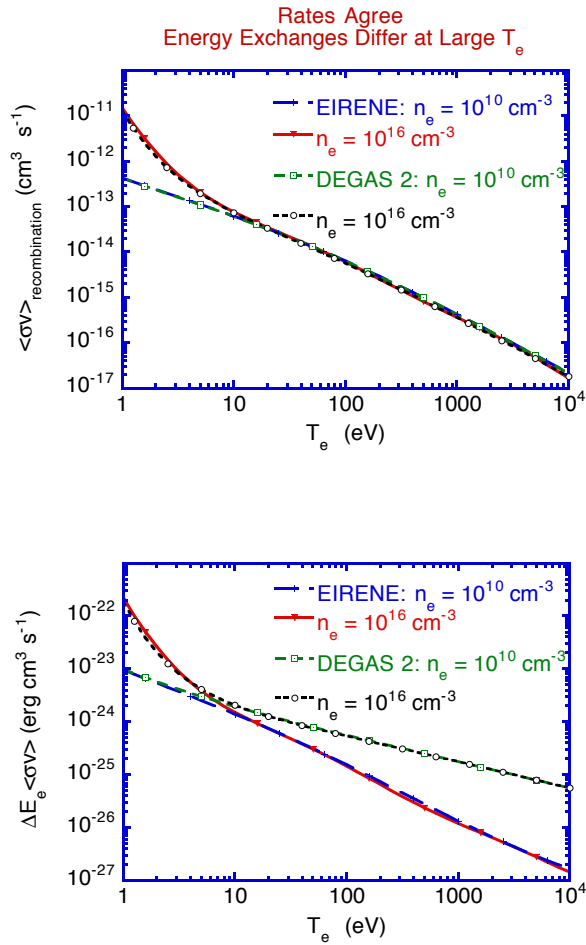


Figure 4.7: Comparison of effective collisional radiative electron recombination rates from EIRENE’s AMJUEL data file and from DEGAS 2’s IRLS code (contained in the publicly distributed file `ehr2.dat`) at densities of  $10^{16} \text{ m}^{-3}$  and  $10^{22} \text{ m}^{-3}$ . The upper figure shows the effective recombination rates; the lower gives the power lost.

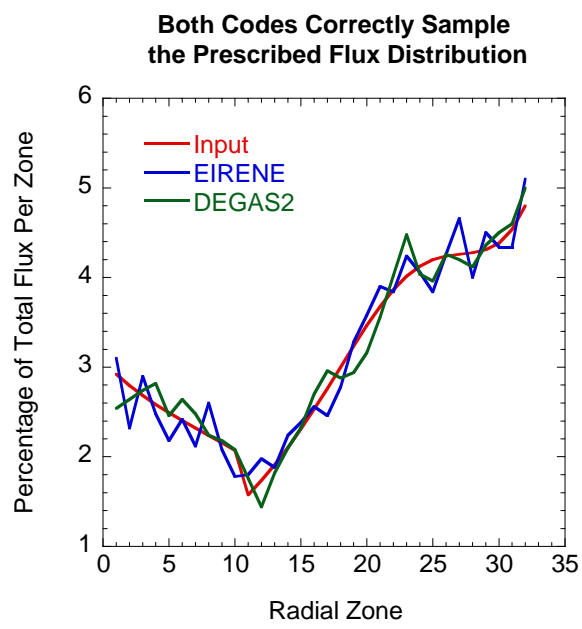


Figure 4.8: Sampled target flux distributions, as a function of radial zone, for DEGAS 2 and EIRENE. The curve labeled “Input” is the ideal result.

We use 50,000 samples of the recombination source. Because of the large number of zones, a simple plot analogous to Fig. 4.8 is unintelligible. Furthermore, not all of the problem zones are adequately sampled to permit the application of a  $\chi^2$  test to the whole problem space. Instead, we isolate the 648 zones with highest recombination rate (the lowest temperature region, chosen somewhat arbitrarily). Applying a  $\chi^2$  test to samples taken in those zones yields for DEGAS 2  $p = 0.94$ . But, for EIRENE  $p = 0.21$ . Sensing that this is small enough to cause concern, we repaired a known problem with the EIRENE random number generator (as received, the code had random number seeds which differed by unity; the fix is to make one of these integers very different). The result is much improved:  $p = 0.79$ . All other EIRENE runs described in this chapter utilize this bug fix.

### 4.5.3 Energy Distribution of Reflected Atoms

The EIRENE surface physics is more detailed than that of the old DEGAS and, hence, DEGAS 2. Consequently, we will not make an overall comparison with different surface physics data. Instead, we have translated the Bateman format data for reflection of D off of Mo taken from EIRENE's TRIM input file into a DEGAS 2 format. To be more precise, the Mo data obtained from Fe data using a scaling argument[43].

These data prescribe the reflection coefficient, the outgoing energy, and two outgoing angles as a function of the incident energy and polar angle. The Bateman format is described in detail elsewhere[3]. Briefly, these data specify these parameter values (e.g., the outgoing energy) at intervals of the cumulative distribution function: 0.1, 0.3, 0.5, 0.7, 0.9. One can also establish data points at each end of the distribution. For example, a minimum energy might be the wall temperature; a maximum would be the incident energy. As originally implemented in DEGAS 2, this additional information to extrapolate beyond the ends of the data. Doing this carefully required specifying additional cumulative distribution values at 0, 0.2, 0.4, 0.6, 0.8, and 1.0 (intermediate values being obtained by linear interpolation).

EIRENE, however, mindlessly extrapolates the data and enforces the minimum and maximum values after sampling. The result is that the sampled maximum and minimum may be noticeably different from what one expects. The first set of benchmark runs indicated that the difference in the handling of the lowest reflected energy atoms was significant. The reason is that the atom density near the target plate (i.e., where ionization is lowest) scales like the inverse of the atom velocity, and hence is impacted strongly by the lowest energy atoms. To eliminate this difference, we reset the lower bound on the energy so DEGAS 2 would mimic

the EIRENE extrapolation. Figure 4.9 shows that the original DEGAS 2 reflected energies for a normally incident 19 eV atom match the input data well (the difference at the lower end is due to the use of logarithmic interpolation in DEGAS 2). The revised DEGAS 2 reflected energies differ from the input, but better match the values obtained from EIRENE.

A second difference becomes significant with the present set of benchmarks including recombination. The temperatures in this plasma are sufficiently low that a significant number of atoms are striking the target with energies below 1 eV. EIRENE assumes that such atoms are always absorbed (and desorbed thermally as molecules in this simulation). DEGAS 2 treats the data literally; the reflection coefficient is about 0.2 at 1 eV. For the initial comparison run (see Sec. 4.3), DEGAS 2 was run in this manner, although the energy and angular extrapolation changes described above and in the next subsection were implemented. For all subsequently discussed benchmark simulations, DEGAS 2 will assume absorption for incident atoms of less than 1 eV energy.

#### 4.5.4 Angular Distribution of Reflected Atoms

The cosines of the angular distribution are sampled in a way analogous to the energy. In this case, the bounds of the sampled parameters are clearer still since they are the cosines of the angles (i.e., 0 and 1). However, during this benchmark exercise, a discrepancy in the near target deuterium density was again connected with the distribution of neutral velocities in the  $Z$  direction. With the difference due to energy extrapolation (see Sec. 4.5.3) having been eliminated, the cause this time was traced to the extrapolation of the cosine of the outgoing polar angle,  $\cos(\theta_{\text{out}})$ .

Figure 4.10 shows the sampled cumulative distribution from two DEGAS 2 runs and from an EIRENE run. These data were compiled from all of the ions incident on the target in a particular zone (normal incidence at 6.88 eV). The curve labeled “original” shows the DEGAS 2 treatment extending down to near  $\cos(\theta_{\text{out}}) \simeq 0$ . The “revised” curve demonstrates that our modifications to the DEGAS 2 data successfully mimic the EIRENE extrapolation behavior.

#### 4.5.5 H<sub>2</sub> Dissociation Rate

Significant differences in the electron energy sink were traced to a discrepancy in the H<sub>2</sub> dissociation rate (reaction 2.2.5 in the Janev book[13]) at the lowest electron temperatures,  $T_e \simeq 1$  eV. Unfortunately, both the plot and the fit for these

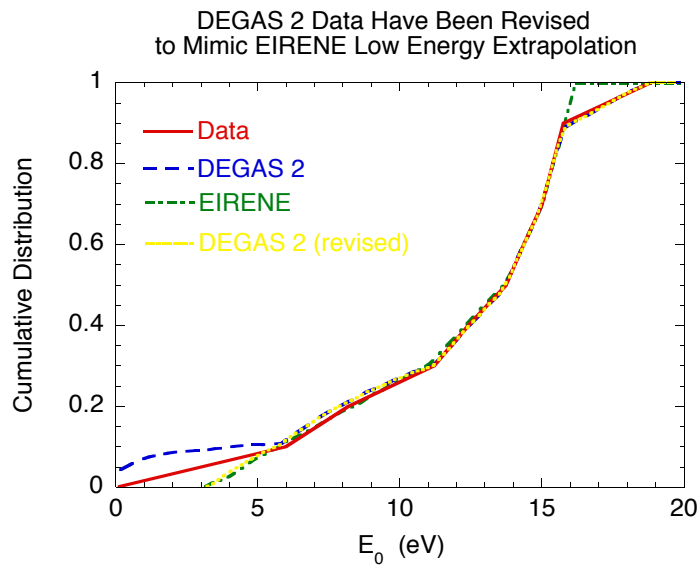


Figure 4.9: Comparison of the cumulative distribution of reflected energies sampled in DEGAS 2 and EIRENE with the input data obtained from EIRENE's TRIM file. The "revised" DEGAS 2 curve indicates that the code is now able to mimic the simple extrapolation used in EIRENE. These data are for a 19 eV deuterium atom incident on molybdenum.

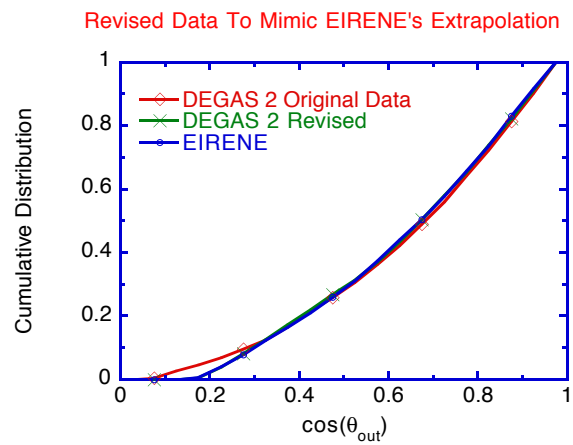


Figure 4.10: Comparison of the cumulative distribution of reflected outgoing polar angles sampled in DEGAS 2 and EIRENE with the input data obtained from EIRENE's TRIM file. These distributions were compiled from all of the initial incident *ions* (i.e., at the start of the flight) in a particular zones. All of these ions strike the target normally with 6.88 eV.

data in the Janev book are *wrong*. One needs to refer to the corresponding preprint even to get the correct values for the fit coefficients. EIRENE has those values, but applies them down to the smallest  $T_e$  used in the code, 1 eV. However, the fit is valid down to only 1.2 eV. The dissociation rate values used in DEGAS 2 at these lowest temperatures were taken directly from the tabular data provided with the original DEGAS code[3], not from the fit. The point is that these values differ from those computed by the fit (presumably due to the fit not being valid there). No record explaining the origin of the DEGAS values, but we assume that they were taken from the initial data compilation from which the fit was derived. Regardless, the remedy for the objectives of this benchmark is to replace these low  $T_e$  dissociation rates with the same values used in EIRENE. The results of Sec. 4.3 have the DEGAS values; runs discussed in subsequent sections will have the EIRENE values.

#### 4.5.6 Estimator Differences

With DEGAS 2 run as in Sec. 4.3, the relative standard deviations for the electron and ion energy sources were substantially larger than those for EIRENE (these differences were most noticeable close to the target). The cause of the higher electron energy source variance was that DEGAS 2 was using a collision estimator for the molecular contributions to that quantity (for historical reasons), while EIRENE was using a track length estimator. Switching the estimator used in DEGAS 2 required a minor change to `tallysetup` (see Sec. 3.4.1). At the same time, we changed the scoring of the electron impact ionization of deuterium contributions to the ion energy and momentum sources from being done “post process” (i.e., computed from the neutral density at the end of the run) to a track length estimator. This allowed the variance contributions from this process to be accounted for in these scores and was essential for comparing with the EIRENE values (see Sec. 4.4).

The main reason for the larger ion energy source variance in DEGAS 2, however, was that charge exchange was being treated by the collision estimator, rather than the track length estimator used in EIRENE. The original reason for choosing the collision estimator in DEGAS 2 was that the charge exchange data file did not have the required integrals of the cross section needed to score the energy and momentum exchanges[14]. We have now worked out the forms these integrals must have to emulate the EIRENE assumption of constant  $\sigma v$  and incorporated them into the charge exchange data file.

The runs of Sec. 4.3 do not employ these estimator changes (and utilize a

different charge exchange cross section altogether, as was noted previously), while runs in subsequent sections have these modifications incorporated.

### 4.5.7 Other Differences

We suspect that there are other differences remaining which will prevent the two codes from being brought into closer agreement. For example, DEGAS 2 uses a logarithmic interpolation in incident energy for the Bateman format reflection data. EIRENE assumes a linear interpolation. The interpolation schemes in DEGAS 2 presently require a uniform spacing, either linearly or logarithmically, between data points (a nonuniform spacing option was tried at one point, but abandoned as too difficult to maintain). Hence, the interpolation technique used by EIRENE cannot be emulated without significant changes to the code. On the other hand, the subtlety of some of the differences which have been detailed in this section suggests that remaining nonstatistical discrepancies in the code results are unlikely to be of physical significance and are consistent with minor numerical differences between the codes.

## 4.6 Characterize Comparison

The principal means of comparing the code results is now considered to be the quantitative prescription given in Sec. 4.4. We will, however, begin this section with plots to illustrate two points.

### 4.6.1 Density Differences

In Fig. 4.11, we show the relative error,

$$\epsilon_{\text{rel}} = \frac{n_D^D - n_E^E}{\sigma_{\text{rsd}}^D \sqrt{(n_D^D)^2 + (n_E^E)^2}}. \quad (4.4)$$

This expression is equivalent to Eq. (4.3) with  $\sigma_{\text{rsd}}$  being the relative standard deviation. Within the *geomtesta* post-processor (see Sec. 3.4.1), we do not have access to the EIRENE error estimates (see Sec. 4.4). However, in the case of the deuterium density, the EIRENE and DEGAS 2 relative standard deviations are sufficiently similar that we can treat them as equal for this purpose. Both are on the order of a one to a few percent near the target. The scale in Fig. 4.11 indicates

the number of standard errors between the DEGAS 2 and EIRENE density values. Note that this is a signed quantity. The white zones indicate areas with differences greater than 3 times the standard error; the black areas indicate likewise that the lower bound has been exceeded.

The dominance of the green areas is indicative of the nearly complete statistical agreement (see Sec. 4.6.3). The red, orange, and yellow zones near the target likely point to a remaining systematic discrepancy between the codes, as suggested in Sec. 4.5.7.

## 4.6.2 Comparison of Momentum Source

As indicated by Figs. 4.12 and 4.13, the deuterium ion parallel momentum sources computed by the two codes are qualitatively (i.e., visually) similar. However, the statistical errors are extremely high (Fig. 4.14), presumably caused by the tight coupling with the background ions through charge exchange (i.e., the net momentum source due to charge exchange is the difference of two nearly equal numbers).

The lack of regions with small relative standard deviations makes comparison of the code results (see Sec. 4.4) problematic since we require a large number of (independent, ideally) zones with “good statistics” (so that the Central Limit Theorem applies) for the analysis. As will be seen in Sec. 4.6.3, relaxing one of these two constraints permits a comparison to be made. In each case, the results are consistent with the two codes being in agreement. The deuterium ion energy source likewise has significant relative standard deviations, although smaller than those shown in Fig. 4.14. The consequences for the stability of a coupling to a plasma transport code may be more serious, however. Future work will assess and remedy this situation, if necessary.

## 4.6.3 Results of Quantitative Comparison

The procedure outlined in Sec. 4.4 must be amended slightly to accommodate the remaining few-percent systematic differences in some of the code results. The relative error is given instead by

$$\epsilon_{\text{rel}} = \frac{\mu_K^{\text{D}} - \mu_{K'}^{\text{E}}}{\max\left(\sqrt{(s_K^{\text{D}})^2 + (s_{K'}^{\text{E}})^2}, \sigma_{\min} \frac{\mu_K^{\text{D}} + \mu_{K'}^{\text{E}}}{2}\right)}, \quad (4.5)$$

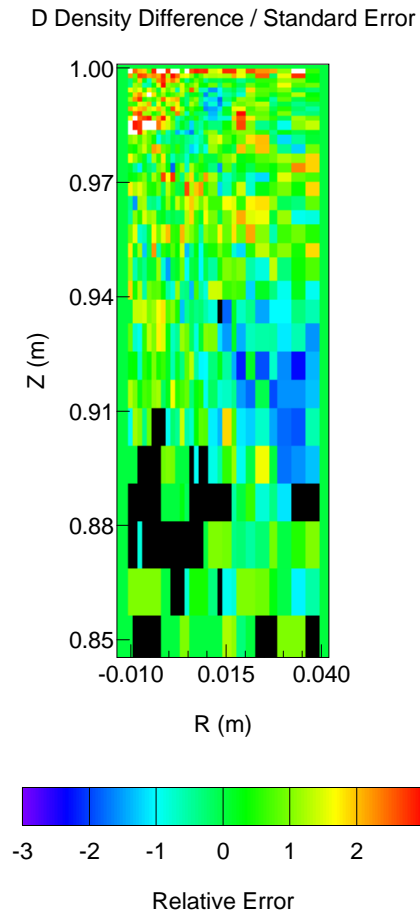


Figure 4.11: Difference between DEGAS 2 and EIRENE deuterium density relative to the standard error estimate.

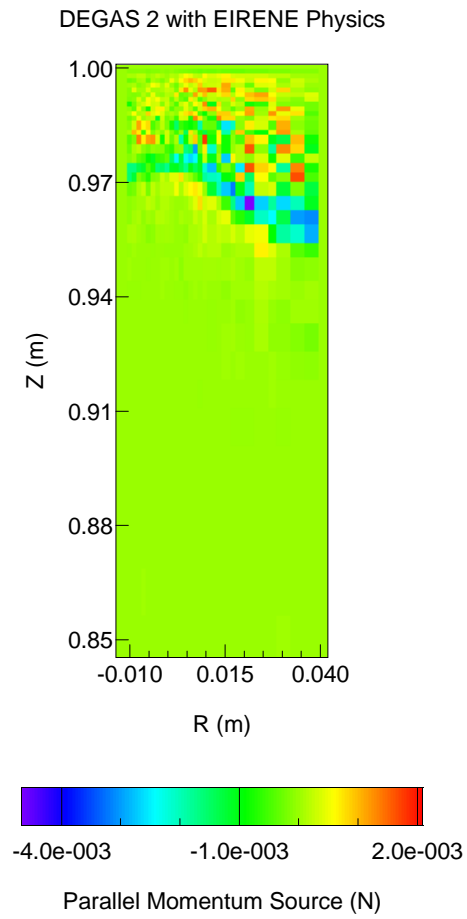


Figure 4.12: Source of deuterium ion parallel momentum computed by DEGAS 2.

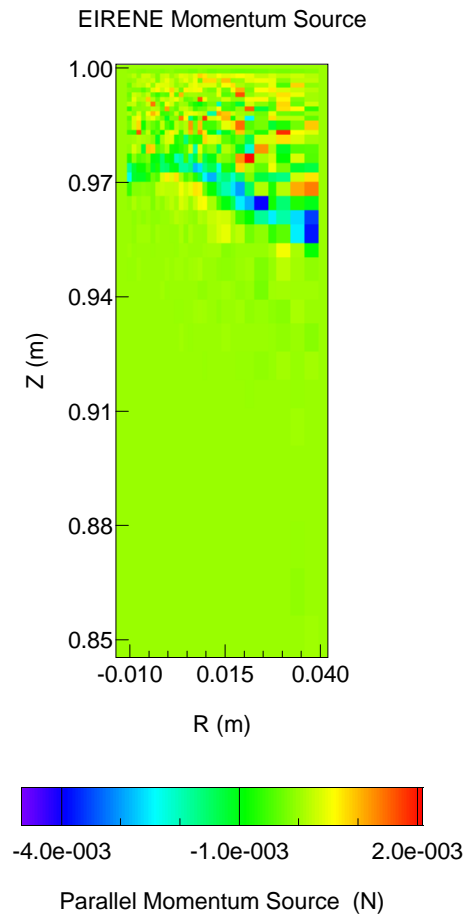


Figure 4.13: Source of deuterium ion parallel momentum computed by EIRENE.

DEGAS 2 Toroidal Momentum R.S.D.

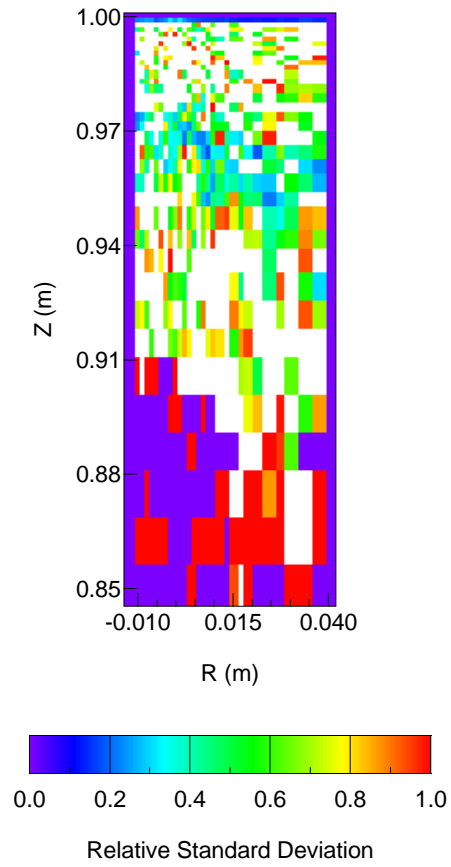


Figure 4.14: Relative standard deviation for the deuterium ion momentum source computed by DEGAS 2.

where again the  $s_K$  refers to the standard error for a simulation of  $K$  flights (i.e.,  $s_K = \sigma_{\text{rsd}}\mu_K$ ). The additional parameter,  $\sigma_{\text{min}}$  is associated with the statistical error (expressed as a fraction, like the relative standard deviation).

For all of these except the ion energy and momentum source,  $\sigma_{\text{max}} = 20\%$  and  $\sigma_{\text{min}}$  is given. For those two,  $\sigma_{\text{min}} = 0$  and  $\sigma_{\text{max}}$  is given. In the former case, the relative standard deviation is required to be  $< 20\%$  to ensure that the Central Limit Theorem is applicable and  $\sigma_{\text{min}}$  represents the systematic error. Of the tested values of  $\sigma_{\text{min}}$  the one which yields a set of percentages most closely matching the Maxwellian ideal (68%, 95%, 99.7%) is taken as our estimate of the systematic error. For the ion energy and momentum sources, we are unable to get “good statistics” with  $\sigma_{\text{max}} = 20\%$ ; hence, larger values are tested. The relative standard deviations are too large for any systematic error to be detected, so we use  $\sigma_{\text{min}} = 0$ .

Source:	Plate			Recombination		
	$1\sigma$	$2\sigma$	$3\sigma$	$1\sigma$	$2\sigma$	$3\sigma$
<b>D Density</b>						
$\sigma_{\min} = 7\%$	82%	99.2%	100%	90%	99.4%	99.9%
$\sigma_{\min} = 5\%$	75%	95%	99.8%	82%	98%	99.9%
$\sigma_{\min} = 0\%$	56%	86%	96%	52%	88%	99%
<b>D<sub>2</sub> Density</b>						
$\sigma_{\min} = 0\%$	64%	92%	98%	59%	92%	99.2%
<b>D<sub>2</sub><sup>+</sup> Density</b>						
$\sigma_{\min} = 0\%$	63%	92%	100%	68%	97%	100%
<b>D<sup>+</sup> Ion Source Rate</b>						
$\sigma_{\min} = 7\%$	74%	99.6%	100%	83%	99.3%	100%
$\sigma_{\min} = 5\%$	57%	94%	100%	63%	98%	99.8%
$\sigma_{\min} = 0\%$	38%	73%	93%	38%	66%	85%
<b>Electron Energy Source Rate</b>						
$\sigma_{\min} = 7\%$	92%	99%	99.1%	93%	99%	99.3%
$\sigma_{\min} = 5\%$	79%	98%	99.1%	86%	98%	99.1%
$\sigma_{\min} = 0\%$	38%	72%	91%	45%	78%	94%
<b>D<sup>+</sup> Ion Energy Source Rate</b>						
$\sigma_{\max} = 70\%$	69%	94%	99%	68%	96%	99.7%
$\sigma_{\max} = 50\%$	69%	94%	99.1%	65%	97%	100%
$\sigma_{\max} = 20\%$	68%	94%	100%	61%	98%	100%
<b>D<sup>+</sup> Ion Parallel Momentum Source Rate</b>						
$\sigma_{\max} = 70\%$	72%	88%	99.2%	75%	92%	99.4%
$\sigma_{\max} = 50\%$	74%	97%	100%	76%	97%	99%
$\sigma_{\max} = 20\%$	58%	89%	100%	0%	0%	0%

The two molecular densities fare the best, given nearly Maxwellian percentages without allowing for any systematic error. The atom density, electron energy source (which is given by the atom density times a function of  $T_e$ , apart from a small contribution due to molecules), and ion source rate are all roughly consistent with a 5% systematic error. Again, the ion energy and momentum sources are too noisy to permit an estimate of the systematic error. However, these numbers indicate that the two codes do agree within the estimated statistical errors.

## 4.7 Performance Benchmark and Optimization

Although efficiency was kept in mind during all stages of the design process, no effort was made to optimize the performance of DEGAS 2 along the way. In this section, we describe the benchmark of the code's performance against EIRENE. Speed bottlenecks were discovered through profiling. Improvements eliminating those bottlenecks were implemented. Some involved significant code revisions; others were effected by simple changes to source or input files. The end result was that the run time for DEGAS 2 was roughly equal to that of EIRENE within the variations normally experienced in a time-sharing environment.

The implemented code revisions were motivated by profiling the code to determine which subroutines were the most time-consuming. At one point, assignments and comparisons of string variables were using significant fractions of the run time. The strings responsible were being used to describe auxiliary data associated with the atomic physics reactions. The code was modified to compile a list of all of these strings at the beginning of the run and to use an integer pointer into that list for the run-time comparisons and assignments. Because these code changes were pervasive, their impact on the run time could not be documented as carefully as the other improvements noted below. Roughly, however, they resulted in a reduction of about 10 seconds per 1000 flights.

### 4.7.1 Starting Point

The starting assumptions were the same as those associated with the code as run for the initial EIRENE benchmark (specifically, the DEGAS 2 version with the CVS tag V1\_8a). The "EIRENE physics" set was used to minimize differences due to the number of collisions and to permit direct comparisons of the variances.

For each code configuration, runs were performed at 1000, 2000, and 4000 flights. The time for the 1000 flight case was subtracted from the other two and the results used to estimate the incremental time required to track 1000 flights. The idea is that production runs would be substantially longer than these (with relative standard deviations on the order of 1%) so that the overhead associated with input and output would be negligible. In a few cases, production length runs (e.g., 80,000 flights) were done; for those, the run time was just taken to be the time consumed divided by 80.

These runs were performed on a Sun UltraSPARC 2 running SunOS 5.5.1 and V. 4.2 of f77 with -O4 optimization. Again, because this computer is a time-sharing system, these run times are only approximate. The estimated error is about

10%. The baseline run time for DEGAS 2 was: 136 seconds per 1000 flights.

### **4.7.2 Charge Exchange Rejection**

The charge exchange cross section depends on the relative ion-neutral velocity. However, collisions are decided upon using a cross section averaged over a Maxwellian distribution. In the baseline, the ion collision partners were chosen so as to be consistent with the actual cross section using a rejection technique, sampling several ions before finding one which is satisfactory. The version of EIRENE used in this benchmark does not do this (neither did the original DEGAS).

For the first change, charge exchange rejection was turned off. A cursory examination of the results showed no significant impact on the neutral density. However, a stronger effect may have occurred elsewhere (e.g., energy transferred to background species). Run time after disabling charge exchange rejection: 119 seconds per 1000 flights.

### **4.7.3 Reduce Number of Scores**

One impressive feature of EIRENE is how thoroughly its default operation has been pared down to the minimum necessary for coupling to the fluid plasma codes. In particular, no data on the variances are kept. DEGAS 2 was written with the philosophy that the mean value for a score is meaningless without a corresponding variance, and the two data values are kept together. For this comparison, a short list of variances was requested in the EIRENE input file. These will be needed later.

As presently distributed, DEGAS 2 by default sets up about 14 scores or tallies. This list was reduced to 7 at this step (later, 3 more will be eliminated leaving the neutral density and the 3 scores representing the particle, momentum, and energy transfer to the background species). Run time after cutting the number of scores to 7: 95 seconds per 1000 flights.

### **4.7.4 Compression of Scores**

The first offender in the profiling exercise was the routine responsible for compiling the scores accumulated during a single flight into the global total. As originally written, both the total and incremental scoring arrays were full-sized (roughly the number of zones times the number of scores times the number of background

species). However, each flight visits only a small fraction of the problem space, and this routine was spending a significant amount of time adding 0 to 0.

These scoring arrays were modified to contain only the non-zero scores, with an array of pointers mapping their contents back to the corresponding locations in the full-sized arrays (which were still used for the final output stage). Run time after implementation of compressed scoring: 49 seconds per 1000 flights.

#### 4.7.5 Other Changes with Minimal Effects

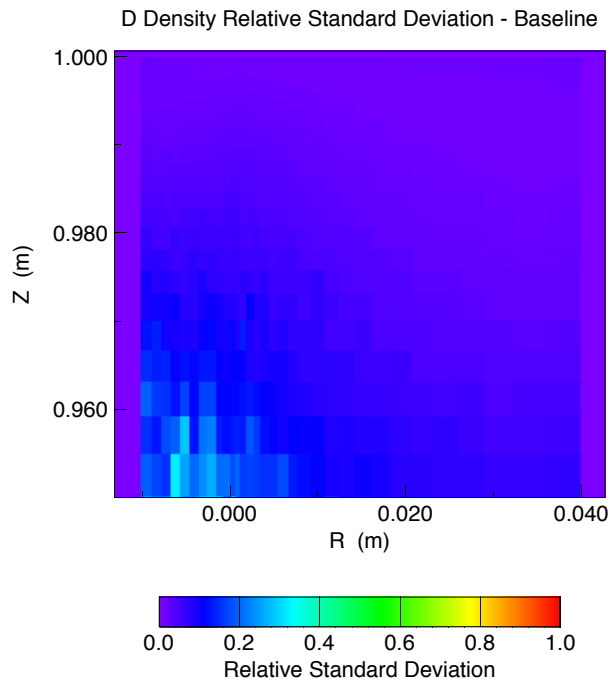
Further reducing the number of scores from 7 to 4 had little impact on the run, probably because of the use of compression at this point.

DEGAS 2 (and EIRENE) employ a 10 term quadratic representation of all surfaces in the geometry. In some problems, such as this one, only the linear terms are needed. The inclusion of the quadratic terms was made a compile-time option so that they could be turned off for fully linear geometries. Earlier tests of the impact of this change showed a reduction of about 4 seconds per 1000 flights. However, in this more systematic series of trials, the improvement could not be quantified with certainty.

#### 4.7.6 Variance-Altering Changes

Thus far, all of the changes made led to the same final results as the run with “EIRENE physics”. Most of the subsequent changes, while reducing the run time, also result in increases in the variance of the results. In a given Monte Carlo calculation, the variance is inversely proportional to the number of flights and, hence, to the run time. So, the performance Figure of Merit (FOM) is the variance times the run time. An attempt will be made below to quantify this FOM, but we can also compare qualitatively the variance over the most relevant portion of the problem space (near the target plate) via the relative standard deviation  $\sigma_{\text{rsd}}$ . Figure 4.15 shows  $\sigma_{\text{rsd}}$  for the deuterium density in the baseline case.

Below we will use  $\sigma_{\text{rsd}}$  for the source rate of  $\text{D}^+$  due to ionization of neutrals. Although not computed for this baseline run, this  $\sigma_{\text{rsd}}$  should be comparable to that shown in Fig. 4.15 except for the first one or two zones adjacent to the plate in which the contributions from  $\text{D}_2$  are significant.



spD\_density\_rsd\_ex vs. ( row, col )

Figure 4.15: Relative standard deviation of the atomic deuterium density in the baseline run of the performance benchmark.

### 4.7.7 Removal of Suppressed Ionization

The simplest (“analog”) Monte Carlo simulation kills off neutrals at their first ionizing collision. However, this makes finding the solution more than one mean free path from the source difficult. The predominant non-analog improvement is to assign a weight to each neutral flight (e.g., initially 1) and reduce that weight at each step to reflect the amount of ionization which should have occurred along the way. As a result, smaller variances are obtained in low probability regions of the problem. Because each flight will thus be tracked for more steps, a run using suppressed ionization will take longer. Whether or not that time is well spent depends on the problem at hand.

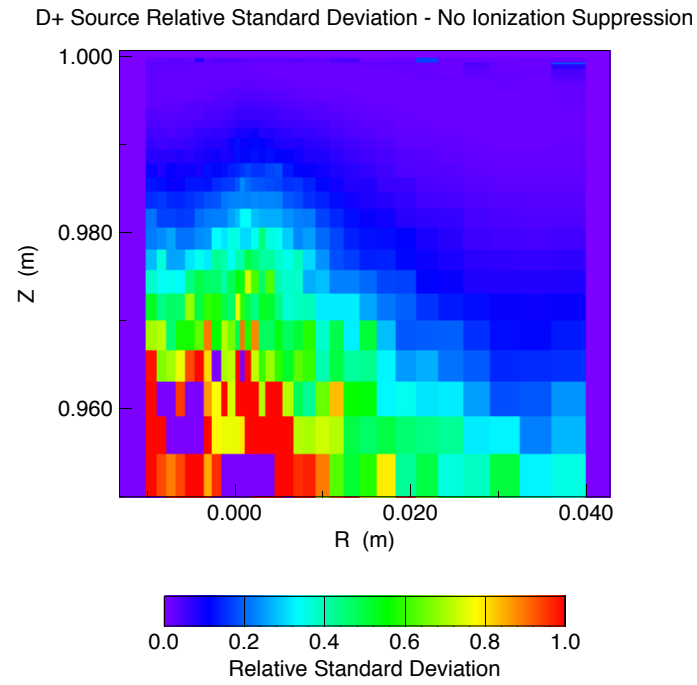
These EIRENE runs do not use suppressed ionization. For the purposes of comparison, we turned it off in DEGAS 2 as well. The run time without suppressed ionization dropped to 15 seconds per 1000 flights. Figure 4.16 shows the resulting  $\sigma_{\text{rsd}}$ .

### 4.7.8 Collision Estimator

Some of the scores in DEGAS 2, e.g., the neutral density and the  $\text{D}^+$  source rate, are computed via the track-length estimator. The other scores are compiled using data only at collisions (though most of these can also be done by track-length). Since the collision routines get executed regardless of whether or not the resulting data are used in the scores, we felt that it would be interesting to switch all of the estimators to collision (except density) and eliminate the overhead associated with generating the track-length scores. Of course, doing this increases the variance as is shown in Fig. 4.17. The run with using the collision estimator (again without suppressed absorption) needed 10 seconds per 1000 flights.

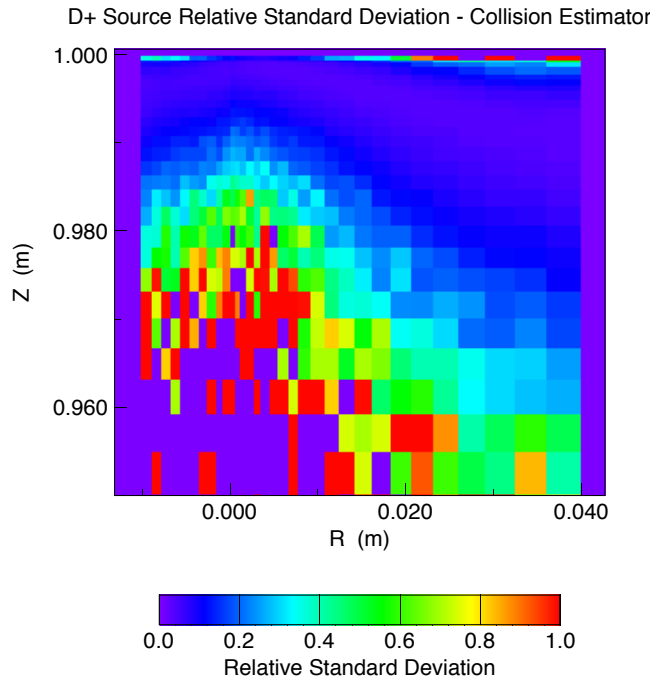
### 4.7.9 Russian Roulette for Molecules

Two of the seven reactions involving  $\text{D}_2$  and  $\text{D}_2^+$  in DEGAS 2 result in two D atoms. DEGAS 2 normally tracks both of these. EIRENE, however, like the original DEGAS, chooses one of the two to follow and “kills” off the other. This is a simple example of a general nonanalog Monte Carlo technique known as “Russian roulette”. Whether the use (or non-use) of this technique improves the variance again depends on the problem. For the purposes of this benchmark, Russian roulette was added to DEGAS 2’s molecular dissociation routine. Those scores switched to collision estimator in the previous section were reverted to the track-



D\_\_lon\_Source\_is\_rsd vs. ( row, col )

Figure 4.16: Relative standard deviation of the  $D^+$  ion source *without* suppressed ionization.



D\_ion\_Source\_col\_rsd vs. ( row, col )

Figure 4.17: Relative standard deviation of the  $D^+$  ion source using a collision estimator and *without* suppressed ionization.

length estimator for this configuration. Figure 4.18 shows the corresponding  $\sigma_{\text{rsd}}$ . This run used only 8 seconds per 1000 flights.

#### 4.7.10 Figures of Merit

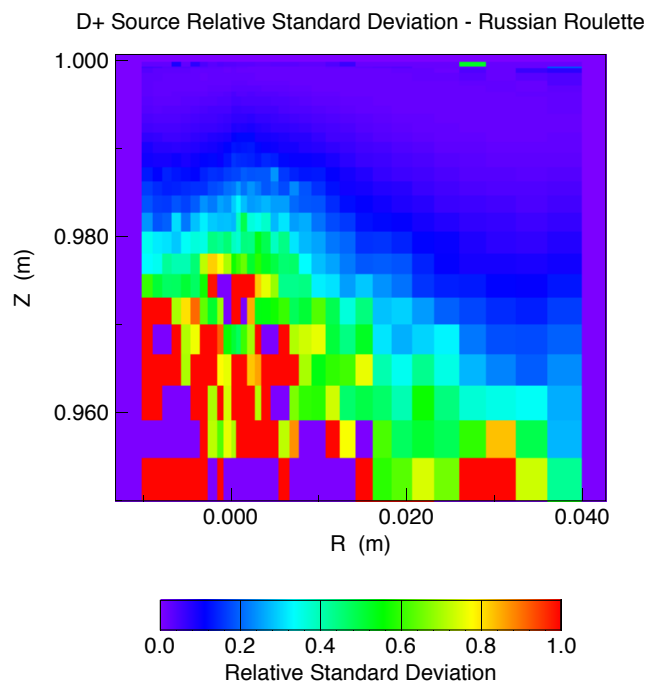
We now have four different configurations with which to evaluate this figure of merit, variance times run time. Presently, there is no single “answer” in these simulations which we can use to compute the FOM. Somewhat arbitrarily, we have selected a region of the problem spanning the width (radius) of this geometry and encompassing most of the integrated  $\text{D}^+$  source (the selection was made by eyeballing the plot; 83% of the integrated source was included). The  $\sigma_{\text{rsd}}$  for each configuration was divided by that of the baseline and integrated over this region. We then defined the FOM as the product of the 1000 flight run times (quoted above) and the square (to get the variance) of this ratio.

Configuration	Seconds / 1000 flights	$\sigma_{\text{rsd}}$ ratio	FOM
Baseline	49	1.0	49
No Suppressed Ionization	15	1.9	54
Collision Estimator	10	4.3	185
$\text{D}_2$ Russian Roulette	8	2.3	41

Clearly, using the collision estimator is not a good idea. The effectiveness of suppressed ionization could go either way. However, doing Russian roulette on the molecular products (this run was done without ionization suppression) looks to be the overall winner. Probably not by accident, this configuration is the closest to the default mode of operation for EIRENE.

#### 4.7.11 EIRENE Performance

Of course, the whole point of this portion of the benchmark is to compare the performance of DEGAS 2 against that of EIRENE. Apart from the addition of the variance output to EIRENE, no other modifications have been made to its default mode of operation. However, the compiler optimization was changed from the `-O3` value specified with the IPP-Garching version to the `-O4` which appears to work well for DEGAS 2 with the Sun FORTRAN 77 compiler. Over several runs of length 1000 to 10000 flights, the incremental time for 1000 flights is 12 seconds. The relative standard deviations computed by EIRENE were consistent with those of the corresponding DEGAS 2 configuration (Russian roulette), although a direct comparison was not made here (see Sec. 4.5.6).



D\_ion\_Source\_rr\_rsd vs. ( row, col )

Figure 4.18: Relative standard deviation of the  $D^+$  ion source using Russian roulette for molecules.

Within normal variations, the two codes are thus running at the same speed. The particular DEGAS 2 configuration should be chosen according to the needs of the problem at hand. Keep in mind that the original objective of DEGAS 2 was to be faster than DEGAS; the hope was that the code would yield performance comparable to that of EIRENE while retaining flexibility. That objective has been met. DEGAS 2 is also able to take full advantage of the substantial benefits of parallel processing.

Note, however, that EIRENE's computation of variances is less than optimal. Disabling them in the input file and turning off unneeded tallies reduces the incremental run time to 3 seconds per 1000 flights. At this point, EIRENE is substantially faster than DEGAS 2 since turning off its variance computation (which has been optimized) will not have a significant impact. The performance comparison between the two codes will be revisited as part of a later benchmark utilizing a more realistic divertor geometry.

The advantages of dynamic memory allocation of all run-time arrays, another design feature of DEGAS 2, have also been demonstrated during this benchmark. The run-time sizes were: DEGAS 2 - 7 MB, EIRENE - 142 MB. By reducing the dimensioning parameters in EIRENE to values more appropriate for this input file, the size of the code was reduced from 142 MB to 55 MB.

# Chapter 5

## Future Work

### 5.1 To Do List

The following are known problems and / or are items which need to be done:

- Sampling from a drifting Maxwellian is fudged or not done at all (sampling recycling ion, recombining ion, charge exchange).
- H / H<sub>2</sub> fraction for gas puffing is not implemented; needed for wall desorption, too.
- Need real sheath physics routine.
- Add fits to reactions, as done for PMI.
- Use FWEB to break up reaction-specific routines into separate files.
- Generalize detectors to treat finite solid angle?
- Might be able to replace eval\_data and pd\_eval\_data with a single routine.
- Generalize setup of detector views to permit chords not lying in poloidal plane.
- Need to add other H<sub>α</sub> emitting molecular reactions (will follow EIRENE here, unlike DEGAS, and explicitly track these reactions rather than fudging the emission rates of the dominant reactions).

- In readgeometry, set up detector views using chords from DEGAS input file.
- Note: in readgeometry, improved treatment of double-null, vacuum, UEDGE option, but didn't do likewise for !vacuum case: it will probably not work.
- Manual and other documentation needs to be updated.
- Add a dump of trajectories? Charles says that we might even be able to plot these in real time using some MPI-based utilities.
- Define default PMI packages which are invoked based on all material and test pairs. Ideally, the user should be presented with the list compiled at problemsetup time and edit it prior to actually running problemsetup.
- Extend sector definition to use two surfaces and a zone. If needed, this could be an ordered pair with the second member optional (or duplicated). Do this only if it cleans up some of the ugly sector related code in readgeometry and sector scoring routines.
- Adapt DG to write DEGAS 2 geometry netCDF file.
- Begin development of hybrid kinetic-fluid neutral transport code.

# Chapter 6

## Troubleshooting

### 6.1 Help!

If you're really in need of help, try contacting  
Charles Karney  
Princeton Plasma Physics Laboratory, MS 28  
P. O. Box 451  
Princeton NJ 08543-0451  
(609) 243-2607  
E-mail: [karney@pppl.gov](mailto:karney@pppl.gov)

or

Daren Stotler  
Princeton Plasma Physics Laboratory, MS 27  
P. O. Box 451  
Princeton NJ 08543-0451  
(609) 243-2063  
E-mail: [dstotler@pppl.gov](mailto:dstotler@pppl.gov)

# Bibliography

- [1] The development of analytic, numerical, and Monte Carlo methods of solving the time-independent Boltzmann equation describing neutral kinetics is reviewed in:  
M. Tendler and D. Heifetz, *Fusion Tech.* **11**, 289 (1987).
- [2] The “bible” of Monte Carlo transport techniques is:  
J. Spanier and E. M. Gelbard, “Monte Carlo Principles and Neutron Transport Problems” (Addison-Wesley Publishing Company, Reading Massachusetts, 1969).  
Other references from the neutron transport field include:  
J. M. Hammersley and D. C. Handscomb, “Monte Carlo Methods” (Metuchen, London, 1964).  
L. L. Carter and E. D. Cashwell, “Particle-Transport Simulation with the Monte Carlo Method” (National Technical Information Service, Springfield, Virginia, 1975).  
Ivan Lux and Laszlo Koblinger, “Monte Carlo Particle Transport Methods: Neutron and Photon Calculations” (CRC Press, Boca Raton, 1991).
- [3] The Algorithm and applications of DEGAS are discussed in:  
D. Heifetz, D. Post, M. Petravic, J. Weisheit, and G. Bateman, *J. Comp. Phys.* **46** 309 (1982).  
The Proceedings from a NATO-sponsored school in Val-Morin, Canada (1984) are an invaluable reference for scrape-off layer physics. In addition to again describing the algorithms and applications of DEGAS, Heifetz covers in his article some of the basics of neutral transport in a plasma: D. B. Heifetz, in *Physics of Plasma-Wall Interactions in Controlled Fusion*, D. Post and R. Behrisch, Eds., (Plenum, New York, 1986), p. 695.
- [4] D. P. Stotler et al., *J. Nucl. Mater.* **196-198**, 894 (1992).

- [5] D. R. Bates, A. E. Kingston, and R. W. P. McWhirter, *Proc. R. Soc. A* **267**, 297 (1962).
- [6] R. W. P. McWhirter, in *Plasma Diagnostic Techniques*, R. H. Huddlestone and S. L. Leonard, Eds. (Academic, New York, 1965).
- [7] [http://w3.pppl.gov/~krommes/fweb\\_toc.html](http://w3.pppl.gov/~krommes/fweb_toc.html) (FWEB home page)
- [8] <http://www.unidata.ucar.edu/packages/netcdf/index.html> (netCDF home page)
- [9] <http://hdf.ncsa.uiuc.edu/> (HDF home page)
- [10] Although never formally published and not readily available online, the EIRENE User's Manual is a very useful reference on the physics and algorithms of Monte Carlo neutral transport:  
 D. Reiter, "The EIRENE Code, Version: Jan. 92, Users Manual", EURATOM-KFA Institut für Plasmaphysik Report JUL-2599 (1992).  
 One source for a recent version of this document is the "SOLPS" package maintained R. Schneider and D. Coster of the Max Planck Insitut für Plasmaphysik in Garching. Try the <http://www.rzg.mpg.de/~dpc/solps.html> SOLPS home page for more information.
- [11] K. M. Case and P. F. Zweifel, *Linear Transport Theory* (Addison-Wesley, Reading, MA, 1967).
- [12] D. P. Stotler, A. Yu. Pigarov, C. F. F. Karney, S. I. Krasheninnikov, B. LaBombard, B. Lipschultz, G. M. McCracken, A. Niemczewski, J. A. Snipes, J. L. Terry, and R. A. Vesey, in *Fusion Energy 1996* (Proc. 16th Int. Conf. Montreal, 1996), Vol. 2 (IAEA, Vienna, 1997) p. 633 (see also the corresponding PPPL Report).
- [13] R. K. Janev, W. D. Langer, K. Evans, Jr., and D. E. Post, Jr., *Elementary Processes in Hydrogen-Helium Plasmas* (Springer-Verlag, Berlin, 1987) (see also the corresponding Aladdin data file).
- [14] D. Reiter, in *Atomic and Plasma-Material Interaction Processes in Controlled Thermonuclear Fusion*, R. K. Janev and H. W. Drawin, Eds., (Elsevier, New York, 1993), p. 243.

- [15] R. K. Janev and J. J. Smith, *Atomic and Plasma-Material Interaction Data for Fusion* (Supplement to the journal Nuclear Fusion) **4** (1993) (see also the corresponding Aladdin data file).
- [16] L. C. Johnson and E. Hinnov, *J. Quant. Spectrosc. Radiat. Transfer* **13**, 333 (1973).
- [17] J. C. Weisheit, *J. Phys. B: Atom. Molec. Phys.* **8**, 2556 (1975).
- [18] R. J. Kanzleiter, D. P. Stotler, C. F. F. Karney, and D. Steiner *Phys. Plasmas* **7**, 5064 (2000).
- [19] P. S. Krstic and D. R. Schultz, *Atomic and Plasma-Material Data for Fusion* **8**, 1 (1998).
- [20] P. Bachmann and d. Reiter, *Contrib. Plasma Phys.* **35**, 45 (1995).
- [21] H. H. Abou-Gabal and G. A. Emmert, *Nucl. Fusion* **31**, 407 (1991).
- [22] A. Dalgarno, *Phil. Trans. R. Soc. London, Ser. A* **250**, 426 (1958).
- [23] T. Holstein, *J. Phys. Chem.* **56**, 832 (1952).
- [24] J. M. Wadehra, *Phys. Rev. A* **20**, 1859 (1979).
- [25] C. F. Barnett, *Atomic Data for Fusion*, Oak Ridge National Laboratory Report ORNL-6086, Vol. 1 (1990).
- [26] J. H. Newman, J. D. Cogan, D. L. Ziegler et al., *Phys. Rev. A* **25**, 2976 (1982).
- [27] A. C. Reviere, *Nucl. Fusion* **11**, 363 (1971).
- [28] J. F. O'Hanlon, *A User's Guide to Vacuum Technology* (John Wiley & Sons, New York, 1989).
- [29] A. Niemczewski, Ph. D. Thesis, Massachusetts Institute of Technology, Plasma Fusion Center Report PFC/RR-95-8 (1995).
- [30] P. L. Bhatnagar, E. P. Gross, and M. Krook, *Phys. Rev.* **94**, 511 (1954).
- [31] P. Welander, *Arkiv Fysik* **7**, 507 (1954).
- [32] Chr. May, Ph. D. Thesis.

- [33] D. Reiter, Chr. May, M. Baelmans, and P. Börner, *J. Nucl. Mater.* **241**, 342 (1997).
- [34] R. J. Kanzleiter, Ph. D. Thesis, Rensselaer Polytechnic Institute (1999).
- [35] S. Chapman and T. G. Cowling, *The Mathematical Theory of Non-Uniform Gases* (Cambridge University Press, 1970).
- [36] T. F. Morse, *Phys. Fluids* **6**, 1420 (1963).
- [37] R. C. Reid, J. M. Prausnitz, B. E. Poling, *The Properties of Liquids and Gases* (McGraw-Hill Book Company, New York, 1987).
- [38] *CRC Handbook of Chemistry and Physics, 75th Edition, 1913–1995*, D. R. Lide, Ed., p. 6-239 (CRC Press, Boca Raton, 1994).
- [39] D. R. Willis, *Phys. Fluids* **5**, 127 (1962).
- [40] C. Cercignani, *J. Stat. Phys.* **1**, 297 (1969).
- [41] C. Cercignani, *Theory and Application of the Boltzmann Equation* (Scottish Academic Press, New York, 1975).
- [42] P. R. Bevington, *Data Reduction and Error Analysis for the Physical Sciences* (McGraw-Hill Book Company, New York, 1969).
- [43] W. Eckstein, *Computer Simulation of Ion-Solid Interactions* (Springer-Verlag, New York, 1991).
- [44] G. Bateman, “Distribution of Neutrals Scattered Off A Wall”, PPPL Applied Physics Division Report # 1 (1980).
- [45] D. B. Macmillan, *SIAM J. Appl. Math.* **15**, 264 (1967).
- [46] J. Spanier, *SIAM J. Appl. Math.* **14**, 702 (1966).
- [47] D. E. Knuth, *The Art of Computer Programming* (Addison-Wesley, Reading, MA, 1997).
- [48] C. S. Pitcher, C. J. Boswell, J. A. Goetz et al., *Phys. Plasmas* **7**, 1894 (2000).
- [49] C. S. Pitcher, C. J. Boswell, T. Chung et al., *J. Nucl. Mater.* **290-293**, 812 (2001).

[50] D. P. Stotler, C. S. Pitcher, C. J. Boswell et al., *J. Nucl. Mater.* **290-293**, 967 (2001).

# Index

- adsorption, 53
- Allocation, memory, 2
- Atomic physics, 21
  
- background species, 53
- BGK, 35
- Boltzmann equation, 1
- boxgen, 48
  
- Charge exchange, 25
- chargex, 52
- collisional-radiative, 21
- CVS, 3, 44
  
- dataexam, 49
- datamatch, 50
- datasetup, 48
- defineback, 46
- defineback input, 54
- definegeometry2d, 45, 46
- definegeometry2d input, 54
- DEGAS, 2
- desorption, 53
- Differential cross section, 25
- Diffusion, 35
- Diffusion cross section, 25
- directories, 45
- dissoc, 52
- dissoc\_rec, 52
- Distribution, probability, 5
  
- elastic, 52
  
- Elastic scattering, 25
- elements\_infile, 52
- elementsfile, 52
- Emacs, 43
- emacs, 42
  
- flighttest, 46
- ftangle, 43
- fweave, 43
- FWEB, 2, 43
  
- Generators, random number, 5
- generic, 52
- generic PMI, 53
- generic reactions, 52
- geometry.inp, 55
- geomtesta, 46
- gmake, 42
  
- HDF, 3, 44
- HOME, 45
  
- ionization, 21
- ionize, 52
- ionize\_suppress, 52
  
- LaTeX, 43
  
- Macros, 2
- make, 42
- Makefile, 42
- Makefile.local, 45

matcheir, 50  
 matchout, 50  
 materials\_infile, 53  
 materialsfile, 53  
 Maxwell molecules, 35  
 Monte Carlo, 5  
  
 ncdum, 43  
 ncdump-filter, 43  
 ncgen, 43  
 ncgen-filter, 43  
 NetCDF, 3  
 netCDF, 43  
 Neutral Transport, 1  
 Neutral-ion scattering, 25  
 Neutral-neutral scattering, 35  
 non-generic PMI, 53  
 non-generic reactions, 52  
  
 Object oriented programming, 2  
 outputscript, 55  
  
 Pcl-cvs, 44  
 PMI, 53  
 pmi\_infile, 53  
 pmitest, 49  
 pmiwrite, 48  
 problem\_infile, 53  
 problemfile, 53  
 problemsetup, 46  
 Processing, parallel, 3  
  
 Random, 5  
 randomtest, 49  
 ratecalc, 48  
 rates, atomic physics, 21  
 reaction type, 52  
 reaction\_infile, 52  
 reactionfile, 52  
  
 reactiontest, 49  
 reactionwrite, 48  
 readbackground, 46  
 readbackground input, 54  
 readgeometry, 46  
 readgeometry input, 54  
 recombination, 21, 52  
 reference level, 53  
 reflection, 53  
  
 Scattering angle, 25  
 Scoring, 5  
 sourcetest, 49  
 species, 52  
 species\_infile, 52  
 speciesfile, 52  
 Spin exchange, 25  
 subset data, 53  
 symbolic name, 51  
 sysdeptest, 49  
  
 Tags, 42  
 tally, 54  
 tally\_infile, 54  
 tallyfile, 54  
 tallysetup, 46, 54  
 test species, 53  
 TeX, 43  
 Theory, transport, 1  
 Total cross section, 25  
 Tracking, 5  
 Transport codes, 1  
 Triangle, 45  
  
 Viscosity, 35  
 Viscosity cross section, 25

# Contents

<b>1</b>	<b>Introduction</b>	<b>1</b>
1.1	Purpose of Monte Carlo Neutral Transport . . . . .	1
1.2	Need for DEGAS 2 . . . . .	2
1.3	DEGAS 2 Features . . . . .	2
<b>2</b>	<b>Background</b>	<b>5</b>
2.1	Generic Monte Carlo Algorithms . . . . .	5
2.1.1	Sampling a Distribution . . . . .	6
2.1.2	Sampling Distance to Next Collision . . . . .	6
2.1.3	Sampling More Complicated Distributions . . . . .	8
2.2	Particle Transport . . . . .	9
2.2.1	Motivating the Integral Equation . . . . .	9
2.2.2	Transport and Collision Kernels . . . . .	10
2.2.3	Integral Equation Details . . . . .	10
2.3	Estimators . . . . .	12
2.3.1	Simple Estimators . . . . .	12
2.3.2	Generalized Collision and Tracklength Estimators . . . . .	13
2.3.3	Specification of Tallies . . . . .	16
2.4	Tracking Procedure . . . . .	19
2.5	Random Numbers . . . . .	21
2.6	Geometry . . . . .	21
2.7	Atomic Physics . . . . .	21
2.7.1	Electron Energy Exchange Rate . . . . .	23
2.7.2	Solutions Used with DEGAS 2 . . . . .	24
2.8	Elastic Scattering . . . . .	25
2.8.1	Neutral-Ion Elastic Scattering . . . . .	25
2.8.2	Neutral-Neutral Elastic Scattering . . . . .	30
2.8.3	Validation of BGK Model and Rates . . . . .	35

<b>3</b>	<b>Running DEGAS 2</b>	<b>41</b>
3.1	Getting DEGAS 2 . . . . .	41
3.2	Getting Supporting Tools . . . . .	42
3.2.1	GNU Software . . . . .	42
3.2.2	netCDF . . . . .	43
3.2.3	FWEB . . . . .	43
3.2.4	Concurrent Version System . . . . .	44
3.2.5	HDF . . . . .	44
3.2.6	Triangle . . . . .	45
3.3	Structure of the DEGAS 2 File System . . . . .	45
3.4	Components of the Code . . . . .	46
3.4.1	Main Code . . . . .	46
3.4.2	Other Setup Routines . . . . .	48
3.4.3	Test Routines . . . . .	49
3.4.4	Miscellaneous Routines . . . . .	50
3.5	Input Files . . . . .	50
3.5.1	degas2.in . . . . .	51
3.5.2	elements_infile . . . . .	52
3.5.3	species_infile . . . . .	52
3.5.4	reaction_infile . . . . .	52
3.5.5	ratecalc Input . . . . .	53
3.5.6	materials_infile . . . . .	53
3.5.7	pmi_infile . . . . .	53
3.5.8	problem_infile . . . . .	53
3.5.9	readgeometry Input . . . . .	54
3.5.10	definegeometry2d Input . . . . .	54
3.5.11	defineback Input . . . . .	54
3.5.12	readbackground Input . . . . .	54
3.5.13	tally_infile . . . . .	54
3.5.14	outputbrowser Input . . . . .	55
3.5.15	geomtesta Input . . . . .	55
3.6	Compiling DEGAS 2 . . . . .	56
3.6.1	Basics . . . . .	56
3.6.2	Making Documents . . . . .	57
3.6.3	Adjustments to Makefile . . . . .	58
3.6.4	Cross-Compiling . . . . .	59
3.6.5	Miscellaneous Targets . . . . .	60
3.6.6	CVS Access to DEGAS 2 . . . . .	60

3.7	Examples . . . . .	61
3.7.1	Analytic_fluid_bench . . . . .	61
3.7.2	Neutral-Neutral Scattering Examples . . . . .	64
3.8	Run Control Parameters . . . . .	80
3.8.1	Checkpoints . . . . .	80
3.8.2	Restarting . . . . .	80
3.8.3	Seed String . . . . .	81
3.8.4	Spaced Seeds . . . . .	82
3.8.5	Direct Sampling . . . . .	82
3.9	Adding Reactions and PMI . . . . .	83
3.9.1	Overview of Data Format . . . . .	83
3.9.2	An Example: Bateman Format Data . . . . .	84
3.9.3	Reaction Processing Routines . . . . .	88
3.10	Defining Radiation Detectors . . . . .	88
3.10.1	Signal Computation . . . . .	89
3.11	Sectors and Diagnostic Surfaces . . . . .	90
3.11.1	Diagnostic Sectors . . . . .	91
3.12	Output File . . . . .	92
3.13	Other Documentation . . . . .	93
<b>4</b>	<b>EIRENE Benchmark</b>	<b>94</b>
4.1	Introduction . . . . .	94
4.2	Problem Description . . . . .	95
4.3	“Out of the Box” Results . . . . .	95
4.4	Statistical Basis for Comparisons . . . . .	100
4.5	Code Differences . . . . .	102
4.5.1	Atomic Physics . . . . .	102
4.5.2	Source Sampling . . . . .	103
4.5.3	Energy Distribution of Reflected Atoms . . . . .	108
4.5.4	Angular Distribution of Reflected Atoms . . . . .	109
4.5.5	H <sub>2</sub> Dissociation Rate . . . . .	109
4.5.6	Estimator Differences . . . . .	112
4.5.7	Other Differences . . . . .	113
4.6	Characterize Comparison . . . . .	113
4.6.1	Density Differences . . . . .	113
4.6.2	Comparison of Momentum Source . . . . .	114
4.6.3	Results of Quantitative Comparison . . . . .	114
4.7	Performance Benchmark and Optimization . . . . .	121

4.7.1	Starting Point . . . . .	121
4.7.2	Charge Exchange Rejection . . . . .	122
4.7.3	Reduce Number of Scores . . . . .	122
4.7.4	Compression of Scores . . . . .	122
4.7.5	Other Changes with Minimal Effects . . . . .	123
4.7.6	Variance-Altering Changes . . . . .	123
4.7.7	Removal of Suppressed Ionization . . . . .	125
4.7.8	Collision Estimator . . . . .	125
4.7.9	Russian Roulette for Molecules . . . . .	125
4.7.10	Figures of Merit . . . . .	128
4.7.11	EIRENE Performance . . . . .	128
<b>5</b>	<b>Future Work</b>	<b>131</b>
5.1	To Do List . . . . .	131
<b>6</b>	<b>Troubleshooting</b>	<b>133</b>
6.1	Help! . . . . .	133